THE FLORIDA STATE UNIVERSITY

COLLEGE OF ARTS AND SCIENCES

ANOMALOUS METALLIC BEHAVIOR IN STRONGLY CORRELATED ELECTRON SYSTEMS WITH DISORDER

By

DARKO TANASKOVIC

A Dissertation submitted to the
Department of Physics
in partial fulfillment of the
requirements for the degree of
Doctor of Philosophy

Degree Awarded:
Summer Semester, 2005

The members of the Committee approve the dissertation of Darko Tanaskovic defended on June 21, 2005.

Vladimir Dobrosavljevic
Professor Directing Dissertation

Naresh Dalal
Outside Committee Member

Efstratios Manousakis
Committee Member

Simon Capstick
Committee Member

Peng Xiong
Committee Member

The Office of Graduate Studies has verified and approved the above named committee members.

ACKNOWLEDGEMENTS

I would like to express my sincere gratitude to my thesis advisor Vlad Dobrosavljević for giving me attractive research topics, making research look fun and easy, and above all for his best judgement and advice in each and every situation.

I would like to thank Eduardo Miranda, with whom I have exchanged numerous e-mails, and who set up an example for me with clarity and elegance in expressing physical ideas.

I thank Satoru Nakatsuji for short, but very fruitful collaboration in analyzing experimental data.

Special thanks to Čedomir Petrović for advising me to come to Florida State University, and introducing me to life in Tallahassee.

Last but not least, I would like to thank numerous friends and colleagues who helped that these five years have become a rewarding life experience. Apologizing to others, I will mention Carol Aguiar, Gonzalo Alvarez, John Janik, Dimitrije Stepanenko and Goran Mihajlović.

TABLE OF CONTENTS

LIST OF FIGURES

ABSTRACT

We study several aspects of the behavior of strongly correlated electron systems with disorder. First we examine the influence of strong electron-electron interactions on the impurity dominated resistivity. In the weak-coupling limit, the resistivity is reduced by the screening effect which is determined by the charge compressibility, which is proportional to the inverse screening length. We show that when strong correlations are present, although the compressibility is reduced, the screening effect is nevertheless strongly enhanced. This phenomenon is traced to the non-perturbative Kondo-like processes captured by dynamical mean field theory, but which are absent in weak coupling approaches. We discuss a possible relevance of our results for the physics of high mobility MOSFETs. In the second part of the thesis we study possible mechanisms of disorder-driven non-Fermi liquid behavior in heavy fermion systems. We present simple analytical arguments explaining the universal emergence of electronic Griffiths phases as precursors of disorder-driven metal-insulator transitions in correlated electronic systems. Then we examine the interplay of the Kondo effect and the RKKY interactions in electronic Griffiths phases using extended dynamical mean-field theory methods. We find that sub-Ohmic dissipation is generated for sufficiently strong disorder, leading to suppression of Kondo screening on a finite fraction of spins, and giving rise to universal spin-liquid behavior.

CHAPTER 1

INTRODUCTION

One of the central goals of condensed matter physics is fabricating of new materials with interesting and unusual transport, optical and thermodynamic properties. Prominent examples include high-temperature superconductors, heavy fermion systems, doped semiconductors, frustrated magnets, and quantum Hall systems. The physical understanding and microscopical description of many aspects of their behavior has remained as a challenge for theorists. The main difficulty for theory lies in the existence of several competing processes. Some of the interactions may favor metallic behavior, superconductivity or ferromagnetism, while others favor localization of carriers, glassy phases or antiferromagnetism. Therefore, these materials are, as a rule, very sensitive to a change of the chemical composition (doping), application of a magnetic field, or pressure.

In this thesis we study several aspects of the low temperature behavior of strongly interacting disordered systems. In particular, we find motivation in puzzling transport properties of high mobility silicon metal-oxide semiconductor field-effect transistors (MOSFETs) [1] and transport and thermodynamic properties of heavy fermion alloys [2]. High mobility two-dimensional (2D) MOSFETs have a very low concentration of carriers, and hence the potential Coulomb energy is much larger than the kinetic (Fermi) energy. Therefore, 2D MOSFETs are strongly interacting electronic systems. On the other hand, the MOSFETs are disordered systems due to the presence of ionized impurities randomly distributed in the oxide layer, and roughness of the Si-SiO_2 interface [3]. The relative importance of the interaction effects in these systems depends on the concentration of charge carriers, which can easily be modified by changing the gate voltage. This makes 2D MOSFETs an excellent probe for a study of the interplay of correlation effects and disorder.

Heavy fermions are strongly correlated systems due to the strong on-site electron-electron interaction in partially filled f-electron shells [4]. Low temperature thermodynamic and

transport properties of these materials can typically be described by the Landau Fermi liquid theory of metals, but with strongly renormalized quasiparticle parameters. In the last fifteen years, however, a large number of heavy fermion alloys has been discovered whose properties clearly deviate from the predictions of the Fermi liquid theory [2]. The origin of this "non-Fermi liquid" (NFL) behavior is still an unresolved problem, and it is hoped that its solution will give us a better understanding of the physics of strongly correlated systems in general. In this thesis we will concentrate on those heavy fermion alloys, like $UCu_{5-x}Pd_x$, whose thermodynamic and transport properties are believed to be dominated by disorder.

There are very few viable theoretical approaches that address the difficult problem of strongly interacting electronic systems with disorder. We will work within the dynamical mean field theory (DMFT) [5] and its extensions to disordered systems [6, 7, 8]. The main advantage of the DMFT approach is that while being reasonably simple, it is controlled in the sense that it becomes exact in the limit of large coordination number. It is similar to the Weiss mean field theory of magnetism in that we solve a problem of a chosen particle embedded in an averaged bath, which has to be determined self-consistently. The difference, however, is that the dynamical mean field theory fully takes into account quantum fluctuations. In other words, it allows hopping of a particle between a given site and its surroundings. Therefore, the DMFT is capable of capturing many physical properties unaccessible in the standard mean field theory. In particular, one of its great successes is a correct description of the interaction effects which lead to the Mott metal-insulator transition.

This thesis is divided into two rather independent parts. The first part of the thesis (Chapters 2, 3 and 4) addresses the questions of the disorder screening in the regime of strong interactions. In Chapter 2, we motivate our research by the description of the metallic phase of high mobility MOSFETs. In particular, we point out the unusually strong temperature dependence of the resistivity in the vicinity of the metal-insulator transition. In the next two chapters we consider the electron scattering on nonmagnetic impurities. Chapter 3 contains critical remarks on the applicability of different versions of the random phase approximation (RPA) to the case of strong coupling. In Chapter 4 we examine how the scattering rate is modified in the presence of a strong electron-electron interaction. We solve this problem within DMFT for a half-filled lattice at zero temperature with short-range

(Hubbard) interactions. To our knowledge, this is a first controlled treatment of the disorder screening in the strong coupling regime. We discuss the limitations of our approach and its applicability to real physical systems.

In the second part of the thesis (Chapters 5, 6, and 7) we examine possible routes that can lead to the non-Fermi liquid behavior in disordered heavy fermion materials. Chapter 5 contains a brief overview of the low temperature thermodynamic and transport properties of heavy fermions. The emphasis is on the experimental data, like the divergence of the low temperature specific heat and magnetic susceptibility, which do not fit into the predictions of the Landau Fermi liquid theory. In Chapter 6, following the previous work within an extended dynamical mean field theory, we develop a simple model of the non-Fermi liquid behavior in disordered Kondo lattice systems which can even be solved analytically. Within this model, rare sites with the lowest Kondo temperatures provide the leading singular low temperature thermodynamic response. We refer to the system described by this model as an electronic Griffiths phase. In Chapter 7 we introduce random inter-site magnetic interactions into the model of the electronic Griffiths phase. We solve this model within an extended dynamical mean field theory and show that a fraction of the f-electrons which decouples from the conduction bath forming a spin liquid, provides the leading logarithmic contribution to the local dynamic magnetic susceptibility. We conclude the thesis in Chapter 8, where we summarize our main results and outline possible directions for the future research.

CHAPTER 2

ANOMALOUS METALLIC PHASE IN TWO-DIMENSIONAL MOSFETS

The synthesis of high mobility silicon metal-oxide semiconductor field-effect transistors (MOSFETs) in early 90's has intensified the efforts to understand the physics of disordered strongly interacting systems. High mobility MOSFETs have many surprising and puzzling transport properties. However, despite the significant number of the experimental data and theoretical papers, many of those properties remained poorly understood. In this chapter, as a motivation for our theoretical work, we will briefly review some of the most important properties of high mobility MOSFETs.

2.1 Metal-insulator transition in two dimensions

According to the scaling theory of localization [9] there can be no metallic state in two dimensions in zero magnetic field. Within this two decades old theory, all carriers are localized in an infinitely large two-dimensional (2D) system at zero temperature. With decreasing temperature the resistance is expected to grow logarithmically ("weak localization") or exponentially ("strong localization"), becoming infinite as $T \to 0$. Although this prediction was made for noninteracting particles, subsequent work showed that weak interaction increases the localization even further [10]. In the opposite limit of very strong interaction between particles, a 2D electron system is expected to become a Wigner crystal [11]. In the presence of even a small amount of disorder, such a crystal is expected to be pinned so that the system of crystallized electrons would not conduct at zero temperature. Therefore 2D systems were not expected to be conducting in either limit: weak (or absent), or very strong interactions between carriers. The experiments in early 1980s seemed to support

that conclusion, and the question whether a conducting state can exist in 2D systems was considered resolved.

Recently, high mobility samples of MOSFETs have become available, which has allowed systematic studies of 2D systems in a very dilute regime, i.e. at electron densities below $10^{11}\,\mathrm{cm}^{-2}$ [1]. Surprisingly, experiments on these samples consistently show the existence of a critical density n_c, above which the resistivity is decreasing with decreasing temperature. This behavior persists up to the lowest accessed temperatures (~ 4 mK), strongly indicating the existence of the metal-insulator transitions at $T = 0$. At the critical density, the resistivity is found to be nearly independent of temperature and of the order of the quantum unit of resistance, $h/e^2 \approx 25.6\,\mathrm{k}\Omega$. Another prominent unusual feature is the strong positive magnetoresistance, both in the conducting and in the insulating phase of MOSFETs. An external magnetic field applied at an arbitrary angle with respect to the 2D plane seems to suppress the metallic behavior and eliminates it completely for fields of order of several tesla. Neither the metallic behavior, nor its suppression by a magnetic field is currently understood.

2.2 Experiments

The first experiments that turned attention to a possible existence of the MIT in 2D systems were performed by Kravchenko *et al.* [12, 13]. The experiments were done on very low-disordered silicon MOSFETs. Peak electron mobilities in these samples exceeded those in the samples used in previous studies by an order of magnitude, reaching more than 4×10^4 cm^2/Vs at $T = 4.2$ K. This allowed measurements at very low electron concentrations n_s, where the electron-electron interaction E_{e-e} becomes the dominant parameter, being much larger than the Fermi energy. Estimates for Si MOSFETs at $n_s = 10^{11}$ cm^{-2} yield

$$E_{e-e} \sim \frac{e^2}{\epsilon}(\pi n_s)^{1/2} \approx 10\,\mathrm{meV}, \tag{2.1}$$

while

$$E_F = \frac{\pi\hbar^2 n_s}{2m^*} \approx 0.58\,\mathrm{meV}, \tag{2.2}$$

where e is the electron charge, ϵ is the dielectric constant, E_F is the Fermi energy, and m^* is the effective electron mass. The dimensionless parameter $r_s \equiv E_{\text{e-e}}/E_F$ thus assumes values

above 10 in these samples. In the very dilute regime, 2D electrons are expected to form a Wigner crystal. Numerical simulation [11] predicted that this should occur at $r_s \approx 37 \pm 5$, and at even higher density when disorder is present [14]. Therefore, it is reasonable to expect that the 2D system is a strongly correlated liquid at $r_s \sim 10$.

Subsequent experiments in dilute silicon MOSFETs with different geometry and oxide thicknesses [15] confirmed the earlier findings, and similar behavior was reported in a variety of other 2D systems (p-GaAs, n-GaAs, p-SiGe, etc.). Fig. 2.1 shows the dependence of the resistivity on the electron density and temperature [12, 13]. We see that there is a critical electron density $n_s = n_c$, at which the systems changes its behavior. For $n_s > n_c$, the system is metallic, and for $n_s < n_c$ the resistivity slope changes sign, and the system becomes insulating. The change in the resistivity is very pronounced. A change of the concentration of only a few percent leads to a change in resistivity of even several orders of magnitude

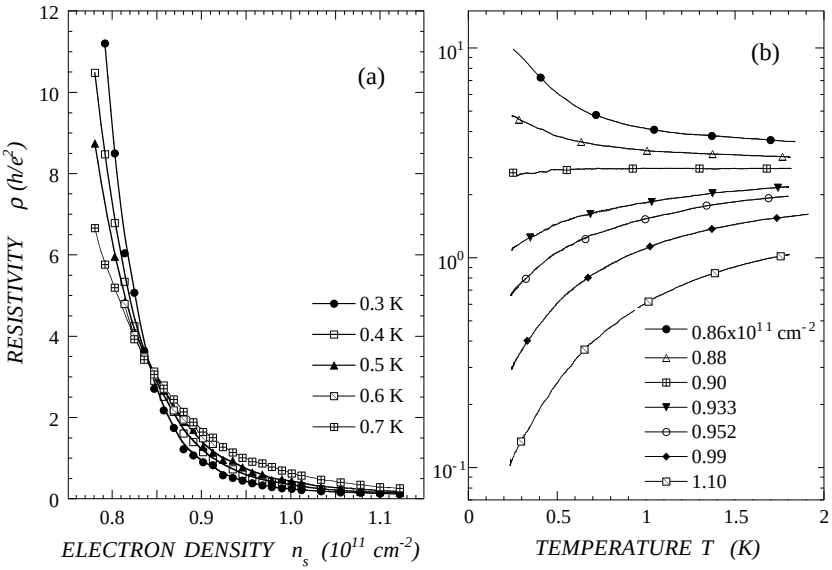

Figure 2.1. (a) Resistivity as a function of electron density for 2D system of electrons in a high-mobility silicon MOSFET; different curves correspond to different temperatures. (b) Resistivity as a function of temperature; here different curves are for different electron densities. From Ref. [13].

at lowest temperatures. At the critical electron density n_c, the resistivity is approximately $3h/e^2$ and almost independent of temperature, while for densities away from n_c the resistivity changes rapidly with decreasing temperature, giving a clear distinction between metallic and insulating behavior. Above $T^* \approx 2$ K the temperature dependence of the resistivity becomes weak. At higher densities, of the order of those used in the experiments in the 1980s, a weak insulating temperature dependence is observed, reminiscent of Anderson localization.

In the critical regime, the resistivity vs. temperature curves can be collapsed onto two branches by applying a single scaling parameter $T_0(n_s)$ [13], Fig. 2.2. The resistivity is given by

$$\rho(T, n_s) = \rho_c f_1[T/T_0(n_s)], \tag{2.3}$$

where ρ_c is the value of the resistivity at the critical density. The scaling relation breaks

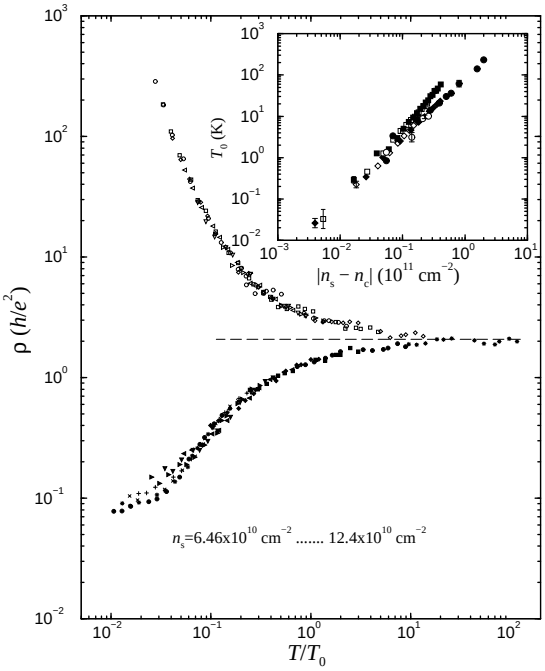

Figure 2.2. For a silicon MOSFET, resistivity versus T/T_0, with T_0's chosen to yield scaling with temperature. The inset shows the scaling parameter, T_0, versus deviation from the critical point, $|n_s - n_c|$; data are shown for silicon MOSFETs obtained from three different wafers. Open symbols correspond to the insulating side and closed symbols to the metallic side of the transition. From Ref. [13].

down at $T > T^*$ and at very low temperatures, where the temperature dependence of the resistivity becomes weak. However, it is remarkable that the scaling is possible over the range of temperatures where the resistivity changes for an order of magnitude. Moreover, $T_0(n_s)$ is independent of the sign of $\delta_n \equiv (n_s - n_c)/n_s$. The inset in Fig. 2.2 shows T_0 as a function of the absolute deviation from the critical density, $|n_s - n_c|$, on a log-log scale for both metallic and insulating curves and for three different samples. It is important to note that the dependence is a power law, $T_0 \propto |\delta_n|^b$, with approximately the same power $b = 1.60 \pm 0.1$ for all three samples and for both metallic and insulating curves. It was also observed that the metallic and insulating curves are reflection symmetric in the temperature range above 300 mK and below T^*. Dobrosavljević *et al.* [16] showed that the observed scaling and reflection symmetry could be consequences of a simple analysis assuming that a $T = 0$ quantum critical point describes the metal-insulator transition. Within quantum critical scaling the power law exponent b in $T_0 \propto |\delta_n|^b$ is given by $b = z\nu$, where z is the dynamical exponent and ν is the correlation length exponent.

Another unusual property of dilute 2D systems is their enormous response to an external magnetic field. A parallel magnetic field of an order of several tesla increases the resistance for more than an order of magnitude [17] (Fig. 2.3). This is true for both the metallic and the insulating side of a transition. Above a characteristic magnetic field B_{sat}, which depends on a density of the electrons, the magnetoresistance becomes saturated. This is associated with a total polarization of the electron spins. A parallel magnetic field suppresses metallic behavior and eventually turns the zero-field metal into a high-field insulator [17] (Fig. 2.4). The effect of the field is negligible at temperatures above T^*, *i.e.*, above the temperature below which the metallic behavior in $B = 0$ sets in. Therefore, T^* signals a temperature below which there is an abrupt onset of metallic behavior and below which the magnetoresistance becomes extremely large. In isotropic systems such as Si MOSFETs, studies have shown that the metallic temperature dependence is suppressed in a similar way by magnetic fields applied at any angle relative to the 2D plane. In this case the magnetoresistance arises from the superposition of two terms: the total field coupled to the electron spins, yielding a large positive magnetoresistance, and the perpendicular field component coupled to the orbital motion, giving rise to the quantum Hall effect.

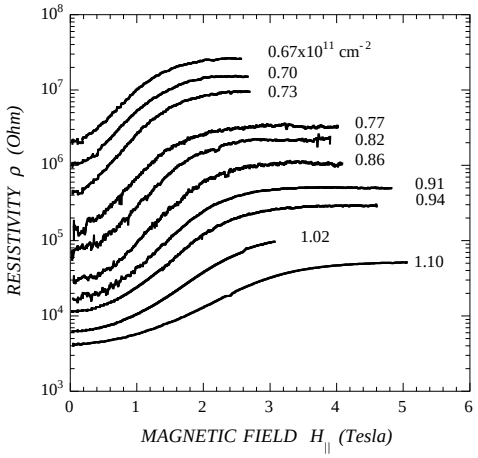

Figure 2.3. Resistivity of a silicon MOSFET at $T = 0.3$ K as a function of magnetic field applied parallel to the plane of the 2D electron system, for several electron densities. The top three curves are insulating in zero field while the lower curves are conducting. Note that B_{sat} decreases as we are getting closer to n_c. From Ref. [17].

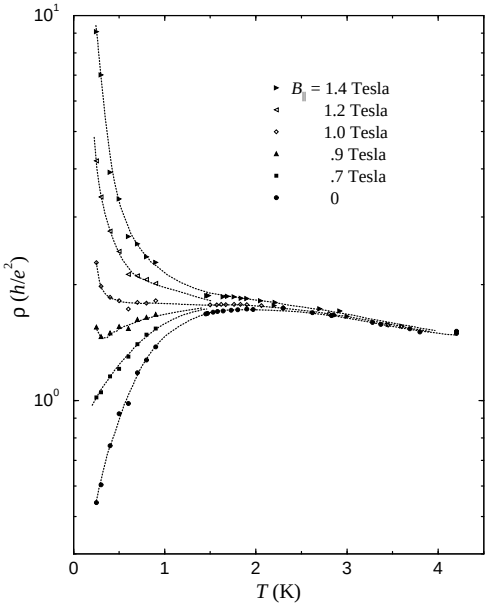

Figure 2.4. Resistivity versus temperature for several values of a magnetic field applied parallel to the plane of a silicon MOSFET. The electron density is 8.83×10^{10} cm^{-2}. From Ref. [17].

2.3 Central open questions and possible explanations

The main observations which need to be explained are:

- Metallic behavior is displayed down to the lowest accessed temperatures and is accompanied by an enormous decrease of resistivity as $T \to 0$. The effects of strong interaction seem to be crucial for this behavior.

- In the metallic side of the transition, for magnetic fields applied parallel to the electron planes, the resistivity increases dramatically by an order of magnitude in response to relatively modest fields of order of a few tesla, saturating to a constant value at higher fields.

- Well defined metallic or insulating behavior is observed only at temperatures lower than a characteristic temperature $T_0(\delta_n)$ that vanishes at the transition. The characteristic magnetic field $B_{sat}(\delta_n)$ which leads to a total spin polarization also tends to zero as $\delta_n \to 0$, while the effective mass becomes divergent, $m^* \to \infty$ as $\delta_n \to 0$.

As in many other interesting open questions in condensed matter physics, both interactions and disorder play a role, and their relative importance is unclear. The transition from insulating to metallic temperature-dependence occurs at very low electron densities ($\approx 10^{11}$ cm^{-2} or lower), where interaction energies are much larger than kinetic energies. The resistivity is of the order of h/e^2, which implies according to the Ioffe-Regel criterion that $k_F l \sim 1$ (here k_F is the Fermi wave number and l is the mean free path). Hence, we also are in the regime where localization due to disorder is expected to be strong.

The possibility that a metallic state can exist in zero magnetic field in two dimensions was first suggested by Finkelstein [18]. He found an interaction driven enhancement of the conductivity at weak disorder, which was expected to overwhelm the localization effects of coherent backscattering (weak localization). However, the analysis revealed that the effective interaction strength diverges upon scaling, making it difficult to determine what will actually happen at long scales or low temperatures. More recent suggested explanations are based on the existence of non-Fermi liquid states [19] and melting of disordered Wigner solid (Wigner glass) [20]. Theories classical in nature are proposed as well, relying on single-particle physics with temperature-dependent scattering on charged traps [21] and temperature-dependent

screening [22, 23, 24, 25]. In a phenomenological, scaling approach [16], the metal-insulator transition is considered as a quantum critical point, and it is shown that no general scaling principles are violated because of the transition. However, none of the proposed theories explains all the important features of diluted 2D systems. The most recent experiments on Si MOSFETs [26, 27, 28] provide a clear indication that the effective mass is strongly enhanced close to the MIT, while the effective Landé g factor remains nearly constant (Fig. 2.5). These conclusions, obtained within the Fermi-liquid framework, may give important guidance for theoretical work.

In the following two chapters, we will consider a metallic system with nonmagnetic impurities. We will concentrate on the question how the interaction effects modify the scattering rate and conductivity. We will emphasize the difference between the well understood weak coupling limit, and the case of a strong interaction and proximity to the Mott metal-insulator transition. We will discuss the limitations of our results and their possible relevance to experiments.

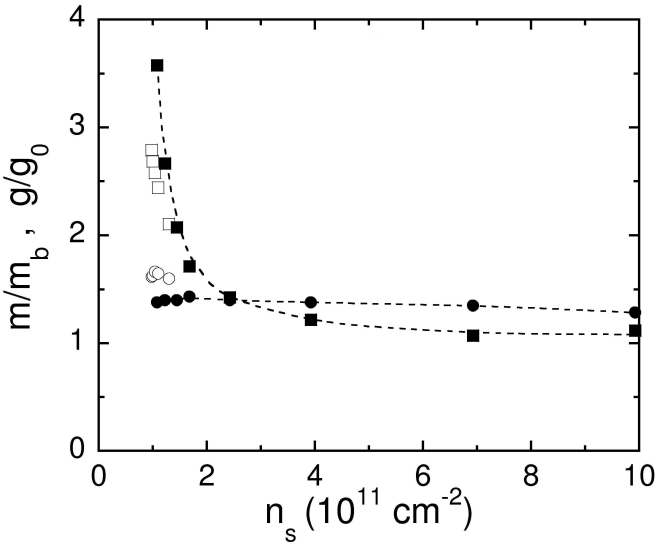

Figure 2.5. Renormalization of the effective mass (filled squares) and g factor (dots) as a function of electron density. The dashed lines are guides to the eye. From [26].

CHAPTER 3

DISORDER SCREENING WITHIN THE RANDOM PHASE APPROXIMATION

There are several attempts of describing the metallic side of the MIT in diluted 2D systems using the Drude-Boltzmann theory [22, 23, 24, 25]. In these papers, the resistivity is dominated by randomly distributed charged impurities. In a spirit of the Boltzmann approach, a weak disorder is assumed, and the conductivity is given by $\sigma = ne^2\langle\tau\rangle/m$, where m is the carrier effective mass, and $\langle\tau\rangle$ is the energy averaged relaxation time. Temperature and magnetic field dependent screening is proposed as the main mechanism leading to strong temperature and magnetic field dependence of the resistivity, $\rho = \sigma^{-1}$, on the metallic side of the transition. While giving a good qualitative picture, these theories still cannot explain the enormous changes in the resistivity for densities very close to n_c. In addition, they are limited to weak disorder and cannot address questions of the MIT. However, the simplicity and robustness of the given arguments, suggest that they should be incorporated in a more comprehensive theory.

In this chapter, we consider a model with short-ranged (Hubbard) interactions within the random phase approximation (RPA). We will show that the results within the local approximation associated with the dynamical mean field theory, where quantities like the self-energy and charge compressibility are momentum-independent, are in a semi-quantitative agreement with the standard RPA solution. We will, however, emphasize and discuss the limitations of the RPA approach in the case of strong electron-electron interactions.

3.1 Disorder screening in the Hubbard model

We consider, following Ref. [24], the disordered Hubbard model for spin 1/2 electrons on a quadratic 2D lattice[1]

$$H = -t \sum_{\langle i,j \rangle \sigma} c^{\dagger}_{i\sigma} c_{j\sigma} + \sum_{i,\sigma} (\varepsilon_i + \sigma H - \mu_0) n_{i\sigma} + \frac{U}{2} \sum_{i,\sigma,\sigma'} n_{i\sigma} n_{i\sigma'}. \tag{3.1}$$

Here, $c_{i\sigma}$ and $c^{\dagger}_{i\sigma}$ are fermionic creation and annihilation operators, $n_{i\sigma} = c^{\dagger}_{i\sigma} c_{i\sigma}$ is the number operator, $\sigma = \uparrow, \downarrow$ labels the projection of spin along the direction of the magnetic field, and μ_0 is the (bare) chemical potential. The magnetic field parallel to the 2D plane is coupled only with the electron spin, and the values of the Bohr magneton and the Lande factor are set to unity. $U > 0$ represents the Hubbard on-site repulsion, and ε_i is a Gaussian random potential with $\overline{\varepsilon_i \varepsilon_j} = W \delta_{i,j}$, where the overbar denotes an average over randomness. (With a redefinition of the chemical potential, the interaction term can be written in a more familiar form $U \sum_i n_{i\uparrow} n_{i\downarrow}$.)

In the Hartree-Fock (or RPA) approach of Ref. [24], one searches for the optimal single-particle approximation to the above Hubbard Hamiltonian

$$H_{HF} = -t \sum_{\langle i,j \rangle \sigma} c^{\dagger}_{i\sigma} c_{j\sigma} + \sum_{i,\sigma} (\tilde{\varepsilon}_i + \sigma H - \mu) n_{i\sigma}, \tag{3.2}$$

where the screened random potential is self-consistently determined as

$$\tilde{v}_{i\sigma} = \varepsilon_i + U \langle n_{i,-\sigma} \rangle - U \overline{\langle n_{i,-\sigma} \rangle}, \tag{3.3}$$

and the thermal average in the last equation is taken over the states of H_{HF}. The chemical potential μ is chosen so that $\overline{\tilde{\varepsilon}_i} = 0$.

[1] In the very dilute regime, 2D electrons form the Wigner crystal [11, 14]. In that case, they can be treated within the tight-binding model, as localized on orbitals belonging to the sites of a (triangular) lattice. An overlap of the adjacent orbitals leads to a formation of the energy band. The electron-electron interaction suppresses the double occupancy of the lattice site. In the case of half-filling, the only possible states where the electrons can hop are the interstitial sites, which form the higher energy band. This naturally introduces a two-band model for a description of this system. The orbitals belonging to the higher energy band, and describing interstitial electrons, are spatially localized between the sites of the original Wigner lattice. When the interaction is strong enough, an energy gap opens between these two bands, which leads to insulating behavior. It is plausible that the low density electron liquid, which is close to the Wigner crystallization, can be treated within this discrete lattice model, similar to how the ^{3}He liquid has been traditionally treated using a lattice Hubbard model [29, 30].

For weak disorder

$$\langle n_{i,-\sigma}\rangle \approx \sum_{j,\sigma'} \chi_{-\sigma\sigma'}(\vec{x}_i - \vec{x}_j)\ \tilde{\varepsilon}_{j\sigma'} + \overline{\langle n_{i,-\sigma}\rangle}, \tag{3.4}$$

where

$$\chi_{-\sigma\sigma'}(\vec{x}_i - \vec{x}_j) \equiv \left.\frac{\partial\langle n_{i,-\sigma}\rangle}{\partial\tilde{\varepsilon}_{j\sigma'}}\right|_{\tilde{\varepsilon}_{j\sigma'}=0} \tag{3.5}$$

is the compressibility of 2D electron gas in the Hartree-Fock approximation. In zero magnetic field, the Fourier components of the screened and the bare random potential are then readily found to be linearly related

$$\tilde{\varepsilon}_\sigma(\vec{q}) = \frac{\varepsilon(\vec{q})}{1 - U\chi(q)}, \tag{3.6}$$

where the compressibility (static polarization function) is given by the standard RPA expression

$$\chi(q) = T\sum_{\omega_n}\int \frac{d^2\vec{p}}{(2\pi)^2}\frac{1}{(i\omega_n - \xi(\vec{p}))(i\omega_n - \xi(\vec{p}+\vec{q}))}, \tag{3.7}$$

and $\xi(\vec{q}) = E(\vec{q}) - \mu$. Eqs. (3.6) and (3.7) describe screening of the weak random potential by the electron liquid. The screened random potential then satisfies

$$\overline{\tilde{\varepsilon}(\vec{q})\tilde{\varepsilon}(\vec{p})} = \widetilde{W}(q)\delta(\vec{q}+\vec{p}), \tag{3.8}$$

with

$$\widetilde{W}(q) = \frac{W}{(1 - U\chi(q))^2}. \tag{3.9}$$

Now it becomes straightforward to calculate the Boltzmann dc conductivity of the Hartree-Fock quasiparticles , which is given by [31]

$$\sigma_B = -\frac{e^2}{m}\mathcal{N}\sum_\sigma \int dE\, E\,\tau(E)\frac{\partial f(E)}{\partial E}, \tag{3.10}$$

where $f(E)$ is the Fermi distribution function and the inverse relaxation time of the quasiparticles with energy E is

$$\tau^{-1}(E) = \mathcal{N}\int_0^{2\pi} d\theta\,(1-\cos\theta)\widetilde{W}(2\sqrt{2mE}\sin\frac{\theta}{2}). \tag{3.11}$$

Here, low-filling is assumed, so that the electron dispersion relation is approximately $E(q) = k^2/2m$, with $m = 1/2t$, and the corresponding density of states per spin is

$\mathcal{N} = m/2\pi$. The expression for the Boltzmann conductivity becomes particularly simple at zero temperature and in zero magnetic field, and is given by the formula

$$\sigma_B = (1+2g)^2\sigma_0, \tag{3.12}$$

where

$$\sigma_0 = \frac{e^2 n_0}{2\pi m \mathcal{N} W} \tag{3.13}$$

is the conductivity without the screening effect, and $g = U\mathcal{N}/2$ is the dimensionless interaction. The conductivity is enhanced by the interactions since the random potential is effectively reduced by the electron liquid.

In a high magnetic field, the electron spins are polarized and there is no screening at all within the Hubbard model. Therefore, the ratio of the conductivities in zero and high magnetic field is $(1+2g)^2$. To get an order of magnitude increase in resistivity in high fields, we need an interaction parameter g of order of one. However, according to the Hartree-Fock theory, a magnetic instability in the electron gas occurs when $U\mathcal{N} = 1$ (the Stoner criterion) [32], i.e. for $g = 1/2$ in our notation. This represents an important constraint in the applicability of the HF theory which was overlooked in Ref. [24], where the value $g = 1.5$ is used for quantitative comparison with the experimental data. We note that the other theories based on the Boltzmann approach [22, 23], but starting from the more realistic long-ranged Coulomb interaction, are still unable to explain the change of the resistivity by an order of magnitude as a result of screening.

3.2 RPA in local approximation

We have explicitly seen in the previous section some of the limitations that appear in the Hartree-Fock (or equivalently RPA) approach. Our goal is to examine the disorder screening and its implications to the scattering time in the presence of a strong interaction. We will do that within dynamical mean field theory (DMFT) [5]. The DMFT is not limited to the Hartree-Fock approximation and weak disorder, but the price that we have to pay is that the quantities that enter the theory have local character. As a preliminary step, we will first calculate the renormalized (screened) disorder $\tilde{\varepsilon}_i$ within the Hartree-Fock theory, but in the approximation where the non-local components of the compressibility are set to zero.

In the local approximation

$$\chi(\vec{x}_i - \vec{x}_j) = \left.\frac{\partial\langle n_i\rangle}{\partial\tilde{\varepsilon}_i}\right|_{\tilde{\varepsilon}_i=0} \delta_{ij} \equiv \chi_{loc}\,\delta_{ij}, \tag{3.14}$$

giving the screened random potential

$$\tilde{\varepsilon}_i = \frac{\varepsilon_i}{1 - U\chi_{loc}}. \tag{3.15}$$

Since $\langle n_i\rangle = \int_{-\infty}^{\infty} d\omega\, f(\omega)D(\omega)$, where the local density of states $D(\omega) = -1/\pi \mathrm{Im} G_{ii}(\omega + i\eta)$, and G_{ii} is the on-site Green's function, the local compressibility, $\chi_{loc} = \partial\langle n_i\rangle/\partial\tilde{\varepsilon}_i|_{\tilde{\varepsilon}_i=0}$, is given by

$$\chi_{loc} = \frac{1}{\pi}\mathrm{Im}\int_{-\infty}^{\infty} d\omega\, f(\omega)\left[G^0_{ii}(\omega + i\eta)\right]^2. \tag{3.16}$$

Here, G^0_{ii} is the noninteracting local (on-site) Green function

$$G^0_{ii}(\omega + i\eta) = \sum_{\vec{q}} \frac{1}{\omega + \mu - E(\vec{q}) + i\eta}. \tag{3.17}$$

In the effective mass approximation, a straightforward calculation gives

$$\chi_{loc} = -\mathcal{N}\left(2\ln\frac{\Omega}{\Omega - \mu} + 2\frac{\mu}{\Omega}\ln\frac{\Omega - \mu}{\mu}\right), \tag{3.18}$$

where Ω is the energy cut-off (upper boundary of the energy band). One can easily check that the function in the parentheses of Eq. (3.18) is of the order of one for half-filling ($\mu = \Omega/2$), and much less than one for low and high filling. Since the standard RPA result gives $\chi(q) = -\mathcal{N}$ for $q < 2k_F$ [3], we conclude that taking the local value of compressibility is a reasonable approximation when we are not too far from half-filling.

In contrast to the Boltzmann theory, in the DMFT approach the conductivity is given by [5]

$$\sigma(\omega) = \frac{2\pi e^2}{dV}\sum_{\boldsymbol{k}} v^2_{\boldsymbol{k}} \int d\omega'\, \bar{\rho}(\boldsymbol{k},\omega')\bar{\rho}(\boldsymbol{k},\omega'+\omega)\,\frac{f(\omega') - f(\omega'+\omega)}{\omega}, \tag{3.19}$$

where

$$\bar{\rho}(\boldsymbol{k},\omega) = -\frac{1}{\pi}\,\mathrm{Im}\,\frac{1}{\omega + i\eta + \mu - \epsilon_{\boldsymbol{k}} - \boldsymbol{\Sigma}(\omega + i\eta)} \tag{3.20}$$

is the spectral function, and $\boldsymbol{\Sigma}$ is the local (momentum-independent) self-energy. It is instructive to show that in absence of the interaction for weak disorder at zero temperature both the Boltzmann theory and DMFT give the same result.

Within DMFT, the disorder averaged Green function

$$G(i\omega_n) = \int d\varepsilon_i P(\varepsilon_i) G_i(i\omega_n) \tag{3.21}$$

can be expressed through the momentum-independent self-energy Σ and "Weiss" field (cavity field, hybridization function) Δ

$$G(i\omega_n) = G_0\left(i\omega_n - \Sigma(i\omega_n)\right) = \frac{1}{i\omega_n + \mu - \Sigma(i\omega_n) - \Delta(i\omega_n)}. \tag{3.22}$$

Here, G_0 is the local Green function for the clean lattice (in the absence of disorder),

$$G_0(i\omega_n) = \frac{1}{i\omega_n + \mu - \Delta(i\omega_n)}. \tag{3.23}$$

Its form is determined by the cavity field Δ, which depends only on the form of the lattice and hopping amplitudes.

For a weak disorder, from Eq. (3.21), we find

$$\begin{aligned} G(i\omega_n) &= \int d\varepsilon_i P(\varepsilon_i) G_i(i\omega_n) = \int d\varepsilon_i P(\varepsilon_i) \frac{1}{i\omega_n + \mu - \varepsilon_i - \Delta(i\omega_n)} \\ &\approx \frac{1}{i\omega_n + \mu - \Delta(i\omega_n)} \int d\varepsilon_i P(\varepsilon_i) \left[1 + \frac{\varepsilon_i}{i\omega_n + \mu - \varepsilon_i - \Delta(i\omega_n)}\right. \\ &+ \left. \frac{\varepsilon_i^2}{\left(i\omega_n + \mu - \varepsilon_i - \Delta(i\omega_n)\right)^2}\right] \\ &= \frac{1}{i\omega_n + \mu - \Delta(i\omega_n)} \left[1 + \frac{W}{\left(i\omega_n + \mu - \varepsilon_i - \Delta(i\omega_n)\right)^2}\right] \\ &= G_0(i\omega_n)\left[1 + W G_0^2(i\omega_n)\right]. \end{aligned} \tag{3.24}$$

Similarly, from Eq. (3.23), for weak disorder

$$G(i\omega_n) = G_0(i\omega_n)\left[1 + G_0(i\omega_n)\Sigma(i\omega_n)\right]. \tag{3.25}$$

Comparing the last two equations, we find that the self-energy is equal to

$$\Sigma(i\omega_n) = W G_0(i\omega_n). \tag{3.26}$$

The spectral function, Eq. (3.20), is equal to

$$\bar{\rho}(\boldsymbol{k}, \omega) = -\frac{1}{\pi} \frac{\Sigma''(\omega)}{(\omega + \mu - \varepsilon_k - \Sigma'(\omega))^2 + \Sigma''(\omega)}, \tag{3.27}$$

where $\Sigma'(\omega) = \mathrm{Re}(\Sigma(\omega + i\eta))$ and $\Sigma''(\omega) = \mathrm{Im}(\Sigma(\omega + i\eta))$. In the weak disorder limit the spectral function assumes its clean case form, $\bar{\rho}(\mathrm{k}, \omega) \to \delta(\omega + \mu - \varepsilon_k)$. From the identity

$$\int_{-\infty}^{\infty} \frac{d\omega}{2\pi} \left(\frac{2a}{\omega^2 + a^2} \right)^2 = \frac{1}{a}, \tag{3.28}$$

we find that in Eq. (3.19) we should replace

$$(\bar{\rho}(\boldsymbol{k}, \omega))^2 \to \frac{1}{-2\pi\Sigma''(\omega)} \delta(\omega + \mu - \varepsilon_k). \tag{3.29}$$

Therefore, for weak disorder and at zero temperature, dc conductivity is equal to

$$\sigma = \frac{2\pi e^2}{dV} \sum_{\boldsymbol{k}} v_{\boldsymbol{k}}^2 \int d\omega' \, \frac{\delta(\omega' + \mu - \varepsilon_k)}{-2\pi\Sigma''(\omega')} \delta(\omega') = -\frac{e^2}{dV} \sum_{\mathrm{k}} v_{\boldsymbol{k}}^2 \frac{\delta(\mu - \varepsilon_k)}{\Sigma''(0)}. \tag{3.30}$$

For two-dimensional ($d = 2$) system in the effective mass approximation ($\varepsilon_k = k^2/2m$), we find

$$\sigma = \frac{e^2 n}{2\pi m \mathcal{N} W}, \tag{3.31}$$

in agreement with Eq. (3.13). In the presence of an electron-electron interaction, the disorder strength W should be replaced by its renormalized value $\widetilde{W} = \sqrt{\overline{\tilde{\varepsilon}_i^2}}$, where $\tilde{\varepsilon}_i$ is given by Eq. (3.20).

To summarize, the conclusions that we have reached are the following: (a) In the presence of weak disorder at zero temperature, the conductivity obtained using the Boltzmann approach is the same as the one obtained within the DMFT. (b) The replacement of the renormalized disorder by its value obtained within the local approximation is justified in the case of an approximately half-filled conduction band.

The reason for doing this simple exercise was to get some feeling about the validity of the local approximation associated with DMFT approach that we are going to use in the next Chapter. Interestingly, the validity of the local approximation for the self-energy has been studied recently in somewhat different context in Refs. [33, 34]. In this work, the behavior of interacting fermions is analyzed near a ferromagnetic Stoner instability. It is shown that as the system approaches a ferromagnetic quantum critical point the fermionic self-energy crosses over from predominantly momentum dependent away from the transition to predominantly frequency dependent in the immediate vicinity of the transition.

3.3 Impossibility of the mass divergence within RPA

Several recent experiments on high mobility MOSFETs [26, 27, 28] indicate very strong mass enhancement in the vicinity of the MIT, and its possible divergence at the critical concentration n_c. The microscopical origin of this mass enhancement is one of the main open problems in the field, and it is discussed by several research groups. In our work presented in the next chapter, we advocate that the strong mass divergence comes from the strong interaction effects in the vicinity of the Mott (or Mott-Anderson) MIT. In this section, we critically review a recent work [35] which uses "on-shell" RPA approximation. We argue, following Ref. [36], that the RPA theory, which is well known to successfully describe weak coupling effects, cannot describe a divergence of the effective mass. A similar conclusion is reached also in Ref. [37].

Let us first recall several definitions. The quasiparticle energy, can be calculated by solving self-consistently the Dyson equation

$$E(\mathbf{k}) = \frac{k^2}{2m} + \Sigma'(\mathbf{k}, E(\mathbf{k}) - \mu), \tag{3.32}$$

where $k^2/2m$ is the single particle energy of the noninteracting electrons, μ is the chemical potential of the interacting system, and Σ' is the real part of the self-energy. The quasiparticle group velocity is defined by $\mathbf{v_k} = \nabla_{\mathbf{k}} E(\mathbf{k})$, and the relation $v_{\mathbf{k}} = k/m^*$ defines the effective mass. Therefore,

$$\frac{1}{m^*} = \frac{1}{k_F} \left. \frac{dE(\mathbf{k})}{dk} \right|_{k=k_F}. \tag{3.33}$$

Combining Eqs. (3.32) and (3.33), we find

$$\frac{m^*}{m} = \left. \frac{Z^{-1}}{1 + \frac{m}{k}\frac{\partial}{\partial k}\Sigma'(\mathbf{k}, \omega)} \right|_{k=k_F, \omega=0}, \tag{3.34}$$

where

$$Z = \frac{1}{1 - \frac{\partial}{\partial \omega}\Sigma'(\mathbf{k}, \omega)\big|_{k=k_F, \omega=0}} \tag{3.35}$$

is the renormalization constant that measures the discontinuity of the momentum distribution at $k = k_F$. From general Fermi liquid arguments $0 < Z \leq 1$, which implies $\frac{\partial}{\partial \omega}\Sigma'(\mathbf{k}, \omega)\big|_{k=k_F, \omega=0} \leq 0$. We see that the divergence of the effective mass is driven

either by an infinite $\frac{\partial}{\partial\omega}\Sigma'(\mathbf{k},\omega)\big|_{k=k_F,\omega=0}$ (which is equivalent to $Z^{-1} \to \infty$), or by $\frac{\partial}{\partial k}\Sigma'(\mathbf{k},\omega)\big|_{k=k_F,\omega=0} = -k_F/m$.

In the so called "on-shell" approximation of Ref. [35], the quasiparticle energy is given by

$$E(\mathbf{k}) = \frac{k^2}{2m} + \Sigma'(\mathbf{k},\xi_{\mathbf{k}}), \tag{3.36}$$

where Σ' is calculated at the energy $\xi_{\mathbf{k}} = k^2/2m - \mu$ which corresponds to the single-particle energy of the noninteracting electrons. In this approximation the effective mass m^* is given by

$$\frac{m^*}{m} = \frac{1}{1 + \frac{m}{k}\frac{\partial}{\partial k}\Sigma'(\mathbf{k},\omega)\big|_{k=k_F,\omega=0}}. \tag{3.37}$$

In the weak coupling limit Eqs. (3.34) and (3.37) give the same result, but in the presence of strong interaction their predictions are qualitatively different. A simple way to see the nonphysical predictions of the on-shell approximation is to consider the case when the self energy is momentum-independent $\Sigma(\mathbf{k},\omega) = \Sigma(\omega)$. Then the effective mass is given by

$$\frac{m^*}{m} = 1 - \frac{\partial}{\partial\omega}\Sigma'(\omega)\bigg|_{\omega=0}. \tag{3.38}$$

Note that, since generally $\frac{\partial}{\partial\omega}\Sigma'(\omega)\big|_{\omega=0} < 0$, the interactions increase the effective mass. The actual divergence is obtained only if the quantity $A \equiv -\frac{\partial}{\partial\omega}\Sigma'(\omega)\big|_{\omega=0}$ itself diverges. This scenario is realized, for example in Brinkman-Rice theory of the Mott transition, as well as in the more recent DMFT solution. Within the same scenario, the quasiparticle weight is simply $Z^{-1} = m^*/m$, so it must diverge at the same place as m^* does.

We contrast this with the application of the on-shell method to our case. We get $\Sigma'(\mathbf{k},\omega = \xi_{\mathbf{k}}) \approx \Sigma'(\omega = \xi_{\mathbf{k}})$. Since

$$\frac{m}{k}\frac{d}{dk}\Sigma'(\omega = \xi_{\mathbf{k}})\bigg|_{k=k_F} = \frac{\partial}{\partial\omega}\Sigma'(\omega)\bigg|_{\omega=0}, \tag{3.39}$$

we get

$$\frac{m^*}{m} \approx \frac{1}{1 + \frac{\partial}{\partial\omega}\Sigma'(\omega)}\bigg|_{\omega=0}. \tag{3.40}$$

In terms of the quasiparticle enhancement factor $A \equiv -\frac{\partial}{\partial\omega}\Sigma'(\omega)\big|_{\omega=0}$, we can write the "on-shell" expression as

$$\frac{m^*}{m} \approx \frac{1}{1 - A}. \tag{3.41}$$

As we can see, this expression is equivalent to the exact expression $m^*/m = 1 + A$, only through leading order, i.e. for infinitesimal A. On the other hand, the positive quantity A is expected to grow with the interaction. As long as it is finite, neither will the properly defined effective mass m^*/m, nor will the inverse quasiparticle wight Z^{-1} ever diverge. In contrast, if one uses the on-shell approximation, than the effective mass will blow up as soon as $A = 1$, and this will happen at some point in any approximation where A grows with the interaction. However, as we can see, this will not lead to the divergence of the inverse quasiparticle weight Z^{-1}. We can see from these expressions that the essence of the on-shell approximation is simply to linearize the expression for $(m^*/m)^{-1}$, by expanding it in the quantity $A = -\frac{\partial}{\partial\omega}\Sigma'(\omega)\big|_{\omega=0}$. Instead of appearing in the numerator of the effective mass expression, it now enters the denominator, and since it has the opposite sign prefactor, it can lead to a spurious effective mass divergence.

CHAPTER 4

DISORDER SCREENING IN THE REGIME OF STRONG CORRELATIONS

This is the central chapter of the first part of the thesis, where we examine how the scattering time changes in the presence of strong electron-electron interactions. We solve this generally very difficult problem for a specific case of on-site Hubbard interactions for half-filled lattice in the limit of large coordination number. We find that the scattering time strongly enhances as we approach the Mott metal-insulator transition. This is a rather counter-intuitive result since we may naively expect that the interactions, which lead to the divergence of the effective mass at the MIT, would tend to localize the quasiparticles and decrease the scattering time. We make a connection of our results with the Kondo pinning which leads to the perfect transmittance through quantum dots, a phenomenon which is very well studied theoretically and also experimentally verified. We discuss the relevance of our results for real physical systems, and make a list of further theoretical questions which remain as a challenge for future work.

4.1 Slave boson approach

In the Kotliar-Ruckenstein (KR) slave boson approach [38] the original Hamiltonian is rewritten in terms of the original fermions and a set of four bosonic operators which keep track of the occupation numbers of the lattice sites. The main formal advantage of this approach is that we are now in a position to write the Hubbard interaction as a bosonic occupation number operator. The operator for the kinetic energy on the other hand becomes much more complicated since the motion of a physical electron changes the numbers of the slave bosons on both lattice sites involved.

Kotliar and Ruckenstein enlarged the Hilbert space of the Hubbard model by introducing four bosonic operators at each site, d_i ($d_i^\dagger$), $p_{i\sigma}$ ($p_{i\sigma}^\dagger$), and e_i ($e_i^\dagger$), corresponding respectively to doubly, singly occupied, and empty state. The physical Hilbert space is recovered if we impose the following local constraints, which have to be fulfilled exactly

$$\begin{aligned} &\sum_\sigma p_{i\sigma}^\dagger p_{i\sigma} + e_i^\dagger e_i + d_i^\dagger d_i = 1, \\ &f_{i\sigma}^\dagger f_{i\sigma} = p_{i\sigma}^\dagger p_{i\sigma} + d_i^\dagger d_i, \qquad \sigma = \uparrow\downarrow . \end{aligned} \tag{4.1}$$

First of these constraints states that only one of the four physical possibilities on a lattice site is allowed, either a double occupancy, a single occupancy, or a hole. The second one expresses the fact that the presence of a physical electron implies either a double, or a single occupancy. In a physical subspace defined by Eqs. (4.1), the Hubbard Hamiltonian obtains the form

$$H = -\sum_{ij,\sigma} t_{ij} f_{i\sigma}^\dagger f_{j\sigma} z_{i\sigma}^\dagger z_{j\sigma} + U \sum_i d_i^\dagger d_i, \tag{4.2}$$

where

$$z_{i\sigma} = e_i^\dagger p_{i\sigma} + p_{i-\sigma}^\dagger d_i. \tag{4.3}$$

In the KR mean-field approximation, equivalent to the saddle-point approximation in the functional integrals formalism, the Bose operators are taken to be independent of space and time, and the constraints (4.1) become satisfied only on average. The slave boson approach is exact while we satisfy the exact constraints, but in order to get sensible results in the mean-field approximation, we have to make use of the fact that the described procedure is not unique. Kotliar and Ruckenstein pointed out that by replacing $z_{i\sigma}$ by another operator $\tilde{z}_{i\sigma}$, given by

$$\tilde{z}_{i\sigma} = (1 - d_i^\dagger d_i - p_{i\sigma}^\dagger p_{i\sigma})^{-1/2} z_{i\sigma} (1 - e_i^\dagger e_i - p_{i-\sigma}^\dagger p_{i-\sigma})^{-1/2}, \tag{4.4}$$

we still obtain the exact Hamiltonian in the physical subspace, but get at the same time a correct mean-field behavior in the limit $U = 0$. It is important to emphasize that as compared to the Hartree-Fock, the Kotliar-Ruckenstein theory introduces not only effective fields, but also renormalizes the hopping which describes the mass renormalization. Therefore, the KR

theory can describe the Mott metal-insulator transition. At $T = 0$ this theory is equivalent to the Gutzwiller variational approach [39].

4.1.1 Clean lattice

To include in the convenient way the effects of disorder, we have applied the KR theory to the Hubbard model with large coordination number - the $D = \infty$ limit where dynamical mean field theory (DMFT) becomes exact. We first consider the clean limit. In the $D = \infty$ Bethe lattice,[1] solving the Hubbard model reduces to solving an Anderson impurity model defined by the action [5]

$$S_{eff} = -\sum_{\omega_n,\sigma} c_\sigma^\dagger(i\omega_n)\left[i\omega_n + \mu - t^2 G(i\omega_n)\right] c_\sigma(i\omega_n) + U\int_0^\beta d\tau\, n_\uparrow(\tau) n_\downarrow(\tau), \tag{4.5}$$

and supplemented by the self-consistency condition

$$G(i\omega_n) = \langle c^\dagger(\omega_n) c(\omega_n)\rangle_{S_{eff}}. \tag{4.6}$$

In the slave boson method $c_\sigma^\dagger$ is replaced by $\tilde{z}_\sigma f_\sigma^\dagger$, where $\tilde{z}_\sigma$ is a bosonic operator given by Eq. (4.4). In the mean field approximation $\tilde{z}$ is replaced by a number $\tilde{z}^\dagger\tilde{z} \to q$. The constraints, Eq. (4.1), are enforced by the Lagrange multipliers, and in the mean field approximation the free energy is given by

$$F = -2\frac{1}{\beta}\sum_{\omega_n} \ln\left[-i\omega_n - \mu + \lambda_0 + qt^2 G(i\omega_n)\right] + Ud^2 - \lambda_0(1 - e^2 + d^2). \tag{4.7}$$

For μ fixed, we have 3 variational parameters λ_0, e, and d. The self-consistency equation (4.6) becomes

$$G(i\omega_n) = q\langle f^\dagger(\omega_n) f(\omega_n)\rangle_{S_{eff}}, \tag{4.8}$$

with

$$G(i\omega_n) = \frac{q}{i\omega_n + \mu - \lambda_0 - qt^2 G(i\omega_n)}. \tag{4.9}$$

If we define the quantity $G_f(\omega_n) = G(i\omega_n)/q$, we get

[1] Bethe lattice (infinite Cayley tree) is a lattice which has a tree-like structure. It has a semicircular (more precisely, semi-elliptic) density of states. While qualitatively the results in the DMFT do not depend on the form of a lattice, often equations simplify for the Bethe lattice, where the "hybridization" function Δ is related to the local Green function simply as $\Delta(i\omega_n) = t^2 G(i\omega_n)$.

$$G_f(i\omega_n) = \frac{1}{i\omega_n + \mu - \lambda_0 - q^2 t^2 G_f(i\omega_n)}. \tag{4.10}$$

$G_f(i\omega_n)$ is identical to the Green's function of noninteracting electrons, with a chemical potential $\tilde{\mu} = \mu - \lambda_0$ and hopping $\tilde{t} = qt$. Note that $G_f(i\omega_n)$ obeys a spectral sum rule (density of states is normalized to one) as opposed to $G(i\omega_n)$, which describes just the quasiparticle part of the physical electron.

For the half filling $\mu = U/2$, $e = d$ and $\lambda_0 = \mu$. Minimizing the free energy with respect to d, we obtain

$$d^2 = \frac{1}{4}\left(1 - \frac{U}{U_c}\right), \tag{4.11}$$

with $U_c = 16\int_0^\infty d\varepsilon\, \varepsilon\rho(\varepsilon)$. This is the critical value of the interaction parameter, which corresponds to the vanishing of the number of doubly occupied states and indicates that the system is undergoing the Mott transition at finite critical value of U.

4.1.2 Disordered lattice

We now concentrate on a disordered Hubbard model described by the Hamiltonian

$$H = -\sum_{ij\sigma} t_{ij} c^\dagger_{i\sigma} c_{j\sigma} + \sum_{i\sigma} \varepsilon_i n_{i\sigma} + U \sum_i n_{i\uparrow} n_{i\downarrow}. \tag{4.12}$$

Here t_{ij} are the hopping matrix elements, $c_{i\sigma}$ and $c^\dagger_{i\sigma}$ are fermionic creation and annihilation operators, $n = c^\dagger_{i\sigma} c_{i\sigma}$ is the number operator, and σ labels the spin projection. U represents the Hubbard on-site repulsion, and the disorder is introduced by random site energies ε_i specified by a distribution function $P(\varepsilon_i)$.

Similarly as in the clean case, the mean-field slave boson equations are obtained by minimizing the local free energy, which now becomes site-dependent

$$F_i = -\frac{2}{\beta}\sum_{\omega_n} \ln\left[-i\omega_n - \mu + \lambda_i + \varepsilon_i + q_i\Delta(\omega_n)\right] + U d_i^2 - \lambda_i\left[1 - e_i^2 + d_i^2\right]. \tag{4.13}$$

We define the renormalized disorder energy as

$$\tilde{\varepsilon}_i = \varepsilon + \lambda_i - \mu. \tag{4.14}$$

Then the free energy assumes the form

$$F_i = -\frac{2}{\beta}\sum_{\omega_n} \ln\left[-i\omega_n + \tilde{\varepsilon}_i + q_i\Delta(\omega_n)\right] + U d_i^2 - \lambda_i\left[1 - e_i^2 + d_i^2\right]. \tag{4.15}$$

Minimizing the local free energy with respect to e_i, d_i and λ_i, we find

$$-\frac{\partial q_i}{\partial e_i}\frac{1}{\beta}\sum_{\omega_n}\Delta(i\omega_n)G_{fi}(i\omega_n) = (\mu + \tilde{\varepsilon}_i - \varepsilon_i)\, e_i, \tag{4.16}$$

$$-\frac{\partial q_i}{\partial d_i}\frac{1}{\beta}\sum_{\omega_n}\Delta(i\omega_n)G_{fi}(i\omega_n) = (U - \mu - \tilde{\varepsilon}_i + \varepsilon_i)\, d_i, \tag{4.17}$$

and

$$\frac{1}{\beta}\sum_{\omega_n} G_{fi}(i\omega_n) = \frac{1}{2}\left(1 - e_i^2 + d_i^2\right), \tag{4.18}$$

where G_{fi} is the quasiparticle Green function given by

$$G_{fi}(i\omega_n) = \frac{1}{i\omega_n - \tilde{\varepsilon}_i - q_i\Delta(i\omega_n)}, \tag{4.19}$$

and

$$q_i = 2\left[1 - (e_i^2 - d_i^2)^2\right]^{-1}(e_i + d_i)^2\left[1 - (e_i^2 + d_i^2)\right]. \tag{4.20}$$

The system of equations (4.16)-(4.20) has to be supplemented by the self-consistency condition, which determines the "hybridization function" Δ describing the environment of a given site. Δ is determined by the self-energy Σ and the hybridization function Δ_o corresponding to the clean lattice of noninteracting electrons,

$$\Delta(i\omega_n) = \Delta_o\left(i\omega_n - \Sigma(i\omega_n)\right). \tag{4.21}$$

The self-energy and the hybridization function are related to the disorder-averaged Green's function

$$G(i\omega_n) = \int d\varepsilon\, P(\varepsilon)G(\varepsilon, i\omega_n), \tag{4.22}$$

by

$$\Sigma(i\omega_n) = i\omega_n + \mu - \Delta(i\omega_n) - \left[G(i\omega_n)\right]^{-1}. \tag{4.23}$$

We emphasize that

$$G(\varepsilon, i\omega_n) = \frac{q_i}{i\omega_n - \tilde{\varepsilon}_i - q_i\Delta(\omega_n)} \equiv q_i G_{fi} \tag{4.24}$$

describes the low-energy (quasiparticle) part of the physical electron. The spectrum (density of states) of this function is not normalized to one, as opposed to G_{fi}, which describes the noninteracting quasiparticles with renormalized hopping. Also, we note that

$\Delta_o(i\omega_n) = i\omega_n + \mu - [G_o(i\omega_n)]^{-1}$, where G_o is the lattice Green's function corresponding to the clean lattice and $U = 0$. Half-filling can be enforced by the requirement $\overline{e_i^2} = \overline{d_i^2}$, or equivalently

$$\int d\varepsilon P(\varepsilon) \frac{1}{\beta} \sum_{\omega_n} G_f(\varepsilon, i\omega_n) = \frac{1}{2}. \tag{4.25}$$

In the following, we will solve the system of equations (4.16)-(4.25) at zero temperature analytically in several important limits, as well as fully numerically for arbitrary values of parameters [40]. We will distinguish the particle-hole symmetric and asymmetric cases, and concentrate particularly on the solution in a vicinity of the Mott metal-insulator transition.

4.2 Particle-hole symmetric lattice

For the particle-hole symmetric lattice, half-filling condition, Eq. (4.23), is automatically satisfied if we set the chemical potential to $\mu = U/2$. We will first solve analytically the slave boson equations in the vicinity of the Mott MIT and derive a remarkable result showing that the system becomes perfectly conducting on the metallic side of the Mott transition. Then we will solve the equations numerically for the full range of parameters and obtain the phase diagram for a disordered Hubbard model.

4.2.1 Weak disorder

The system of equations further simplifies if we concentrate on the Bethe lattice. In this case the hybridization function is very simply related to the Green function,

$$\Delta(i\omega_n) = t^2 G(i\omega_n), \tag{4.26}$$

which significantly simplifies the self-consistency condition. We will find a solution for weak disorder in the vicinity of the MIT, where the slave boson parameters are small.

For clarity, we will rewrite the the system of equations (4.16)-(4.23), which now assume the form

$$-\frac{\partial q}{\partial e} t^2 \frac{1}{\beta} \sum_{\omega_n} \frac{G(i\omega_n)}{i\omega_n - \tilde{\varepsilon}(\varepsilon) - q(\varepsilon) t^2 G(i\omega_n)} = \left(\frac{U}{2} + \tilde{\varepsilon}(\varepsilon) - \varepsilon \right) e(\varepsilon), \tag{4.27}$$

$$-\frac{\partial q}{\partial d} t^2 \frac{1}{\beta} \sum_{\omega_n} \frac{G(i\omega_n)}{i\omega_n - \tilde{\varepsilon}(\varepsilon) - q(\varepsilon) t^2 G(i\omega_n)} = \left(\frac{U}{2} - \tilde{\varepsilon}(\varepsilon) + \varepsilon \right) d(\varepsilon), \tag{4.28}$$

$$\frac{1}{\beta}\sum_{\omega_n}\frac{1}{i\omega_n-\tilde{\varepsilon}(\varepsilon)-q(\varepsilon)t^2G(i\omega_n)}=\frac{1}{2}\left(1-e^2(\varepsilon)+d^2(\varepsilon)\right), \tag{4.29}$$

and

$$G(i\omega_n)=\int d\varepsilon\, P(\varepsilon)\frac{q(\varepsilon)}{i\omega_n-\tilde{\varepsilon}(\varepsilon)-q(\varepsilon)t^2G(i\omega_n)}, \tag{4.30}$$

with

$$q=2\left[1-(e^2-d^2)^2\right]^{-1}(e+d)^2\left[1-(e^2+d^2)\right]. \tag{4.31}$$

The renormalized disorder is defined as $\tilde{\varepsilon}(\varepsilon)=\varepsilon+\lambda(\varepsilon)-\mu$, and $\mu=U/2$.

We assume the solution in the form

$$e(\varepsilon)=e_0\left(1+\frac{2\varepsilon}{U}+A\varepsilon^2+\mathcal{O}(\varepsilon^3)\right), \tag{4.32}$$

$$d(\varepsilon)=e_0\left(1-\frac{2\varepsilon}{U}+B\varepsilon^2+\mathcal{O}(\varepsilon^3)\right), \tag{4.33}$$

where the constants A and B are to be determined. (The coefficient $2/U$ is obtained by solving the system (4.27)-(4.30) to the first order in ε.) Then,

$$q(\varepsilon)\approx(e+d)^2\approx q_0(1+C\varepsilon^2), \tag{4.34}$$

where $q_0\equiv q(\varepsilon=0)=8e_0^2$ and $C=A+B$. We now make a further assumption that $\tilde{\varepsilon}\sim q_0^2$. This assumption will be justified a posteriori, from the explicit solution of the slave boson equations.

One can easily check that, under the assumption $\tilde{\varepsilon}\sim q_0^2$, the renormalized disorder $\tilde{\varepsilon}$ can be neglected in Eq. (4.30). Then the averaged Green's function of the form

$$G(i\omega_n)=q_0(1+C\overline{\varepsilon^2})G_f(i\omega_n), \tag{4.35}$$

with

$$G_f(i\omega_n)=\frac{1}{i\omega_n-q_0^2(1+C\overline{\varepsilon^2})^2t^2G_f(i\omega_n)}, \tag{4.36}$$

satisfies the self-consistency condition, Eq. (4.30). Note that the density of states still has semicircular form, but with the bandwidth which is broadened by the disorder, as respect

to the clean case. Inserting this expression into the variation equation for the parameter λ (Friedel sum rule), Eq. (4.29), we obtain

$$\frac{1}{\beta}\sum_{\omega_n} G_f(i\omega_n)\frac{1}{1-\tilde{\varepsilon}G_f(i\omega_n) - Cq_0^2t^2G_f^2(i\omega_n)\times\mathcal{O}(\varepsilon^2)} = \frac{1}{2} - \frac{1}{2}q_0\left[\frac{\varepsilon}{U} + 2(A-B)\varepsilon^2\right]. \quad (4.37)$$

Since $\frac{1}{\beta}\sum_{\omega_n} G_f(i\omega_n) = 1/2$ and $\frac{1}{\beta}\sum_{\omega_n} G_f^2(i\omega_n) = -4/(3\pi t q_0(1+C\overline{\varepsilon^2}))$, to the first order in ε, renormalized disorder is equal to

$$\tilde{\varepsilon}(\varepsilon) = \frac{3\pi t}{8}q_0^2\frac{\varepsilon}{U}, \quad (4.38)$$

Note that this justifies the assumption $\tilde{\varepsilon} \sim q_0^2$.

Now we go back to the equations for the variational parameters e and d. The renormalized disorder $\tilde{\varepsilon}$ can be neglected in these equations. Inserting the expressions for $e(\varepsilon)$, $q(\varepsilon)$ and $G(i\omega_n)$ into Eq. (4.27), and using $\frac{1}{\beta}\sum_{\omega_n} G_f^4(i\omega_n) = 8/(15\pi q_0^3(1+C\overline{\varepsilon^2})^3t^3)$, to the second order in ε we obtain

$$e_0U_c^0\left[1+\frac{2}{5}(A+B)\overline{\varepsilon^2}\right]\left[1+\frac{1}{10}(A+B)\varepsilon^2\right] = e_0U\left[1+\left(A-\frac{4}{U^2}\right)\varepsilon^2\right]. \quad (4.39)$$

Similarly, Eq. (4.28) assumes the form

$$e_0U_c^0\left[1+\frac{2}{5}(A+B)\overline{\varepsilon^2}\right]\left[1+\frac{1}{10}(A+B)\varepsilon^2\right] = e_0U\left[1+\left(B-\frac{4}{U^2}\right)\varepsilon^2\right]. \quad (4.40)$$

The above equations have to be satisfied for each ε. Therefore, $A = B$ and $(A+B)/10 = A - 4/U^2$, which gives

$$A = B = \frac{C}{2} = \frac{5}{U^2} \approx \frac{5}{(U_c^0)^2}. \quad (4.41)$$

The critical value of the interaction parameter is

$$U_c = U_c^0\left[1+\frac{2}{5}C\overline{\varepsilon^2}\right]. \quad (4.42)$$

To find q_0 as a function of U, we need to expand q to the forth order in e and d

$$q(e,d) = 2e^2 + 4ed + 2d^2 - 2e^4 - 4e^3d - 4e^2d^2 - 4ed^3 - 2d^4. \quad (4.43)$$

Then, $\partial q/\partial e|_{\varepsilon=0} = 8e_0(1-4e_0^2)$, and from Eq.(4.27) we obtain $e_0^2 = \frac{1}{4}(1-U/U_c)$, i.e.

$$q_0 = 2\left(1-\frac{U}{U_c}\right). \quad (4.44)$$

This completes the solution of the system (4.27)-(4.30) for weak disorder.

Let us summarize the results. Close to the Mott transition, to the second order in disorder, we have shown the following:

(i) The quasiparticle weight q depends on the site energy ε as $q(\varepsilon) = q_0(1 + C\varepsilon^2)$, where the constant $C = 10/(U_c^0)^2 = 0.867$, and $U_c^0 = 64t/3\pi = 3.395$ is the critical interaction parameter in the absence of disorder.[2] For a given disorder distribution $q_0 = 2(1 - U/U_c)$, where the critical interaction is given by $U_c = U_c^0(1 + \frac{2}{5}C\overline{\varepsilon^2})$.

(ii) Quasi-particle density of states remains semicircular. The averaged Green's function is given by $G(i\omega_n) = q_0(1 + C\overline{\varepsilon^2})G_f(i\omega_n)$, where G_f is determined by the equation $G_f(i\omega_n) = [i\omega_n - q_0^2(1 + C\overline{\varepsilon^2})^2 t^2 G_f(i\omega_n)]^{-1}$.

(iii) Renormalized disorder strength is equal to $\tilde{\varepsilon}(\varepsilon) = 3\pi t q_0^2 \varepsilon/8U$.

4.2.2 Scattering rate: perfect screening

In the following, we will derive the expression for the scattering rate as a function of the renormalized disorder, and show that it goes to zero as we approach the Mott transition. This leads to perfect conductivity at the metallic side of the Mott MIT.

Scattering rate. The conductivity σ is proportional to the scattering time (inverse scattering rate) τ determined by the imaginary part of the self-energy at zero frequency

$$\frac{1}{\sigma} \sim \frac{1}{2\tau} = -\mathrm{Im}\,\Sigma(0). \tag{4.45}$$

The average Green function

$$G(i\omega_n) = \int d\varepsilon\, P(\varepsilon) \frac{q(\varepsilon)}{i\omega_n - \tilde{\varepsilon}(\varepsilon) - q(\varepsilon)\Delta(i\omega_n)} \tag{4.46}$$

expressed through the self-energy Σ is given by

$$G(i\omega_n) = \frac{1}{i\omega_n - \Sigma(i\omega_n) - \Delta(i\omega_n)}. \tag{4.47}$$

We make an expansion of Eq. (4.46) with respect to $\tilde{\varepsilon}$, which gives

[2] We will set $t = 1/2$, which corresponds to the half-bandwidth $D = 1$.

$$
\begin{aligned}
G(i\omega_n) &= \int d\varepsilon\, P(\varepsilon) \frac{q(\varepsilon)}{i\omega_n - q(\varepsilon)\Delta(i\omega_n)} \left[1 - \frac{\tilde{\varepsilon}(\varepsilon)}{i\omega_n - q(\varepsilon)\Delta(i\omega_n)}\right]^{-1} \\
&= \int d\varepsilon\, P(\varepsilon)\, \widetilde{G}(\varepsilon, i\omega_n) \left[1 - \frac{\tilde{\varepsilon}(\varepsilon)}{q(\varepsilon)} \widetilde{G}(\varepsilon, i\omega_n)\right]^{-1} \\
&\approx \int d\varepsilon\, P(\varepsilon)\, \widetilde{G}(\varepsilon, i\omega_n) \left[1 + \frac{\tilde{\varepsilon}(\varepsilon)}{q(\varepsilon)} \widetilde{G}(\varepsilon, i\omega_n) + \left(\frac{\tilde{\varepsilon}(\varepsilon)}{q(\varepsilon)} \widetilde{G}(\varepsilon, i\omega_n)\right)^2\right] \\
&= \widetilde{G}(i\omega_n) + \int d\varepsilon\, P(\varepsilon)\, \frac{\tilde{\varepsilon}(\varepsilon)}{q(\varepsilon)} \left[\widetilde{G}(\varepsilon, i\omega_n)\right]^2 + \int d\varepsilon\, P(\varepsilon)\, \left[\frac{\tilde{\varepsilon}(\varepsilon)}{q(\varepsilon)}\right]^2 \left[\widetilde{G}(\varepsilon, i\omega_n)\right]^3. \quad (4.48)
\end{aligned}
$$

The Green functions $\widetilde{G}(i\omega_n)$ and $\widetilde{G}(\varepsilon, i\omega_n)$ are defined as

$$
\widetilde{G}(i\omega_n) = \int d\varepsilon\, P(\varepsilon) \frac{q(\varepsilon)}{i\omega_n - q(\varepsilon)\Delta(i\omega_n)}. \quad (4.49)
$$

and

$$
\widetilde{G}(\varepsilon, i\omega_n) = \frac{q(\varepsilon)}{i\omega_n - q(\varepsilon)\Delta(i\omega_n)}. \quad (4.50)
$$

Due to the particle-hole symmetry $q(\varepsilon)$ and $\widetilde{G}(i\omega_n)$ are even functions in ε, while $\tilde{\varepsilon}(\varepsilon)$ is odd. Therefore the second integral is equal to zero and we find

$$
G(i\omega_n) = \widetilde{G}(i\omega_n) + \int d\varepsilon\, P(\varepsilon)\, \left[\frac{\tilde{\varepsilon}(\varepsilon)}{q(\varepsilon)}\right]^2 \left[\widetilde{G}(\varepsilon, i\omega_n)\right]^3. \quad (4.51)
$$

Following the same idea, we define the self-energy $\widetilde{\Sigma}$ by

$$
\widetilde{G}(i\omega_n) = \frac{1}{i\omega_n - \widetilde{\Sigma}(i\omega_n) - \Delta(i\omega_n)}, \quad (4.52)
$$

and denote $\Sigma_s(i\omega_n) = \Sigma(i\omega_n) - \widetilde{\Sigma}(i\omega_n)$. Then we can expand $G(i\omega_n)$ to the first order in $\Sigma_s(i\omega_n)$

$$
\begin{aligned}
G(i\omega_n) &= \frac{1}{i\omega_n - \Sigma_s(i\omega_n) - \widetilde{\Sigma}(i\omega_n) - \Delta(i\omega_n)} \\
&= \frac{1}{i\omega_n - \widetilde{\Sigma}(i\omega_n) - \Delta(i\omega_n)} \left[1 - \frac{\Sigma_s(i\omega_n)}{i\omega_n - \widetilde{\Sigma}(i\omega_n) - \Delta(i\omega_n)}\right]^{-1} \\
&= \widetilde{G}(i\omega_n) \left[1 - \widetilde{G}(i\omega_n)\Sigma_s(i\omega_n)\right]^{-1} \\
&\approx \widetilde{G}(i\omega_n) \left[1 + \widetilde{G}(i\omega_n)\Sigma_s(\omega_n)\right] \\
&= \widetilde{G}(i\omega_n) + \left[\widetilde{G}(i\omega_n)\right]^2 \Sigma_s(i\omega_n). \quad (4.53)
\end{aligned}
$$

By comparison with Eq. (4.51), we find

$$\Sigma_s(i\omega_n) = \frac{1}{\left[\widetilde{G}(i\omega_n)\right]^2} \int d\varepsilon\, P(\varepsilon)\, \left[\frac{\tilde{\varepsilon}(\varepsilon)}{q(\varepsilon)}\right]^2 \left[\widetilde{G}(\varepsilon, \omega_n)\right]^3. \tag{4.54}$$

In a particle-hole symmetric system with random hopping only, it is easy to see that the Green function at zero frequency is pinned to its noninteracting value, $\widetilde{G}(\varepsilon, \omega = 0) = \widetilde{G}(\omega = 0) = G_0(\omega = 0)$, and the self-energy is equal to zero, $\widetilde{\Sigma}(\omega = 0) = 0$. Therefore

$$\Sigma_s(0) = G_0(0) \int d\varepsilon\, P(\varepsilon)\, \left[\frac{\tilde{\varepsilon}(\varepsilon)}{q(\varepsilon)}\right]^2. \tag{4.55}$$

Hence $\mathrm{Im}\Sigma(0) = \mathrm{Im}\Sigma_s(0)$, which gives

$$\frac{1}{\tau} = -2\left[\mathrm{Im}G_0(0)\right] \int d\varepsilon\, P(\varepsilon)\, \left[\frac{\tilde{\varepsilon}(\varepsilon)}{q(\varepsilon)}\right]^2. \tag{4.56}$$

This equation explicitly shows that the renormalized disorder, as seen by the physical quasiparticle at the Fermi energy, should be defined as

$$v_i = \frac{\tilde{\varepsilon}_i}{q_i}. \tag{4.57}$$

In the case of weak disorder, from Eq. (4.38), we find

$$\frac{1}{\tau} = -2\left[\mathrm{Im}G_0(0)\right] \left[\frac{3\pi t}{4U_c}\left(1 - \frac{U}{U_c}\right)\right]^2 \langle\varepsilon^2\rangle. \tag{4.58}$$

This is a remarkable result showing that $\tau \to 0$ as $U \to U_c$. In other words, the conductivity becomes infinite at the metallic side of the Mott metal-insulator transition. This one of our main results, and we will discuss its physical origin and applicability to real physical systems in the remaining sections of this chapter. We will refer to this phenomenon as "perfect screening".

Perfect screening. We have seen that the renormalized disorder $v_i = \tilde{\varepsilon}_i/q_i$ goes to zero at the MIT. However, we have derived this result for weak disorder and Bethe lattice. Now we will show that $v_i \to 0$ as $U \to U_c$ for an arbitrary particle-hole symmetric lattice and for arbitrary disorder strength.

Similarly as in the case of weak disorder, we will concentrate on the slave boson equation (4.18) (Friedel sum rule)

$$\frac{1}{\beta}\sum_{\omega_n} G_{fi}(\omega_n) = \frac{1}{2}\left(1 - e_i^2 + d_i^2\right), \tag{4.59}$$

and make an expansion with respect to $\tilde{\varepsilon}_i$.

$$\frac{1}{\beta}\sum_{i\omega_n} G_{fi}(\omega_n) = -\frac{1}{\pi}\int_{-D}^{0} d\omega\, \mathrm{Im}\left[\widetilde{G}_{fi}(i\omega_n)\frac{1}{1-\tilde{\varepsilon}_i\widetilde{G}_{fi}(i\omega_n)}\right]$$
$$= -\frac{1}{\pi}\int_{-D}^{0} d\omega\, \mathrm{Im}\left[\widetilde{G}_{fi}(i\omega_n) + \tilde{\varepsilon}_i\left(\widetilde{G}_{fi}(i\omega_n)\right)^2 + \cdots\right], \qquad (4.60)$$

where

$$\widetilde{G}_{fi}(i\omega_n) = \frac{1}{i\omega_n - q_i\Delta(i\omega_n)}. \qquad (4.61)$$

If the system has global particle-hole symmetry, then

$$\frac{1}{\beta}\sum_{\omega_n}\widetilde{G}_{fi}(i\omega_n) = \frac{1}{2}. \qquad (4.62)$$

(Note that that the local Green function $\widetilde{G}_{fi}$ is particle-hole symmetric as opposed to G_{fi}.) Therefore,

$$\frac{1}{\beta}\sum_{i\omega_n} G_{fi}(\omega_n) \approx \frac{1}{2} + \tilde{\varepsilon}(\varepsilon)\int_{-D}^{0} d\omega\, \mathrm{Im}\left(\widetilde{G}_{fi}(\omega)\right)^2. \qquad (4.63)$$

We express the hopping in a form $q_i = A_i\, q_o$, where $q_o \equiv q(\varepsilon = 0)$ goes (linearly) to zero as $U \to U_c$, while $A_i \equiv A(\varepsilon_i)$ remains constant. Then

$$\widetilde{G}_{fi}(\omega) = \frac{1}{\omega - q_i\Delta(\omega, \{q_i\}, \{\tilde{\varepsilon}_i\})} = \frac{1}{q_i}\frac{1}{\frac{\omega}{q_i} - \Delta(\omega, \{A_i q_o\}, \{\tilde{\varepsilon}_i\})}$$
$$= \frac{1}{q_i}\frac{1}{\frac{\omega}{q_i} - \Delta\left(\frac{\omega}{q_o}, \{A_i\}, \{\tilde{\varepsilon}_i/q_o\}\right)} = \frac{1}{q_i}\widetilde{G}_f\left(\frac{\omega}{q_i}, \{A_i\}, \{\tilde{\varepsilon}_i/q_o\}\right), \qquad (4.64)$$

where the curly brackets denote that the the Green function depends on the distribution of A_i and $\tilde{\varepsilon}_i$. The bandwidth $2\widetilde{D}_f$ corresponding to $\widetilde{G}_f$ is $1/q_o$ times larger than the bandwidth $2\widetilde{D}_{fi}$ of $\widetilde{G}_{fi}$, while the density of states is $1/q_o$ times smaller. Both the bandwidth $2\widetilde{D}_f$ and the density of states $-\mathrm{Im}\widetilde{G}_f(\omega + i0^+)/\pi$ remain finite as $q_o \to 0$ which is the reason why we scaled the energy with q_i and defined the Green function $\widetilde{G}_f$. We emphasize that the exact form of $\widetilde{G}_f$ depends on the bare disorder distribution and interaction (through q_i), but the corresponding density of states and the bandwidth will be of the order of the bandwidth $2D$ of the clean lattice of noninteracting electrons.

Eq. (4.63) now assumes the form

$$\frac{1}{\beta}\sum_{i\omega_n} G_{fi}(\omega_n) \approx \frac{1}{2} + \tilde{\varepsilon}_i\int_{-D}^{0} d\omega\, \frac{1}{q_i^2}\mathrm{Im}\left[\widetilde{G}_f\left(\frac{\omega}{q_i}\right)\right]^2. \qquad (4.65)$$

After the change of variables, $\omega \to \omega/q_i$, we obtain

$$\frac{1}{\beta}\sum_{i\omega_n} G_{fi}(\omega_n) \approx \frac{1}{2} + \tilde{\varepsilon}_i \int_{-\tilde{D}}^{0} d\omega' q_i \,\mathrm{Im}\left[\frac{1}{q_i}\widetilde{G}_f(\omega')\right]^2$$
$$= \frac{1}{2} + \frac{\tilde{\varepsilon}_i}{q_i}\int_{-\tilde{D}}^{0} d\omega' \,\mathrm{Im}\left[\widetilde{G}_f(\omega')\right]^2, \tag{4.66}$$

and Eq. (4.59) reduces to

$$\frac{\tilde{\varepsilon}_i}{q_i}\int_{-\tilde{D}}^{0} d\omega \,\mathrm{Im}\left[\widetilde{G}_f(\omega)\right]^2 + \mathcal{O}\left(\frac{\tilde{\varepsilon}_i}{q_i}\right)^2 = \frac{1}{2}\left(-e_i^2 + d_i^2\right). \tag{4.67}$$

The integral remains constant as we approach the Mott transition, while the right-hand side goes to zero. Therefore, the renormalized disorder $v_i = \tilde{\varepsilon}_i/q_i$ goes to zero as $q_i \to 0$.

4.2.3 Numerical results

We have solved the slave boson equations (4.27) - (4.31) numerically for the full range of parameters at zero temperature. The goal is twofold: first we want to check and illustrate our analytical results, and second, we want to obtain a full metal-insulator transition phase diagram.

We have solved the equation on imaginary frequency axis using the following identity [41]

$$\lim_{\eta\to 0} T\sum_{\omega_n} G(i\omega_n)e^{-i\omega_n\eta} = 2T{\sum_{\omega_n\geq 0}}' \mathrm{Re}\, G(i\omega_n) - \frac{1}{2}\,\mathrm{sgn}\,\eta, \tag{4.68}$$

where the prime on the summation sum means that the $\omega_n = 0$ term is taken with weight $1/2$. At zero temperature the sum over ω_n can be replaced by an integral

$$T\sum \cdots \to \frac{1}{2\pi}\int \cdots, \tag{4.69}$$

which gives

$$\lim_{\eta\to 0} T\sum_{\omega_n} G(i\omega_n)e^{-i\omega_n\eta} = \frac{1}{\pi}\int_0^\infty d\omega \,\mathrm{Re}\, G(i\omega) - \frac{1}{2}\,\mathrm{sgn}\,\eta. \tag{4.70}$$

Then we obtain a system of integral equations

$$-\frac{\partial q_i}{\partial e_i}\frac{1}{\pi}\int_0^\infty d\omega \,\mathrm{Re}\left[\Delta(i\omega)G_{fi}(i\omega)\right] = \left(\mu + \tilde{\varepsilon}_i - \varepsilon_i\right)e_i, \tag{4.71}$$

$$-\frac{\partial q_i}{\partial d_i}\frac{1}{\pi}\int_0^\infty d\omega \,\mathrm{Re}\left[\Delta(i\omega)G_{fi}(i\omega)\right] = \left(U - \mu - \tilde{\varepsilon}_i + \varepsilon_i\right)d_i, \tag{4.72}$$

and

$$\frac{1}{\pi}\int_0^\infty d\omega\, \mathrm{Re}\, G_{fi}(i\omega) = \frac{1}{2}\left(-e_i^2 + d_i^2\right). \tag{4.73}$$

We have solved the system of Eqs. (4.71)-(4.73) using the codes dcadre1.f from the NIST archive for the numerical integration, and DNSQE.f as a root search. The self-consistent solution is reached by iterations. Figure 4.1(a) shows how the quasiparticle weight changes as the interaction U is increased. The noninteracting lattice has semicircular density of

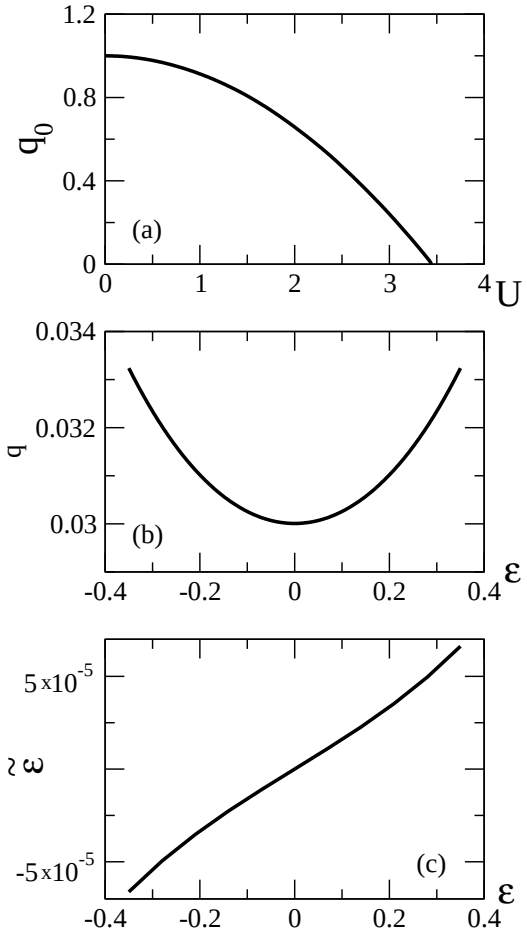

Figure 4.1. (a) Quasiparticle weight for $\varepsilon = 0$ site as a function of the interaction U. (b) Quasiparticle weight as a function of the site disorder for $U = 3.4$. (c) Renormalized disorder as a function of the (bare) site disorder for $U = 3.4$. The plots are obtained for the semicircular density of states and W=0.7.

states. The disorder is taken to be uniformly distributed in the interval $(-W/2, W/2)$, where W is set to 0.7, expressed in units of the half-bandwidth D of the noninteracting clean system. This value of W corresponds to moderate disorder since $\sqrt{\langle\varepsilon^2\rangle} = 0.216$. The disorder averaging is done by choosing a finite number of site energies which sample the distribution. Typically we used $m = 11$ site energies distributed equidistantly in the interval $(-W/2, W/2)$. The frequency grid is taken to be 0.01. Numerically obtained critical interaction $U_c = 3.445$ is in good agreement with the analytical result for weak disorder, $U_c = U_c^0(1 + \frac{2}{5}C\overline{\varepsilon^2}) = 3.452$. Figure 4.1(b) shows the value of the quasiparticle weight for sites with different site energies. The data are taken for $U = 3.4$ and $W = 0.7$. Function $q(\varepsilon)$ has a parabolic form $q = 0.3(1 + 0.878\varepsilon^2)$ in very good agreement with the analytical result, $q = q_o(1 + 0.867\varepsilon^2)$. Figure 4.1(c) shows the renormalized disorder $\tilde{\varepsilon}$ as a function of site energies. A linear fit gives the slope 1.79×10^{-4} in good agreement with analytical result $3\pi t q_o^2/8U = 1.53 \times 10^{-4}$.

The scattering rate, $\tau^{-1} = -2\mathrm{Im}\,\Sigma(0)$, normalized with the noninteracting value, for different amounts of disorder is shown in Figure 4.2. At the Mott transition the scattering rate goes to zero.

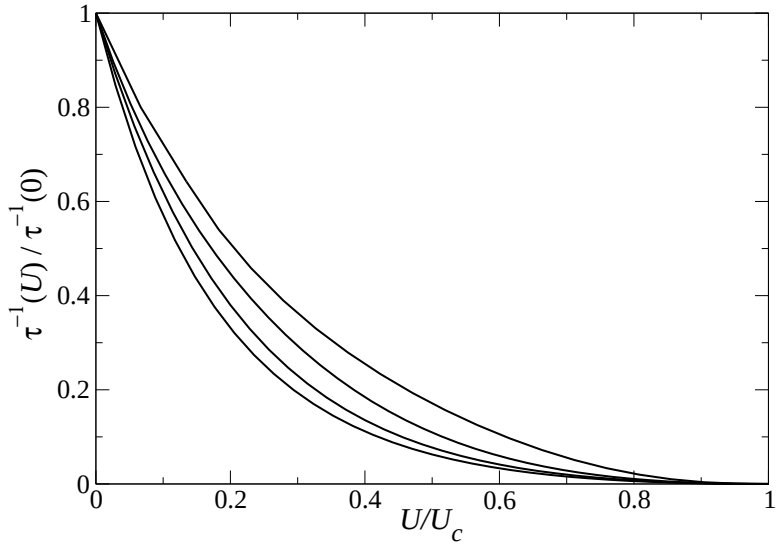

Figure 4.2. Scattering rate normalized with the noninteracting value. From the lower to the upper curves: W=0.1,1,2,4.

4.2.4 Phase diagram

The metal-insulator phase diagram for the disordered Hubbard model at zero temperature is shown in Figure 4.3. The Mott insulating phase is completely suppressed for $W > U$, since the disorder tends to fill in the Mott-Hubbard gap. The phase boundary separating the correlated metal and the Mott insulator is identified by the simultaneous vanishing of the quasiparticle weights q_i on all lattice sites.

The DMFT approach is too simple to describe Anderson localization effects, which cannot be neglected for strong enough randomness. Nevertheless, it is interesting to estimate the disorder strength necessary for localization. In the absence of interactions, localization is expected to set in when the disorder scale W is comparable to the kinetic (i.e. Fermi) energy [42], as indicated by a dotted line in Fig. 1.[3] However, we have shown that correlations lead to strong screening, with a renormalized disorder scale $\widetilde{W} \sim (\overline{v_i^2})^{1/2} \ll W$, which we can numerically compute for any U and W, and analytically in several limits. In particular, in the atomic limit ($E_F \to 0$), we find $\widetilde{W} \sim (1 - U/W)^{3/2}$. In the presence of interactions, the onset of localization should be estimated by comparing $\widetilde{W}$ to E_F, and the resulting boundary is shown by a dashed line in Fig. 4.3. Hence, the metallic phase is found to be strongly stabilized by screening in the intermediate regime $W \sim U$. Of course, such an interplay of the correlation and localization effects should be studied in more detail by extensions of DMFT which can explicitly incorporate the localization effects. Interestingly such a work has been done very recently [43] within an extended DMFT which uses geometrically averaged ("typical") density of states as an order parameter for the Anderson localization [8]. The DMFT equations are solved using numerical renormalization group and the results are in excellent agreement with our phase diagram.

4.3 Particle-hole asymmetric lattice

The behavior of the scattering time in a vicinity of the Mott transition is qualitatively different in the case of a particle-hole asymmetric lattice. However, although the disorder is not perfectly screened, the renormalized disorder v_i becomes very small, leading to the very large increase in the scattering time and conductivity.

[3] In the case of a particle-hole symmetric lattice the Fermi energy is equal to the half-bandwidth D.

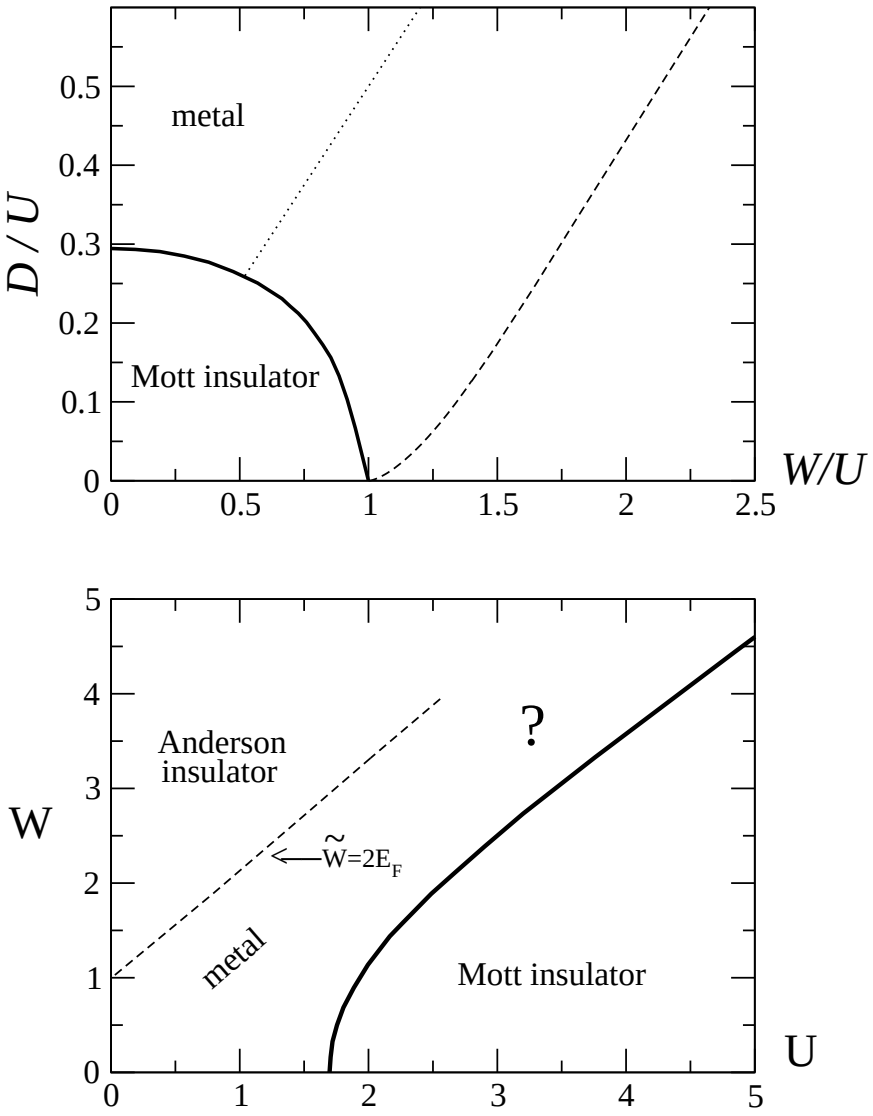

Figure 4.3. DMFT phase diagram of the Hubbard model with random site energies. The Mott insulator can be suppressed by sufficiently strong (bare) disorder $W > U$. Also shown is an estimate of the regime where Anderson localization effects are important, as obtained by comparing the Fermi energy E_F to bare disorder W (dotted line) or screened disorder $\widetilde{W}$ (dashed line). Localization is strongly suppressed by correlation effects in the intermediate regime where the disorder is comparable to the on-site repulsion U. The lower panel shows the same phase diagram, but with the disorder W and the interaction U as explicit parameters. The question mark corresponds to the crossover between the Anderson and Mott insulator, which cannot be described within standard DMFT.

4.3.1 Clean lattice

It is instructive to familiarize first with a solution of the slave boson equations in the clean case. We will start from the mean field expression for the free energy at zero temperature (this expression is not restricted to DMFT)

$$F = 2\int d\epsilon\, \rho(\epsilon)(q\epsilon - \mu + \lambda)\, n_F(q\epsilon - \mu + \lambda) + Ud^2 - \lambda(1 - e^2 + d^2). \tag{4.74}$$

The minimization of the free energy with respect to the slave boson parameters gives[4]

$$-2\frac{\partial q}{\partial e^2}\int_{-\infty}^{\frac{\mu-\lambda}{q}} d\epsilon\, \epsilon\rho(\epsilon) = \lambda, \tag{4.75}$$

$$-2\frac{\partial q}{\partial d^2}\int_{-\infty}^{\frac{\mu-\lambda}{q}} d\epsilon\, \epsilon\rho(\epsilon) = U - \lambda, \tag{4.76}$$

and

$$\int_{-\infty}^{\frac{\mu-\lambda}{q}} d\epsilon\, \rho(\epsilon) = \frac{1}{2}. \tag{4.77}$$

At half-filling in the clean case $e = d$, and from Eqs. (4.75) and (4.76) we find $\lambda = U/2$. From Eq. (4.77), $(\mu - \lambda)/q = \mu_0$, where μ_0 is the chemical potential of the noninteracting lattice at half-filling. (Note that for the particle-hole symmetric lattice $\mu_0 = 0$.) If we write

$$\mu - \frac{U}{2} = q\mu_0, \tag{4.78}$$

we see that the chemical potential goes to $U/2$ as we approach to the Mott transition. Then, since $q = 8d^2(1 - 2d^2)$, from Eq. (4.76)

$$-8(1 - 4d^2)\int_{-\infty}^{\mu_0} d\epsilon\, \epsilon\rho(\epsilon) = \frac{U}{2}, \tag{4.79}$$

which gives

$$U_c = -16\int_{-\infty}^{\mu_0} d\epsilon\, \epsilon\rho(\epsilon), \tag{4.80}$$

and

$$d^2 = \frac{1}{4}\left(1 - \frac{U}{U_c}\right). \tag{4.81}$$

[4] $\partial n_F(q\epsilon - \mu + \lambda)/\partial\lambda = -\delta(q\epsilon - \mu + \lambda)$. Since $\int dx\, x\delta(x) = 0$, this partial derivative after integration gives zero. The same is true for partial derivatives with respect to e and d.

4.3.2 Disordered lattice: strong screening

In the case of a particle-hole asymmetry it is convenient to define the renormalized disorder as

$$\tilde{\varepsilon}_i = \varepsilon_i + \lambda_i - \mu + \tilde{\mu}_o, \tag{4.82}$$

where $\tilde{\mu}_o$ sets $\tilde{\varepsilon}(\varepsilon = 0)$ to be equal to 0. Note that $\tilde{\mu}_o \sim q\mu_0$, see Eq. (4.78). The local free energy has the form

$$F_i = -\frac{2}{\beta}\sum_{\omega_n} \ln\left[-i\omega_n - \tilde{\mu}_o + \tilde{\varepsilon}_i + q_i\Delta(\omega_n)\right] + Ud_i^2 - \lambda_i\left[1 - e_i^2 + d_i^2\right]. \tag{4.83}$$

As in the particle-hole symmetric case, we consider λ variation equation

$$\frac{1}{\beta}\sum_{\omega_n} \frac{1}{i\omega_n + \tilde{\mu}_0 - \tilde{\epsilon}_i - q_i\Delta(i\omega_n)} = \frac{1}{2}\left(1 - e_i^2 + d_i^2\right). \tag{4.84}$$

First note that, by a definition of $\tilde{\mu}_0$, $\tilde{\epsilon}(0) = 0$ and

$$\frac{1}{\beta}\sum_{\omega_n} \frac{1}{i\omega_n + \tilde{\mu}_0 - q_o\Delta(i\omega_n)} = \frac{1}{2}. \tag{4.85}$$

Close to the transition $\tilde{\mu}_0 \sim q_o$. The bandwidth corresponding to the conduction bath Δ is also of the order of q_o, while $\Delta(\omega) \sim \mathcal{O}(1)$. Since $q_i - q_o \sim \mathcal{O}(q_o)$, in order to fulfill Eq. (4.84), $\tilde{\epsilon}_i$ has to be of the order of q_o. In this analysis, the right-hand side of Eq. (4.84) can be approximated by $1/2$.[5] Now we can interpret $\tilde{\epsilon}_i$ as a correction in the local chemical potential, which provides simultaneous formation of the local moments on every site (simultaneous $q_i \to 0$). This correction obviously has to be much smaller than the width of the quasiparticle band, which gives the conclusion that $\tilde{\epsilon}_i/q_i \ll 1$. This means that the disorder screening is strong (though not perfect), even in the case of a strong particle-hole asymmetry and strong disorder. This is the central result of this section, which we will now present in more quantitative form in the case of weak disorder.

4.3.3 Weak disorder

For weak disorder and weak particle-hole asymmetry we can obtain an explicit expression for the renormalized disorder. q_i can be written as $q_i = q_o(1 + \alpha_i)$, where $\alpha_i \ll 1$. Then

[5] This means that $\tilde{\epsilon}(\epsilon) = \tilde{\epsilon}(-\epsilon)$ when $U \to U_c$, which agrees with the numerical results. We will come back to this interesting feature in the next subsection.

$$\frac{1}{\beta}\sum_{\omega_n}\frac{1}{i\omega_n+\tilde{\mu}_o-\tilde{\epsilon}_i-q_i\Delta(i\omega_n)}=\frac{1}{\beta}\sum_{\omega_n}\frac{1}{i\omega_n+\tilde{\mu}_o-\tilde{\epsilon}_i-q_o\Delta(i\omega_n)-\alpha_i q_o\Delta(i\omega_n)}$$
$$=\frac{1}{\beta}\sum_{\omega_n}\frac{1}{\left[i\omega_n+\tilde{\mu}_o-q_o\Delta(i\omega_n)\right]\left[1-\frac{\tilde{\epsilon}_i+\alpha_i q_o\Delta(i\omega_n)}{i\omega_n+\tilde{\mu}_o-q_o\Delta(i\omega_n)}\right]}$$
$$\approx\frac{1}{\beta}\sum_{\omega_n}\frac{1}{i\omega_n+\tilde{\mu}_o-q_o\Delta(i\omega_n)}\left[1+\frac{\tilde{\epsilon}_i+\alpha_i q_o\Delta(i\omega_n)}{i\omega_n+\tilde{\mu}_o-q_o\Delta(i\omega_n)}\right]$$
$$=\frac{1}{\beta}\sum_{\omega_n}\frac{1}{i\omega_n+\tilde{\mu}_o-q_o\Delta(i\omega_n)}+\frac{1}{\beta}\sum_{\omega_n}\left[\frac{1}{i\omega_n+\tilde{\mu}_o-q_o\Delta(i\omega_n)}\right]^2\left[\tilde{\epsilon}_i+\alpha_i q_o\Delta(i\omega_n)\right]$$
$$=\frac{1}{2}+\frac{1}{\beta}\sum_{\omega_n}\left[\frac{1}{i\omega_n+\tilde{\mu}_o-q_o\Delta(i\omega_n)}\right]^2\left[\tilde{\epsilon}_i+\alpha_i q_o\Delta(i\omega_n)\right]. \tag{4.86}$$

Eq. (4.84) then reduces to

$$\frac{1}{\beta}\sum_{\omega_n}\left[\frac{1}{i\omega_n+\tilde{\mu}_o-q_o\Delta(i\omega_n)}\right]^2\left[\tilde{\epsilon}_i+\alpha_i q_o\Delta(i\omega_n)\right]=0. \tag{4.87}$$

Here the cavity function $\Delta(i\omega_n)$ can be approximated by its value for a clean lattice. For a semicircle Green's function $\Delta(i\omega_n)=q_o t^2 G_f(i\omega_n)$, where $G_f(i\omega_n)=1/(i\omega_n-q_o^2t^2G_f(i\omega_n))$.

Now we calculate the sums

$$\frac{1}{\beta}\sum_{\omega_n}\left[\frac{1}{i\omega_n+\tilde{\mu}_o-q_o\Delta(i\omega_n)}\right]^2\approx\frac{1}{\beta}\sum_{\omega_n}\left[\frac{1}{i\omega_n-q_o\Delta(i\omega_n)}\right]^2$$
$$=\frac{1}{\beta}\sum_{\omega_n}G_f^2(i\omega_n)=-\frac{4}{3\pi q_0 t}, \tag{4.88}$$

and

$$\frac{1}{\beta}\sum_{\omega_n}\left[\frac{1}{i\omega_n+\tilde{\mu}_o-q_o\Delta(i\omega_n)}\right]^2 q_o\Delta(i\omega_n)=\frac{1}{\beta}\sum_{\omega_n}\left[\frac{1}{i\omega_n-q_0 o\Delta(i\omega_n)}\,\frac{1}{1+\frac{\tilde{\mu}_o}{i\omega_n-q_o\Delta(i\omega_n)}}\right]^2 q_o\Delta(i\omega_n)$$
$$=\frac{1}{\beta}\sum_{\omega_n}\left[G_f(i\omega_n)\,\frac{1}{1+\tilde{\mu_o}G_f(i\omega_n)}\right]^2 q_o^2t^2G_f(i\omega_n)\approx q_o^2t^2\frac{1}{\beta}\sum_{\omega_n}G_f^3(i\omega_n)\left[1-2\tilde{\mu}_oG_f(i\omega_n)\right]$$
$$=q_o^2t^2\frac{1}{\beta}\sum_{\omega_n}G_f^3(i\omega_n)-2\tilde{\mu_o}q_o^2t^2\frac{1}{\beta}\sum_{\omega_n}G_f^4(i\omega_n)=-\frac{16}{15\pi}\frac{\tilde{\mu}_0}{q_o t}\approx-\frac{16}{15\pi}\frac{\mu_o}{t}. \tag{4.89}$$

Here we assumed that $\mu_o\ll t$, and used that $\frac{1}{\beta}\sum_{\omega_n}G_f^3(i\omega_n)=0$ and $\frac{1}{\beta}\sum_{\omega_n}G_f^4(i\omega_n)=8/(15\pi q_o^3t^3)$. Eq. (4.87) then gives

$$\frac{\tilde{\epsilon}_i}{q_0}=-\frac{4}{5}\mu_o\alpha. \tag{4.90}$$

Since for weak disorder $q_i \approx q_o(1 + C\epsilon^2)$, we obtain that[6]

$$\frac{\tilde{\epsilon}_i}{q_o} \approx -0.7\mu_o\epsilon^2. \tag{4.91}$$

We can find the expression for the scattering rate similarly as in the particle-hole symmetric case, and here the derivation will be just outlined. We start from the relations which define the disorder-averaged Green function

$$G(i\omega_n) = \int d\varepsilon\, P(\varepsilon) \frac{q(\varepsilon)}{i\omega_n + \tilde{\mu}_o - \tilde{\varepsilon}(\varepsilon) - q(\varepsilon)\Delta(i\omega_n)} \tag{4.92}$$

and the corresponding self-energy

$$G(i\omega_n) = \frac{1}{i\omega_n + \tilde{\mu}_o - \Sigma(i\omega_n) - \Delta(i\omega_n)}. \tag{4.93}$$

Note that as compared with Eq. (4.46), G includes the "chemical potential" $\tilde{\mu}_o$. Then in full analogy with the symmetric case we define

$$\widetilde{G}(\varepsilon, i\omega_n) = \frac{q(\varepsilon)}{i\omega_n + \tilde{\mu}_o - q(\varepsilon)\Delta(i\omega_n)}, \tag{4.94}$$

the corresponding disorder-averaged Green function $\widetilde{G}(i\omega_n)$, and the self-energy $\widetilde{\Sigma}(i\omega_n)$. We define $\Sigma_s(i\omega_n) = \Sigma(i\omega_n) - \widetilde{\Sigma}(i\omega_n)$, and expand Eqs. (4.92) and (4.93) to the second order in $\tilde{\varepsilon}(\varepsilon)/q(\varepsilon)$. Using Eq. (4.91), we find $\mathrm{Im}\,\Sigma_s(\omega = 0) = \mathrm{Im}\,G_0(0)\,\mu_o^2 C^2[0.96\langle\varepsilon^4\rangle + 1.6\langle\varepsilon^2\rangle^2]$, and $\mathrm{Im}\,\widetilde{\Sigma}(\omega = 0) = \mathrm{Im}\,G_0(0)\,\mu_o^2 C^2[\langle\varepsilon^4\rangle - \langle\varepsilon^2\rangle^2]$, which gives

$$\mathrm{Im}\,\Sigma(\omega = 0) \approx 0.8\,[\mathrm{Im}\,G_0(0)]\;\mu_o^2\left[2\langle\varepsilon^4\rangle + 0.6\langle\varepsilon^2\rangle^2\right]. \tag{4.95}$$

Therefore, we have found that for weak disorder, close to the Mott transition, the scattering rate $\tau^{-1} = -2\mathrm{Im}\,\Sigma(0)$ approaches very small asymptotic value

$$\frac{1}{\tau} \sim \mu_o^2\langle\varepsilon^4\rangle, \tag{4.96}$$

instead of $1/\tau \sim \langle\varepsilon^2\rangle$ as for weak interaction. In addition, for any realistic lattice at half-filling, μ_o is small number ($\lesssim 0.1$), explaining the smallness of the scattering rate.

[6] $C \approx 0.9$ for weakly asymmetric Bethe lattice. We will keep this value as an estimate for C.

4.3.4 Numerical results

Typical numerical results are shown in Fig. 4.4, where the full line corresponds to the (symmetric) semicircular density of states $\rho_o = -\frac{1}{\pi}\,\mathrm{Im}\,G_0(\omega + i\eta)$, and the dashed line is obtained for the particle-hole asymmetric lattice described by the Green function $G_{0a}(\omega) = [\omega - t^2 G_0(\omega + a)]^{-1}$. In this plot, the asymmetry parameter a is chosen to be $0.3D$ (strongly asymmetric lattice), where D is the half-bandwidth. The data are obtained for $W = 1$, which corresponds to moderate disorder strength. For weaker interaction the behavior of the scattering time is almost the same in the symmetric and asymmetric case. The difference appears very close to the critical interaction U_c, where the scattering rate in the case of a particle-hole asymmetric lattice saturates to a very small, but nonzero value.

Fig. 4.5(a) shows renormalized disorder as a function of the bare site energy. Interestingly, renormalized disorder is a nonmonotonic function of its bare value, as opposed to the results in the particle-hole symmetric case, but in agreement with the analytical arguments from the previous subsection. The average occupation number, Fig. 4.5(a), however, decreases with the increase of the site disorder, as expected.

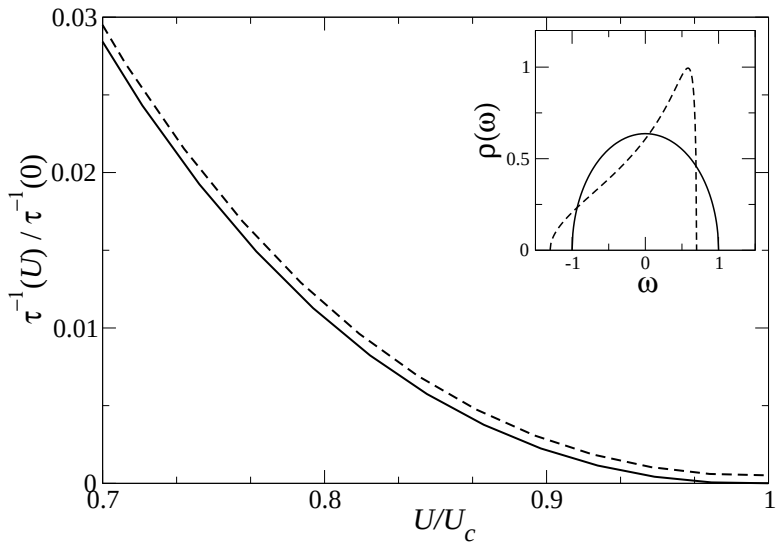

Figure 4.4. Scattering rate normalized with the noninteracting value. Results close to U_c for the particle-hole symmetric lattice (full line), and the asymmetric lattice (dashed line), with $W = 1$. The inset shows the density of states in these two cases.

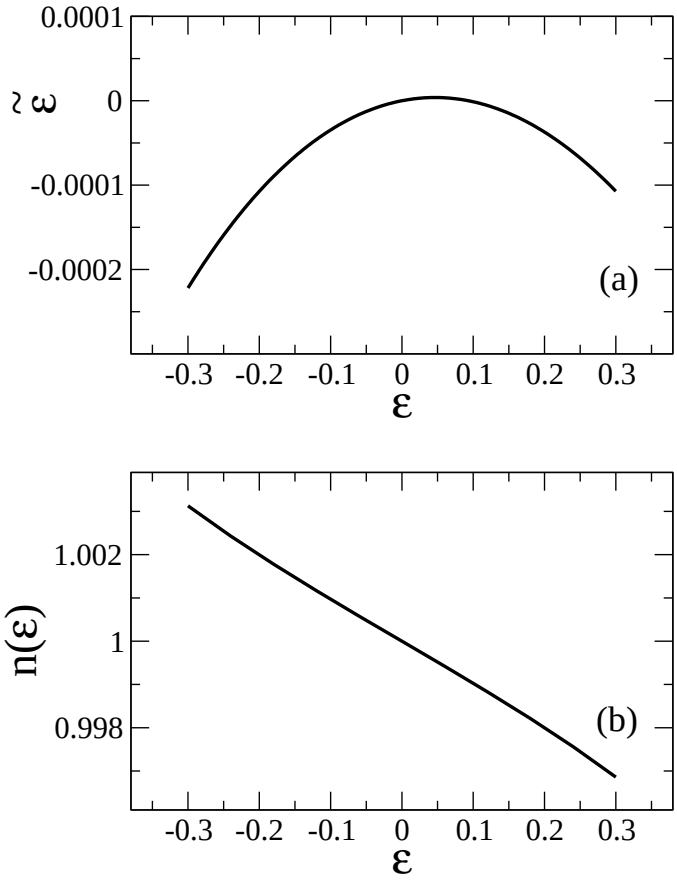

Figure 4.5. Renormalized disorder (a), and average occupation number (b), as a function of the bare site energy. Here, asymmetry parameter $a = 0.3D$, $W = 0.6$, and $U = 3.3$. For these parameters $U_c = 3.355$.

4.4 Breakdown of conventional theory

In the strongly correlated regime our DMFT results are in sharp discrepancy with the results obtained within the Hartree-Fock theory. In this section, working within the DMFT limit of large coordination number, we will compare the results for the scattering time in the slave boson and Hartree-Fock approach. This provides an explicit example how an uncontrolled extrapolation of the Hartree-Fock theory to the regime of strong correlation may lead to nonphysical results.

In the Hartree-Fock theory the screening appears as a consequence of finite (nonzero) compressibility of the electron gas. We can think of it semiclassically, as a result of the

redistribution of electrons in the presence of a random potential. In DMFT the renormalized (screened) disorder is equal to

$$v_{i\sigma} = \epsilon_i - \Sigma_{i\sigma}(\omega = 0), \tag{4.97}$$

where $\Sigma_{i\sigma}$ is the momentum-independent self-energy, which is equal to $U\delta n_{i,-\sigma}$ in the Hartree-Fock approximation. Here δn is the deviation of the occupation number from its average value. For weak disorder $\delta n_{i\sigma} = \chi_\sigma \epsilon^{sc}_{i\sigma}$, where the local compressibility (charge susceptibility) is given by $\chi_\sigma = -\partial\langle n_{i\sigma}\rangle/\partial v_{i\sigma}|_{v_{i\sigma}=0}$. The renormalized disorder is then

$$v_{i\sigma} = \frac{1 - U\chi_{-\sigma}}{1 - U^2\chi_{-\sigma}\chi_\sigma}\,\epsilon_i. \tag{4.98}$$

This result obtains much more familiar form in the nonmagnetic case

$$v_i = \frac{1}{1 + U\chi}\,\epsilon_i. \tag{4.99}$$

But what is the charge compressibility in the vicinity of the Mott metal-insulator transition? It is well established that it is very small, and in fact within the slave boson mean field theory $\chi \to 0$ as $U \to U_c$ [5]. Therefore, Eq. (4.99), applicable in the weak coupling limit, predicts very weak disorder screening close to the Mott transition.

To further elaborate our arguments, we will complete the Hartree-Fock solution, though at this point it is already obvious that we can expect spurious results for two different reasons: (i) In the strong coupling limit the simple relation between the renormalized disorder and the charge compressibility is not valid. (ii) The Hartree-Fock theory does not describe correctly the Mott metal-insulator transition.

The local compressibility expressed through the local Green function $G^\sigma_i(i\omega_n) = [i\omega_n + \mu - \tilde{\varepsilon}_i - \Delta_\sigma(i\omega_n)]^{-1}$ is equal to

$$\begin{aligned}
\chi_\sigma &= -\left.\frac{\partial\langle n_{i\sigma}\rangle}{\partial v_{i\sigma}}\right|_{v_{i\sigma}=0} = -\left.\frac{\partial G^\sigma_i(\tau,\tau^+)}{\partial v_i}\right|_{v_{i\sigma}=0} \\
&= -\frac{\partial}{\partial v_i}\left(\frac{1}{\beta}\sum_{\omega_n} e^{i\omega_n\eta} G^\sigma_i(i\omega_n)\right)\Bigg|_{v_{i\sigma}=0} = \frac{1}{\beta}\sum_{\omega_n}\left(G^\sigma_0(i\omega_n)\right)^2.
\end{aligned} \tag{4.100}$$

Then the renormalized disorder, Eq. (4.98) assumes the form

$$v_{i\sigma} = \frac{1 + U\frac{1}{\beta}\sum_{\omega_n}\left(G^{-\sigma}_0(i\omega_n)\right)^2}{1 - U^2\frac{1}{\beta}\sum_{\omega_n}\left(G^{-\sigma}_0(i\omega_n)\right)^2\frac{1}{\beta}\sum_{\omega_n}\left(G^\sigma_0(i\omega_n)\right)^2}\,\epsilon_i, \tag{4.101}$$

where

$$G_0^\sigma(i\omega_n) = \frac{1}{i\omega_n + \mu_0 - U\overline{n_{-\sigma}} - \Delta_0^\sigma(i\omega_n)}. \tag{4.102}$$

Half-filling condition, $\overline{n_{-\sigma}} + \overline{n_\sigma} = 1$, can be imposed by setting $\mu_0 = U/2$. We have solved Eq. (4.101) for semicircular density of states for the full rang of the interaction parameter. For small U, Hartree-Fock and slave boson methods both give similar results, but closer to the transition Hartree-Fock theory (dashed line in Fig. 4.6), predicts a reduced disorder screening, while full DMFT (full line) shows that the screening remains strongly enhanced. The reduction of screening found in the Hartree-Fock approximation reflects the decrease of the compressibility near the Mott transition. We note that the Mott gap within Hartree-Fock theory opens at much smaller value of interaction ($U = 2D$) than in the full DMFT solution ($U = 3.39$). The reason is that the Hartree Fock theory misses non-perturbative interaction effects, reflected in the formation of the quasiparticle Kondo peak. The decrease in the Hartree-Fock compressibility seen in Fig. 4.6 appears as a result of a Stoner instability in the magnetic Hartree-Fock solution, which sets in for $U = 1/\rho_0(0) = \pi D/2$ as a precursor to a gap opening at the transition [32].

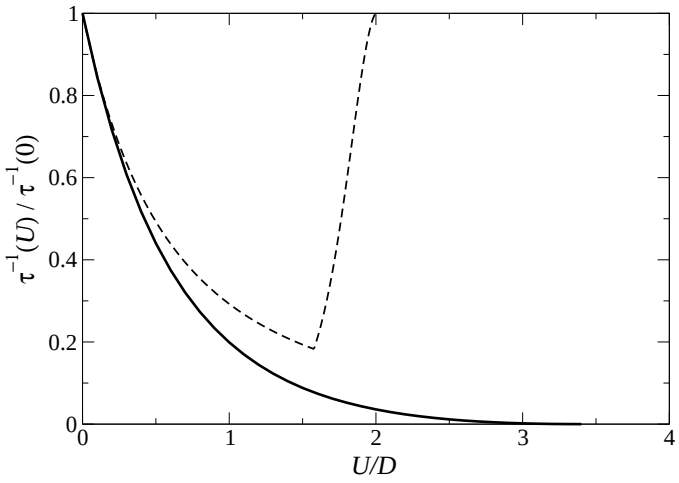

Figure 4.6. Normalized scattering rate for weak disorder as a function of U, from the full DMFT solution (full line), and the corresponding Hartree-Fock approximation (dashed line). For moderate interaction both methods predict the same screening, but diametrically opposite results are obtained in the strongly-correlated regime, where DMFT predicts enhanced screening, while a strong suppression is obtained within Hartree-Fock theory.

We would like to stress once again a difference between the renormalized disorder and the disorder screening as defined in our paper with the "static charge response" and "static overscreening" as defined and studied, e.g. in Ref. [44]. In this work the "screening charge" is essentially equal to the local compressibility. The Hubbard model is studied for the full range of the parameter U, using a combination of numerical Monte Carlo approach and slave boson mean field theory, and a comparison is made with the RPA results. However, as we have seen, there is no simple connection between the charge compressibility and transport properties in the strong coupling limit, and a study of solely the static charge response is not sufficient to determine the impurity scattering dominated conductivity.

4.5 Physical picture: enhanced screening as Kondo pinning

In this section we establish a connection between enhanced disorder screening in a vicinity of the Mott transition and the well studied phenomenon of increased low temperature transmittance of quantum dots. This provides simple physical interpretation of of our results in terms of the Kondo physics.

In the DMFT approach that we use, the solution of the full Hubbard model is mapped to solving an ensemble of auxiliary Kondo-Anderson impurity problems. Accordingly, the approach to the Mott transition can be described as the decrease of the local Kondo temperature, corresponding to the reduction of the local quasiparticle weight. This is illustrated in Fig. 4.7, which is obtained for a clean lattice using the iterated perturbation theory [5].

But what happens in the presence of a site disorder? For a single impurity in a given conduction bath this corresponds to ordinary Kondo problem. It is well known that in the local moment limit at zero temperature, in the case of a particle-hole symmetric lattice, the renormalized site energy level coincides with the Fermi energy [4]. This "pinning" of the renormalized energy to the Fermi level is responsible for increased resonant tunneling through quantum dots, as first theoretically predicted by [46, 47]. A strong increase of the resonant conductivity through a quantum dot is also experimentally verified [45]. A schematic plot of the experiment is shown in Figure 4.8. Note how the appearance of the quasiparticle peak at the Fermi energy resembles the quasiparticle peak in the Hubbard model. Therefore,

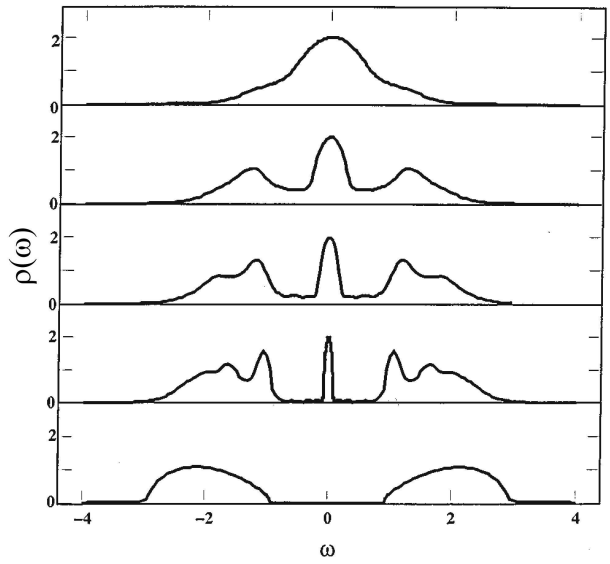

Figure 4.7. Local spectral density at $T = 0$, obtained by the iterated perturbation theory. The first four curves ($U/D = 1, 2, 2.5, 3$) correspond to an increasingly correlated metal, while the bottom one ($U/D = 4$) corresponds to an insulator. From [5].

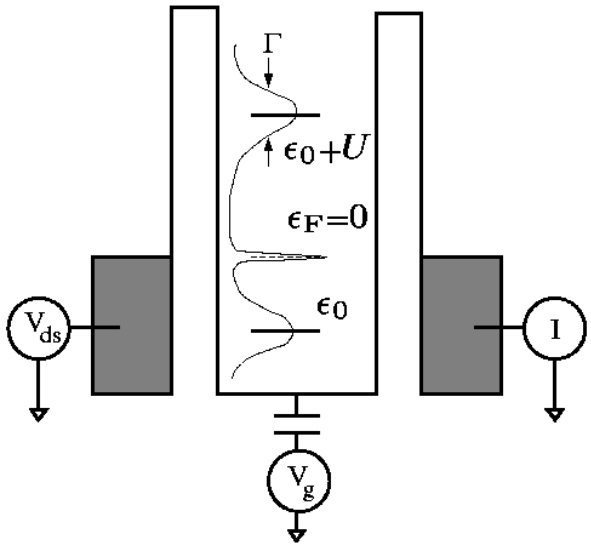

Figure 4.8. Schematic plot of the density of states of a quantum dot connected to the conduction leads. From [45].

the renormalized energy level v_i in the disordered Hubbard model can be identified as the position of the Kondo resonance, which is pinned to the Fermi energy in the Kondo limit $Z_i \to 0$. We can thus interpret the surprising enhancement of disorder screening in the strongly-correlated regime as a reflection of the non-perturbative Kondo physics captured by our DMFT method, but not by standard weak-coupling theories.

4.6 Finite temperature conductivity: importance of inelastic scattering

In good metals electron-electron scattering is relatively unimportant even at room temperature since the Fermi energy is very large ($\sim 10^4$ K). At these temperatures the scattering is dominated by electron-phonon interactions, which reduce at low temperatures, where the resistivity appears primarily due to the scattering on impurities. High mobility MOSFETs, however, have very low Fermi energy ($E_F \sim 10$ K), and the role of (inelastic) electron-electron scattering has to be reexamined.

Slave boson mean field theory describes only the quasiparticle part of the spectrum, and cannot describe the incoherent processes at finite (nonzero) temperature. The same model that we have studied at $T = 0$ can be studied at finite temperature using iterated perturbation theory. This has been done in Ref. [48]. The results show that the Fermi liquid coherence occurs only at rather low temperatures, while strong inelastic scattering (leading to decoherence) sets in rapidly as the temperature is raised, as shown in the upper panel in Fig. 4.9. The solution within Hartree-Fock theory does not capture inelastic processes, and shows weak temperature dependence of the scattering rate, lower panel in Fig. 4.9. Note that at very low temperatures the DMFT solution gives a much smaller scattering rate than the Hartree-Fock approximation, in agreement with our zero temperature results.

4.7 Conclusions and discussion

In this Chapter we have examined the influence of strong short-ranged interactions on the electron scattering on nonmagnetic impurities. We have formulated and solved this problem in the DMFT limit of large coordination number, where physical quantities like the self-energy and compressibility become local in space, i.e. momentum-independent.

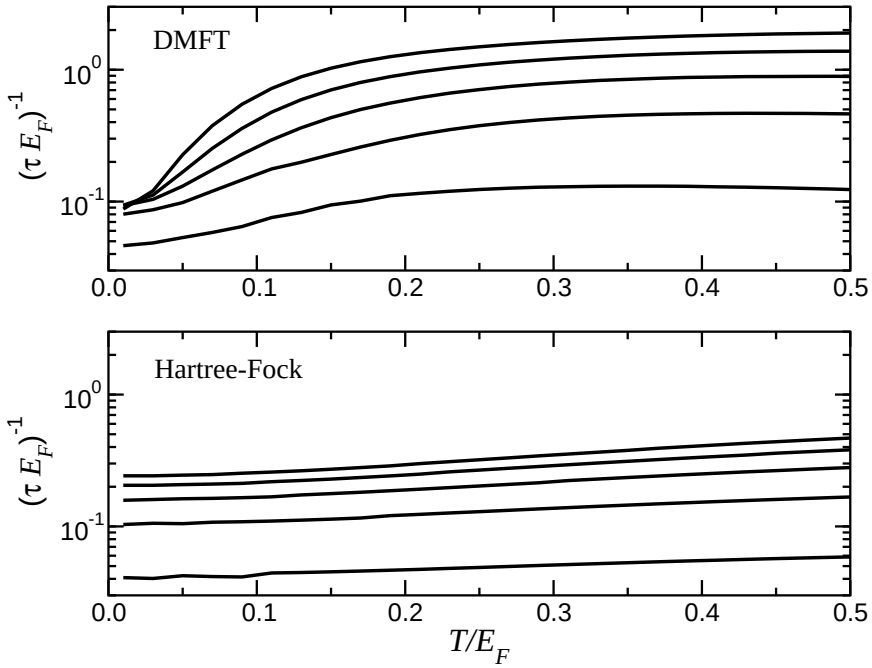

Figure 4.9. Scattering rate $\tau^{-1}(\sim$ resistivity) as a function of temperature. Results are shown for the disorder strength W equal to the interaction U, as we reduce the Fermi energy $E_F/U = 2.0,\ 1.0,\ 0.67,\ 0.5,\ 0.4$ (bottom to top curves). Note the large resistivity drop in the DMFT solution (upper panel), but much weaker temperature dependence within the Hartree-Fock approach (lower panel). From [48].

Within this model, the site disorder is strongly renormalized in the presence of strong electron-electron interactions, which leads to the large enhancement of the scattering time and conductivity. This happens exactly in the regime where the effective mass becomes very large, while the charge compressibility decreases. Therefore, a simple semiclassical connection between the renormalized disorder and charge compressibility from the weak coupling (RPA) theories is not valid in the strong coupling regime. In the following, we will make further connections of our work with the related results from other research groups, discuss the applicability of the results to real physical systems, and outline several important questions which should be addressed in the future research.

After publication of our work, several other research groups have independently solved the same disordered Hubbard model using (extended) DMFT, and obtained essentially the same results. S. Florens [49] has solved the DMFT equations at zero temperature using numerical renormalization group method, and reached the same conclusion that the renormalized

disorder is perfectly screened at the metallic side of the Mott metal-insulator transition in the case of a particle-hole symmetric lattice. Byczuk, Hofstetter, and Vollhardt [43] have obtained the MIT phase diagram within an extended DMFT ("typical medium theory") [8] which includes the Anderson localization effects even on the mean-field level, using the geometrically averaged (typical) local density of states as an order parameter. This work has shown that the Anderson localization effects are strongly suppressed by the electron-electron interactions. Balzer and Potthoff [50] applied another extension of the DMFT ("self-energy-functional" approach) to the Hubbard model with binary site disorder, and obtained a very similar phase diagram.

What are the the implications of our results for a formulation of theory which would realistically describe the metal-insulator transition in high mobility 2D MOSFETs, and in particular, explain the anomalously strong temperature dependence of conductivity in the metallic phase? These questions have raised a lot of dispute within the scientific community in the last ten years, and we cannot claim to provide here definite answers. However, we believe that the amount of evidence favoring the Mott-Anderson metal-insulator scenario, which we advocate, is increasing. In particular, a consensus seems to be reached that the effective mass is strongly enhanced close to the MIT. This is consistent with a picture of the interaction-driven Mott transition. However, as we discussed in some detail in Chapter 3, a strong enhancement of the effective mass cannot be described by different versions of the RPA theory advocated, for example, by Zhang and Das Sarma [35].

Following the idea that the temperature dependent screening is the main mechanism for the large temperature dependence of the conductivity, several authors have suggested that the observed MIT transition is essentially a (semi)classical percolation transition [51, 52]. It is proposed that at low enough carrier densities, the spatial fluctuations associated with the long-range disorder potential arising from the random charged impurity centers, become too strong to be effectively screened by the carriers, leading to screening breakdown that provides spatial inhomogeneities ("hills" and "puddles") giving rise to a percolation MIT transition in conductivity. The percolation theory again assumes a semiclassical, essentially Thomas-Fermi picture of screening, where the "screening cloud" smoothes out the long-ranged Coulomb interaction of randomly displaced charged impurities. However, our results presented in this Chapter seriously question the applicability of the semiclassical

picture of disorder screening in the strong coupling limit, at least in the case of short range interactions.

What are the predictions of our theory in its current stage? First we will discuss its zero temperature predictions as the concentration of carriers is varied. An important question is what is the physical trajectory on the phase diagram, Fig. 4.3, which corresponds to the change of the carrier (electron) density. For a two-dimensional system the Fermi energy (equal to the half-bandwidth D) depends on the carrier density as $E_F \sim n$, while the interaction U goes as $U \sim n^{1/2}$. Therefore, $E_F/U \sim n^{1/2}$. On the other hand, the density of charged impurities does not change with the change of the gate voltage and carrier density. This gives, $W/U \sim n^{1/2}$, and the physical trajectory on the phase diagram should be a hyperbola, $E_F/U \sim W/U$. This hyperbola intersects a dashed line on the phase diagram which corresponds to the Anderson localization. Accordingly, our theory predicts that the metal-insulator transition is of the Anderson localization type, however, modified by the presence of strong electron-electron interaction. A natural extension of our theory to finite temperatures [48], described in Section 4.5, predicts that the strong temperature dependence of the conductivity is a consequence of the inelastic electron-electron scattering. Though these results are to some extent similar to those based on the temperature dependent charged impurity screening [22, 23, 24, 25], the physical origin of the results is completely different. The inelastic scattering, which is argued to be the dominant scattering mechanism at low temperatures for systems with very small Fermi energy, is completely neglected in the impurity scattering based theories.

What are the limitations of our theory? Obviously, in order to have a realistic description of low density 2D MOSFETs, we need to include into the theory long-range Coulomb interactions, and go beyond the large coordination limit in order to describe realistic two-dimensional systems. Also, a further study of Anderson localization effects is necessary for a reliable description of a system close to the metal-insulator transition. Each of these questions by itself poses a difficult and challenging theoretical problem and a step towards a complete understanding of the long standing problem of strongly correlated systems with disorder. We believe that our work further emphasizes a need for developing such a theory, and also presents a promising direction for future research.

CHAPTER 5

DISORDER-DRIVEN NON-FERMI LIQUID BEHAVIOR IN HEAVY FERMION SYSTEMS

In the second part of the thesis we will present our work on the disordered Kondo lattice systems. This research is motivated by the intensive debate among the scientific community about the origin of the non-Fermi liquid (NFL) behavior observed in a large number of heavy fermion alloys. This is considered to be one of the most important problems in contemporary condensed matter physics. Its solution should give us deeper understanding of the competing processes in strongly correlated electronic systems, which lead to the enormous sensitivity of their thermodynamic and transport properties to a change of the chemical composition (doping), application of a magnetic field, or pressure. Also, the physics of heavy fermion materials may give us important guidance in the search to fully understand the mechanism leading to the high temperature superconductivity in cuprates.

5.1 Landau Fermi liquid theory

The Landau Fermi liquid theory [53] forms the foundation of our understanding of the behavior of electrons in metals. It is based on two premises. First, it is recognized that the low energy excitations of a Fermi sea have a very long life time due to the restricted space available for their scattering. Second, these excitations are in one to one correspondence to those of a non-interacting Fermi gas. In another words, switching on the interactions does not qualitatively change the excitation spectrum. We refer to this second premise as the adiabatic continuity.

As a consequence, the thermodynamic properties of metals at low temperatures are very similar to those of a non-interacting Fermi gas. The interaction leads only to the renormalization of the physical parameters which can be described by only a few phenomenological Landau parameters. For example, the effective mass is equal to $m^* = m(1+F_1^s/3)$, and the density of states $N(0) = m^* k_F/\pi^2$. To leading order in the temperature, the specific heat is linear in temperature and the magnetic susceptibility is temperature independent

$$\frac{C_V(T)}{T} \equiv \gamma = \frac{1}{3} m^* k_F, \quad \chi(T) = \frac{m^* k_F \mu_B^2}{\pi^2(1+F_0^a)}. \tag{5.1}$$

Here F_1^s and F_0^a are the Landau parameters. Several predictions about the transport properties come out of the Fermi liquid framework as well. In particular, the resistivity increases as a second power of temperature

$$\rho = \rho_0 + AT^2, \tag{5.2}$$

where ρ_0 is the residual resistivity due to impurities and lattice imperfections, and A is a non-universal constant.

The Landau Fermi liquid theory is originally formulated for clean systems, but its concepts remain applicable also in the presence of disorder [42, 54, 55]. In particular, the magnetic susceptibility χ and specific heat parameter γ remain finite even in the disordered metallic phase. The perturbative quantum corrections to the conductivity are calculated in the case of weak disorder [42], predicting singular terms in the conductivity temperature dependence, which can typically be seen at the experiments at millikelvin temperatures.

Predictions of the Fermi liquid theory survive even in the presence of very strong electron correlation, as in the case of a number of Ce and U compounds. In these systems a strong electron-electron interaction in partially filled f-electron shells leads to a very strong renormalization of the quasiparticle mass which is of the order 10^2 to 10^3 larger then the mass of an electron (hence the name heavy fermions). Experiments on a very well studied heavy fermion compound $CeAl_3$ nicely illustrates Fermi liquid features. The specific heat,

Fig. 5.1(a), is linear with T at the lowest temperatures, with the very large value of the parameter γ. The inverse magnetic susceptibility, Fig. 5.1(b) saturates to a constant at zero temperature, while at higher temperatures follows usual Curie-Weiss law. The electrical resistivity increases with the decreasing temperature, due to the strong scattering of the conduction electrons on f electron local moments. However, at low temperatures the scattering becomes coherent and the resistivity suddenly decreases, Fig. 5.2. At the lowest temperatures, the resistivity follows the predictions of the Fermi liquid theory, Eq. (5.2).

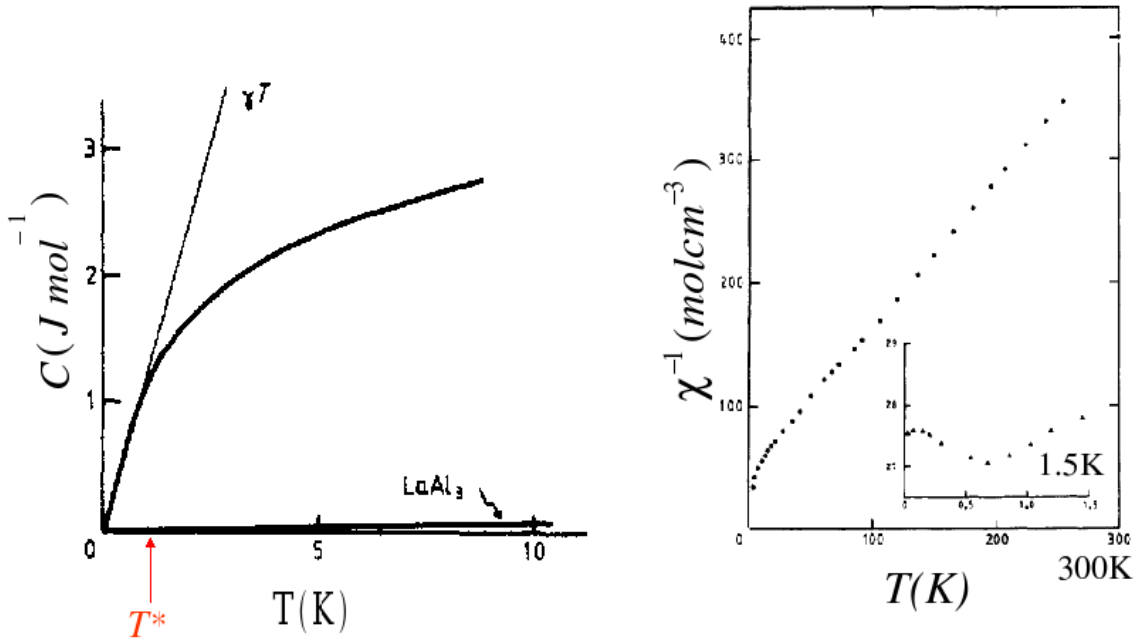

Figure 5.1. (a) Specific heat of $CeAl_3$ as a function of temperature. Bellow a crossover temperature T^*, linear temperature dependence of the specific heat is restored. Note that the specific heat of the "conventional" metal $LaAl_3$ is much smaller (due to the smaller effective mass), and also exhibits Fermi liquid behavior in a much wider temperature region. (b) Inverse magnetic susceptibility of $CeAl_3$ as a function of temperature. At higher T the f-electron of Ce^{3+} act as free local moment which leads to Curie-Weiss $\chi \sim 1/T$ law, but at low temperatures the f-electron spin is "quenched" (screened) by the conduction electrons and Fermi liquid picture with the Pauli form of the magnetic susceptibility takes over. From [56].

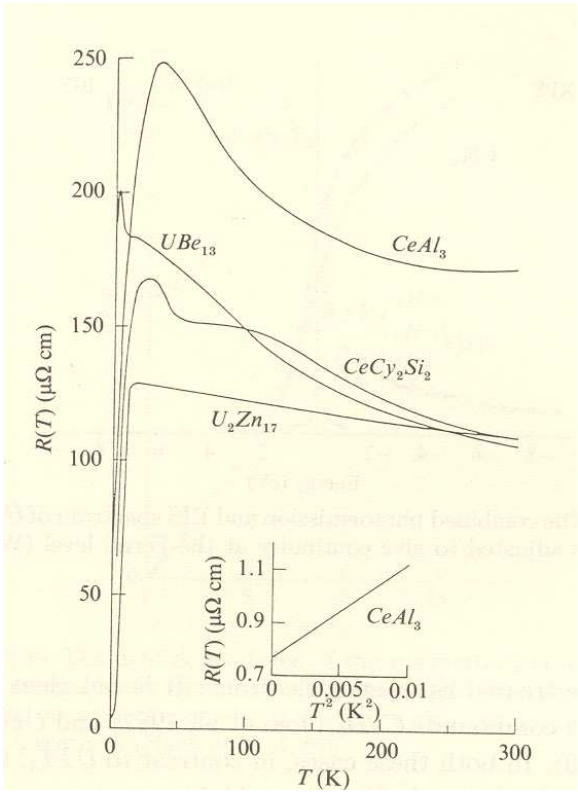

Figure 5.2. Temperature dependence of the electrical resistivity for $CeAl_3$, UBe_{13}, $CeCu_2Si_2$, and U_2Zn_{11}. The inset shows the T^2 behavior for $CeAl_3$ for $T < 0.1$ K. From [57].

5.2 Non-Fermi liquid behavior in heavy fermion alloys

The study of the possible routes which may lead to the breakdown of the Fermi liquid picture in metals has strongly intensified in the last twenty years. The motivation came from experiments on high temperature superconductors and many heavy fermion alloys. In this Section, we will briefly describe two classes of heavy fermion materials, which are extensively studied both experimentally and theoretically.

5.2.1 NFL behavior in the vicinity of the quantum critical point

Heavy fermion metals are generically close to the magnetic ordering due to the antiferromagnetic interaction between f-shell local moments. This interaction is mediated by the

conduction electrons. Many of these materials can easily be tuned to the critical point by changing chemical composition, applying magnetic field or pressure. This makes them ideal for a study of the processes which are driven by strong electron-electron interaction, and/or disorder.

The low temperature region in a vicinity of the quantum critical point is characterized by strong deviations from Landau's Fermi liquid theory. In many cases, the following properties are observed:

- A diverging specific heat coefficient, often logarithmically, $C(T)/T = -\gamma_o \log(T/T_o)$.
- An anomalous temperature dependence of the resistivity, $\rho(T) = \rho_o + AT^\alpha$, where $\alpha < 2$.
- An anomalous Curie-Weiss law, $\chi^{-1}(T) = \chi_0^{-1} + CT^\beta$, where $\beta < 1$.

A typical phase diagram for these materials is presented on Fig. 5.3(a). Undoped $CeCu_6$ is paramagnetic metal, which enters into antiferromagnetic metallic phase by doping with gold. At the critical doping the specific heat coefficient diverges logarithmically, $C/T \sim -\log(T/T_o)$ (Fig. 5.3(b)), magnetic susceptibility follows $\chi = \chi_o(1-\alpha\sqrt{T})$ behavior, and electrical resistivity increases linearly with temperature, $\rho = \rho_0 + AT$.

The first theoretical study of zero temperature magnetic phase transitions in metals was done by John Hertz in 1976 [62]. It assumes that the only important low energy degrees of freedom are long-wavelength paramagnons. This weak coupling spin density wave approach, however, cannot explain properties observed in the vicinity of a quantum critical point in heavy fermions. For example, Hertz theory predicts nonsingular specific heat coefficient and the Fermi liquid form for resistivity. Many attempts have been made to amend the Hertz picture of quantum phase transitions. For example, the apparent momentum independence of the localized critical correlations at the quantum critical point [63] has led to the suggestion that the explanation of the non-Fermi liquid behavior should be searched within the local quantum criticality [64], which follows the ideas of the dynamical mean field theory.

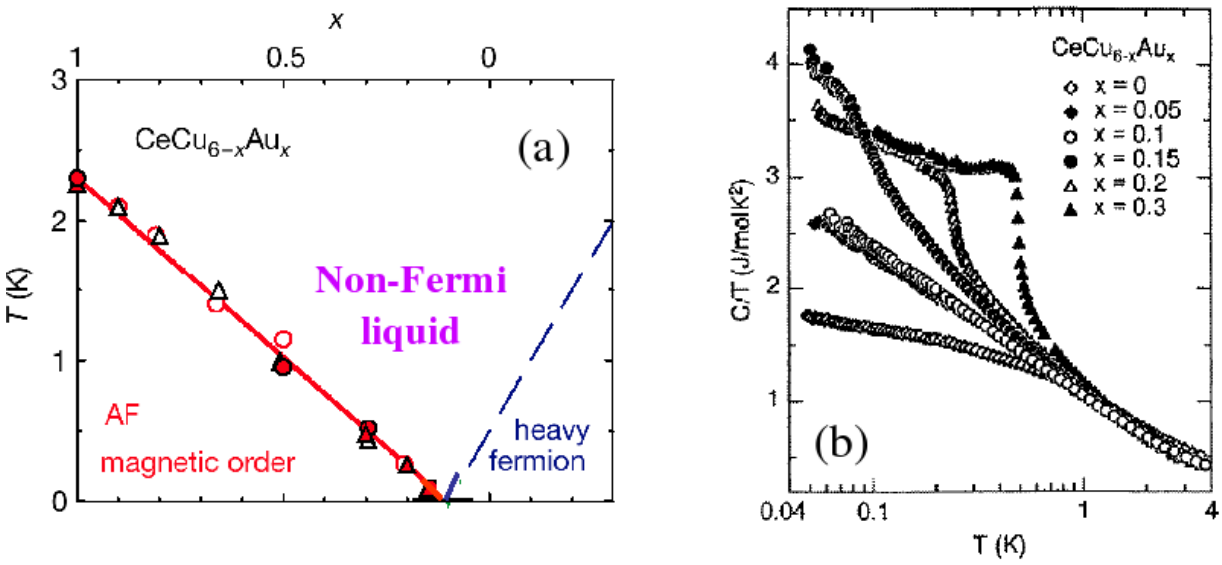

Figure 5.3. (a) Temperature vs. doping phase diagram for $CeCu_{6-x}Au_x$. Paramagnet-antiferromagnet quantum critical point is reached for $x \approx 1$. The region above the critical point has NFL transport and thermodynamic properties. (b) Temperature dependence of the specific heat coefficient, $\gamma \equiv C/T$, for several levels of doping. Note that at the critical concentration the logarithmic behavior persists up to the lowest measured temperatures. From [58].

5.2.2 Disorder-driven NFL behavior

Another class of heavy fermion materials exhibits non-Fermi liquid behavior at the lowest temperatures even away from the critical point. These materials are typically non-stoichiometric compounds with very large residual resistivity. The disorder effects are believed to be crucial for their thermodynamic and transport properties.

A very well studied material from this class is $UCu_{5-x}Pd_x$. Its phase diagram is shown on Fig. 5.4. For doping larger than the critical value $x \approx 1$, the antiferromagnetic order is destroyed, but the properties of the low temperature metallic region clearly deviate from the Fermi liquid framework. The resistivity linearly decreases with temperature, $\rho = \rho_o - AT$,

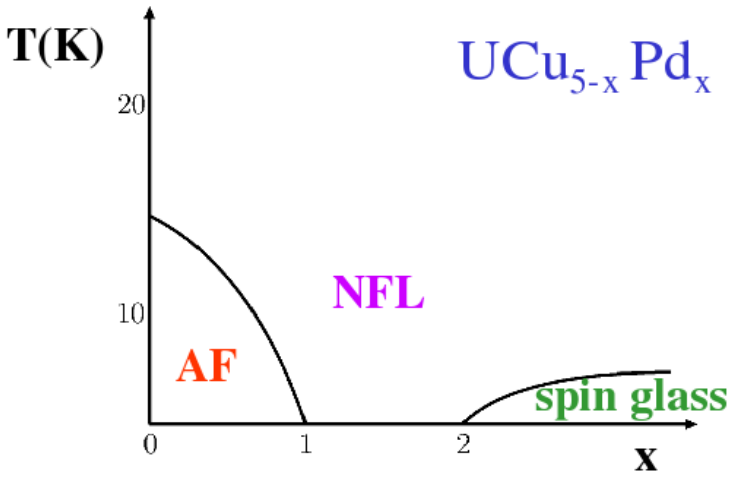

Figure 5.4. Phase diagram for $UCu_{5-x}Pd_x$. From [59].

Fig. 5.5(a), showing no traces of coherent scattering. The magnetic susceptibility, Fig. 5.5(b), and the specific heat diverge approximately logarithmically as $T \to 0$. At even larger doping, $x \gtrsim 2$, the neutron scattering experiments [65] show spin glass ordering at low temperatures. This is to be expected as a consequence of the inter-site RKKY interactions in the strongly disordered environment.

I the remaining part of the thesis, we will concentrate on a theoretical description of disordered heavy fermion compounds. In particular, the emphasis will be to shed light on the interplay of the RKKY interactions which induces magnetic ordering and the Kondo effect which screens the local moments and favors paramagnetic phase.

5.3 NFL behavior in disordered Kondo lattice systems

Kondo (Anderson) lattice models have been established to provide excellent theoretical description of heavy fermion materials. In this Section we will summarize the work which generalizes these models to the case of disordered systems. The results provide strong evidence for the relevance of the disordered Kondo lattice models for description of the thermodynamic and transport properties of $UCu_{5-x}Pd_x$. We will point out, however, to the

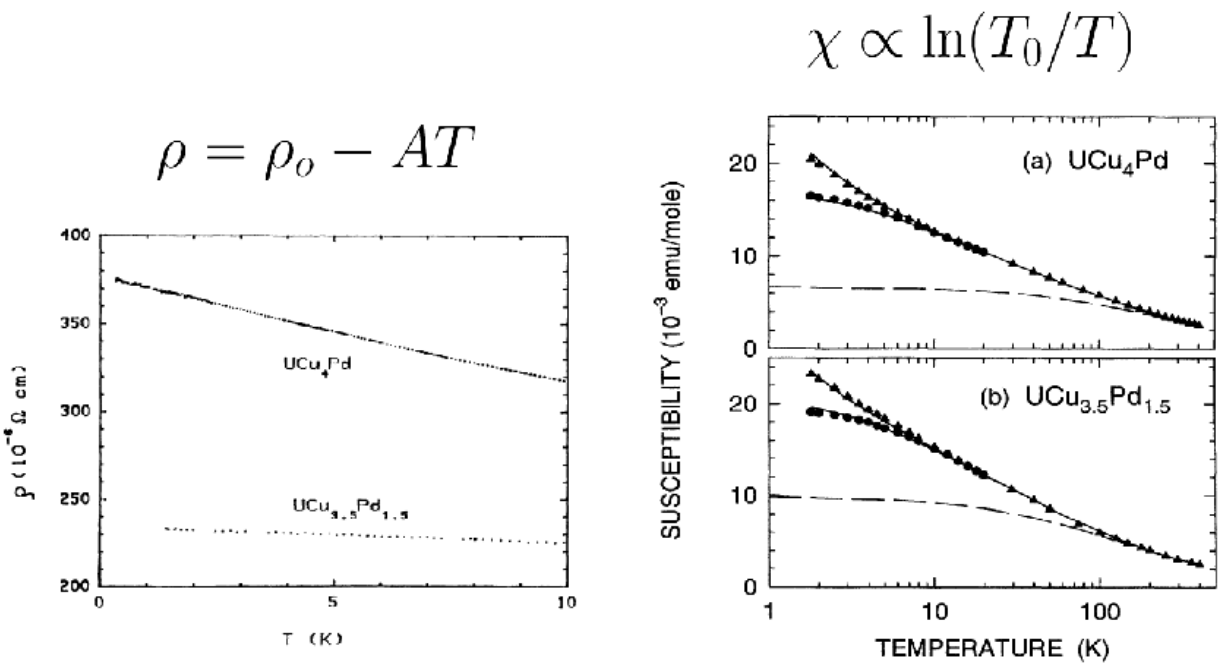

Figure 5.5. Left panel: Electrical resistivity as a function of temperature for $UCu_{5-x}Pd_x$ [60]. Right panel: Magnetic susceptibility vs. temperature measured at $H = 5$ kOe (triangles), and in a stronger magnetic field $H = 50$ kOe [61]. Solid curves: fits to χ (see next Section).

limitations of these studies, which sets up a direction for our subsequent work presented in the final Chapters of the thesis.

5.3.1 Phenomenological Kondo disorder model

The disorder based mechanism for explanation of the non-Fermi liquid thermodynamic properties of $UCu_{5-x}Pd_x$ has been first proposed by Bernal *et al.* [61] It came out of the nuclear magnetic resonance (NMR) measurements which have shown large broadening of resonances in NMR spectra. Since the Knight shift (the shift in resonant frequency) is proportional to the local susceptibility, $K(R) \propto \chi(R)$, the broadening of the resonances is ascribed to the inhomogeneous distribution of the local susceptibility associated with the U ions.

The local susceptibility in the Kondo system is related to the local Kondo temperature by a simple formula due to Wilson [4]

$$\chi(T, T_K) = \frac{C}{T + aT_K}. \tag{5.3}$$

The Kondo temperature is, as usual, approximatelly equal to

$$T_K = De^{-1/\rho J}, \tag{5.4}$$

where ρ is the local density of states, J is the local Kondo coupling, and D is the bandwidh of the conduction electrons. Bernal *et al.* obtained a fit for the NMR line-widths by adjusting the distribution $P(T_K)$ of the Kondo temperatures. The results, Fig. 5.6, show that $P(T_K)$ has a finite intercept with x-axis, meaning that at arbitrary small temperature T, there will always be a finite fraction of spins with $T_K < T$. These spins are effectively decoupled from the conduction bath and provide dominant contribution to the magnetic susceptibility and specific heat. The leading temperature dependence of the uniform susceptibility can easily be obtained as an average value of the local susceptibility

$$\begin{aligned} \chi(T) &= \overline{\chi(T, T_K)} = \int_0^\infty P(T_K)\chi(T, T_K)dT_K = \int_0^\Lambda dT_K P(T_K)\frac{C}{T + aT_K} \\ &= \int_0^\Lambda dT_K P(0)\frac{C}{T + aT_K} + \text{const.} \sim \ln\left(\frac{T_0}{T}\right). \end{aligned} \tag{5.5}$$

The results for the uniform (bulk) susceptibility are in excellent agreement with the experimental data, Fig. 5.5. It is interesting to notice that a successful fit to the experimental data is obtained for fitting parameter which corresponds to moderate amount of disorder.

5.3.2 Disordered Kondo lattice model within DMFT: transport properties

Phenomenological Kondo disorder model treated local moments as independent though U ions form a dense lattice. The limitations of this approach are the most obvious in calculating the transport properties where, for example, the effects of coherent scattering at low temperatures are completely omitted. The disorder effects are studied within more

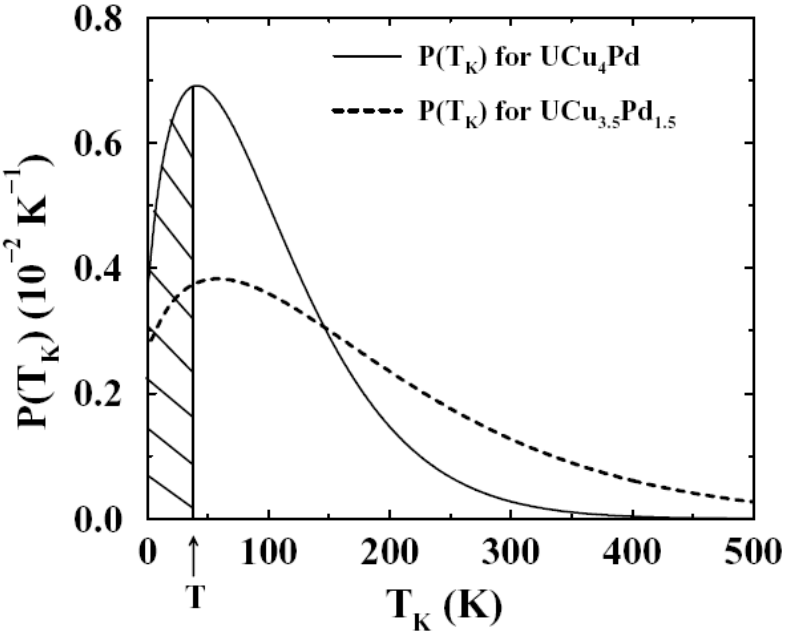

Figure 5.6. Distribution of Kondo temperatures obtained within the Kondo disorder model from an analysis of the NMR data for $UCu_{5-x}Pd_x$ [61]. Spins with $T_K < T$ (shaded area) dominate the thermodynamic response.

realistic microscopical model by Miranda *et al.* [6, 66]. They considered Anderson lattice model as given by the Hamiltonian

$$\begin{aligned} H &= -t\sum_{\langle ij\rangle\sigma}(c^\dagger_{i\sigma}c_{j\sigma} + \text{H.c.}) + \sum_{j\sigma}\left(V_j c^\dagger_{j\sigma}f_{j\sigma} + \text{H.c.}\right) \\ &+ \sum_{j\sigma} E_{fj} f^\dagger_{j\sigma}f_{j\sigma} + U\sum_j f^\dagger_{j\uparrow}f_{j\uparrow}f^\dagger_{j\downarrow}f_{j\downarrow}. \end{aligned} \tag{5.6}$$

Here $f_{j\sigma}$ and $c_{j\sigma}$ are annihilation operators for f- and conduction electrons, respectively. The kinetic energy of the conduction electrons is proportional to the hopping parameter t. The largest energy scale in the model is the Coulomb repulsion energy U of the f-electrons occupying the same site j, and this energy is set to infinity, thus preventing the double occupancy of the f-sites. V_j is the hybridization parameter, and E_{fj} is the f-electron energy on the site j. The local Kondo temperature in the Anderson model is

$$T_{Kj} \approx De^{-|E_{fj}|/(2\rho V_j^2)}, \tag{5.7}$$

and the connection to the Kondo model is obtained from $J_j = 2V_j^2/|E_{fj}|$.

The disordered Anderson lattice model has been solved within dynamical mean field theory, and various thermodynamic and transport properties have been obtained. The disorder distribution in both V_j and E_{fj} is considered, and it is fitted to reproduce the same distribution of local Kondo temperatures as in the work of Bernal *et al.* [61]. The main results of this work are the following:

(i) Bulk thermodynamic responses in the Anderson/Kondo lattice models can be very accurately obtained through an ensemble average of the individual contribution from each site, thus justifying the procedure of Ref. [61].

(ii) Although the clean system has low resistivities due to the onset of coherence at low T, moderate amounts of f-shell disorder are capable of destroying this low-T coherence, leading to characteristic incoherent Kondo scattering behavior. The essential condition for the linear dependence in low temperature resistivity is that $P(T_K = 0) \neq 0$.

The work of Miranda *et al.* [6, 66] has explained the anomalous linear temperature dependence of resistivity, but several important questions remained unanswered. In particular, the results are very sensitive on the form of the disorder distribution, and rely on the finite value of $P(T_K = 0)$. There are no apparent physical reasons favoring this type of distribution. Also, there are many other compounds which exhibit power low divergence in thermodynamic properties instead of the logarithmic one, but again fine tuning of the disorder distribution is needed to explain such properties. This problem is resolved within an extended DMFT approach described in the next Section.

5.3.3 Statistical DMFT approach: electronic Griffiths phase as a precursor to the Mott-Anderson MIT

Within standard DMFT approach, even in the presence of disorder, each site "sees" the same conduction bath and spatial fluctuations of the electronic wave functions are completely neglected. This is one of the most severe limitations of DMFT, and it is an immediate consequence of the assumption of large (infinite) coordination number which is embedded into the standard formulation of DMFT. Spatial fluctuations in the electronic wave functions (density of states) are included within "statistical" dynamical mean field theory (statDMFT) developed by Dobrosavljević and Kotliar [67, 68]. The assumption of retaining only on-site correlations, as in DMFT, is maintained in statDMDF. In another words,

the self-energy remains to have only the frequency, and not the momentum dependence. However, in the disordered case statDMFT treats the lattice with finite coordination number, and the self-consistency condition is no longer a simple algebraic equation, but rather a set of stochastic equations in the local Green functions whose distribution has to be determined numerically. If the interactions are turned off, the treatment of disorder is equivalent to the self-consistent theory of localization [69].

The inclusion of spatial fluctuations in the local density of states has important consequences on the thermodynamic properties of disordered Kondo lattice systems which can be anticipated already from the expression for the local Kondo temperature $T_K(x) \approx D\exp(-1/\rho(x)J(x))$. We notice that the fluctuations in the conduction bath lead to the disorder in the Kondo temperatures even in the absence of disorder in the Kondo couplings. Miranda and Dobrosavljević [70] have established a remarkable universality in the form of the distribution functions for Kondo temperatures. The most important results are the following:

(a) For weak disorder the distribution of Kondo temperatures $P(T_K)$ has log-normal form, and for stronger disorder it assumes the power law form $P(T_K) \sim T_K^{\alpha-1}$. A crossover to the NFL region is obtained for $\alpha = 1$. For $\alpha = 1$, $P(T_K = 0) = \text{const.}$, there is a logarithmic divergence in magnetic susceptibility, and for $\alpha < 1$, $P(T_K = 0) = \infty$, and the divergence assumes the power law form, $\chi \sim T^{\alpha-1}$, Fig. 5.7.

(b) The results are qualitatively and semi-quantitatively the same in the presence of disorder in the Kondo couplings J (i.e. E_f and V) and in the presence of a site disorder in the conduction bath. Furthermore, the distribution of the Kondo temperatures has the same form for both discrete and continuous, bounded and unbounded distribution of the bare disorder. (A detailed discussion of these features is presented in the next Chapter of the thesis.)

(c) The NFL region generically appears before the Mott-Anderson metal-insulator transition is reached. A schematic phase diagram for the disordered Kondo/Anderson lattice is shown in Fig. 5.8.

The thermodynamic and transport properties in the NFL region are dominated by the small fraction of sites with the lowest Kondo temperatures. This resembles to the situation in disordered insulating magnets studied originally by Griffiths [71], and later

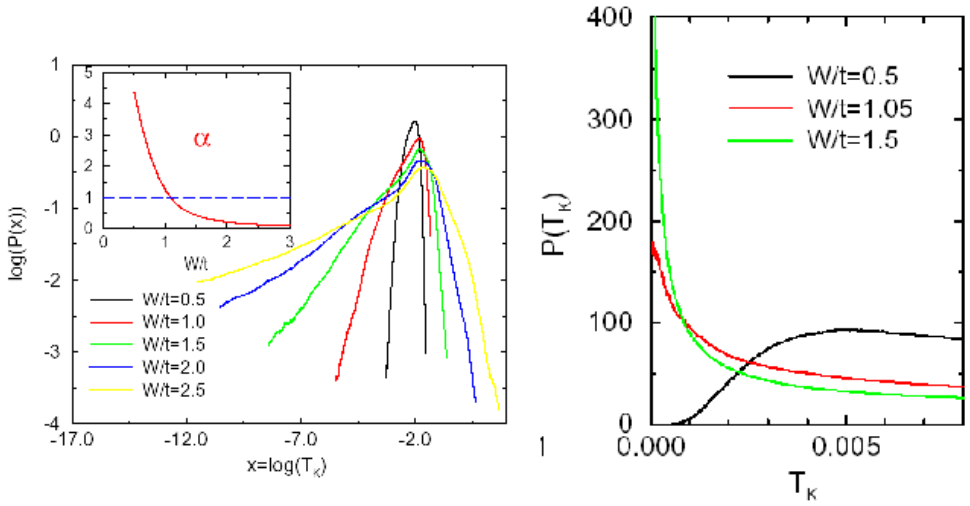

Figure 5.7. Distribution of local Kondo temperatures within *stat*DMFT [70]. For stronger disorder W the distribution assumes a power law form $P(T_K) \sim T_K^{\alpha-1}$.

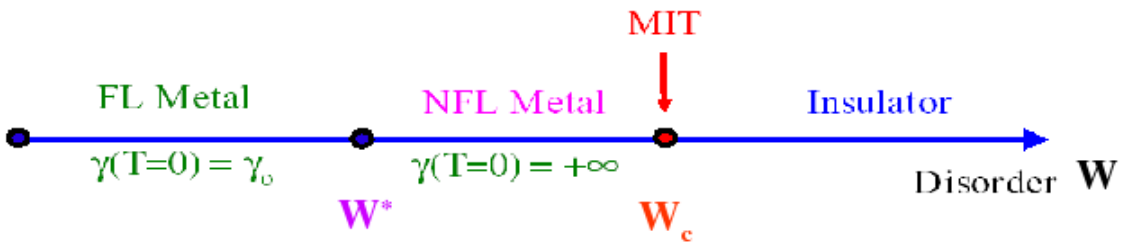

Figure 5.8. Schematic phase diagram for the disordered Kondo/Anderson lattice.

by McCoy and Wu [72]. In these systems a formation of rare large magnetic clusters is well established. Although their number is exponentially rare, they provide the leading thermodynamic response with power low singularities with disorder-dependent power law exponent. Such systems whose properties are dominated by the rare events are classified as Griffiths phases. Therefore NFL region that appears in the Kondo lattice systems as a precursor to the Mott-Anderson MIT is named *electronic Griffiths phase* (EGP). Note that the Griffiths phase in this model is not connected to any form of magnetic ordering, and in this sense it is an alternative to the magnetic Griffiths phase scenario in the disordered

Kondo lattice systems introduced by Castro Neto and Jones [73, 74] which has provoked a lot of controversy and debate [75, 76].

5.3.4 Limitations of the statDMFT picture of the electronic Griffiths phase

The model of the electronic Griffiths phase within statDMFT is not completely satisfactory because of the following reasons:

(a) The magnetic susceptibility and specific heat exhibit power law divergence with the disorder dependent power law exponent. For stronger disorder this would lead to very strong power law singularities while in the experiments only logarithmic, or weak power law singularities are seen.

(b) Quite generally, the spins which are Kondo unscreened at temperature T, and act as local moments, are not completely free due to the long ranged RKKY interactions (see Fig. 5.9 for a schematic illustration). The RKKY interaction favors spin glass phase at low temperatures as seen in experiments.

Therefore, our subsequent work has concentrated on the study of the influence of additional RKKY interactions on the properties of the electronic Griffiths phase. As a preliminary step, we have derived a simplified effective model of the EGP within standard DMFT [77], which qualitatively and semi-quantitatively reproduces all the features obtained within more generic statDMFT. This work is presented in detail in Chapter 6. The effects of

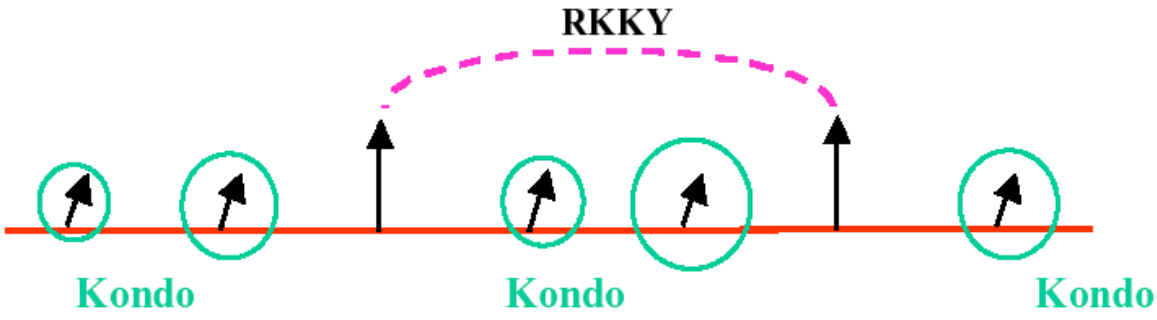

Figure 5.9. Schematic illustration of the interplay of the RKKY interactions and the Kondo effect.

additional inter-site RKKY interactions are studied within the effective model of the EGP in Chapter 7.

CHAPTER 6

EFFECTIVE MODEL FOR THE ELECTRONIC GRIFFITHS PHASE

In this Chapter we introduce and solve an effective model for the electronic Griffiths phase as a DMFT model with a Gaussian distribution of random site energies. We should emphasize that localization is not present in this effective model, but the Griffiths phase emerges in qualitatively the same fashion as in the more realistic calculations within "statistical" DMFT [70, 78]. We discuss how the specific disorder distribution which is hand-picked in the effective model is dynamically generated by fluctuation effects within the *stat*DMFT formulation, elucidating the origin of the universality of the Griffiths phase behavior. In addition, the simplicity of this DMFT effective model makes it possible to describe all the qualitative features of the solution using simple analytical arguments, thus eliminating the need for large scale numerical computations in the description of the electronic Griffiths phase. This is crucial in order to address more complicated issues, such as the role of additional RKKY interactions in disordered Kondo alloys [79].

6.1 Model

We consider the Anderson lattice model where the disorder is introduced by random site energies ε_i in the conduction band, as given by the Hamiltonian

$$\begin{aligned} H &= -t\sum_{\langle ij\rangle\sigma}(c^\dagger_{i\sigma}c_{j\sigma}+\text{H.c.})+\sum_{j\sigma}(\varepsilon_j-\mu)c^\dagger_{j\sigma}c_{j\sigma} \\ &\quad +V\sum_{j\sigma}\left(c^\dagger_{j\sigma}f_{j\sigma}+\text{H.c.}\right)+\sum_{j\sigma}E_f f^\dagger_{j\sigma}f_{j\sigma} \\ &\quad +U\sum_j f^\dagger_{j\uparrow}f_{j\uparrow}f^\dagger_{j\downarrow}f_{j\downarrow}, \end{aligned} \tag{6.1}$$

where $f_{j\sigma}$ and $c_{j\sigma}$ are annihilation operators for f- and conduction electrons, respectively. V is the hybridization parameter, and E_f is the f-electron energy. We assume $U \to \infty$, and choose a Gaussian distribution of random site energies for the conduction band

$$P(\varepsilon_i) = (2\pi W^2)^{-1/2} \exp\{-\frac{1}{2}\varepsilon_i^2/W^2\}. \tag{6.2}$$

In Sec. 6.4 we will explain how this particular disorder distribution comes out naturally from the more generic *stat*DMFT approach.

To solve these equations, we use the DMFT approach [5], which is formally exact in the limit of large coordination. We concentrate on a generic unit cell j, containing an f-site and its adjoining conduction electron Wannier state. After integrating out the conduction electron degrees of freedom, we obtain the effective action for the f-electron on site j

$$\begin{aligned} S_{imp}(j) &= \sum_\sigma \int_0^\beta d\tau \int_0^\beta d\tau' f_{j\sigma}^\dagger(\tau) \left[\delta(\tau-\tau')(\partial_\tau + E_f)\right. \\ &+ \left. \Delta_{fj}(\tau-\tau')\right] f_{j\sigma}(\tau'). \end{aligned} \tag{6.3}$$

Here, the restriction of no double f-site occupancy is implied. The hybridization function Δ_{fj} between the f-electron and the conduction bath Δ_c is given by

$$\Delta_{fj}(i\omega_n) = \frac{V^2}{i\omega_n - \varepsilon_j + \mu - \Delta_c(i\omega_n)}. \tag{6.4}$$

The self-consistency condition for the conduction bath (cavity field) assumes a simpler form for the semi-circular model density of states [5], which we use for simplicity. All the qualitative features of our solution are independent of the the form of the lattice, and the quantitative results depend only weakly on the details of the electronic band structure. For this model $\Delta_c(i\omega_n) = t^2\overline{G_c}(i\omega_n)$, where $\overline{G_c}(i\omega_n)$ is the disorder-averaged Green's function of the conduction electrons, and the self-consistency is enforced by

$$\overline{G_c}(i\omega_n) = \langle [i\omega_n - \varepsilon_j + \mu - t^2\overline{G_c}(i\omega_n) - \Phi_j(i\omega_n)]^{-1} \rangle, \tag{6.5}$$

where

$$\Phi_j(i\omega_n) = \frac{V^2}{i\omega_n - E_f - \Sigma_{fj}(i\omega_n)}, \tag{6.6}$$

and Σ_{fj} is the f-electron self-energy derived from the impurity action of Eq. (6.3). From a technical point of view, within DMFT the solution of the disordered Anderson lattice

problem reduces to solving an ensemble of a single impurity problems supplemented by a self-consistency condition.

We will solve the system of Eqs. (6.3)-(6.6) at zero temperature using the slave boson mean field theory approach [80, 81]. This approximation is known [70, 82, 78] to reproduce all the qualitative and even most of the accurately quantitative features of the exact DMFT solution at $T = 0$. It introduces renormalization factors (quasi-particle weights) Z_j and renormalized f-energy levels ε_{fj}, which are site-dependent quantities in the case of a disordered lattice. These parameters are determined by the saddle-point slave boson equations (see Ref. [6] for more details) which, on the real frequency axis, assume the form

$$-\frac{1}{\pi}\int_{-\infty}^{0} d\omega \,\mathrm{Im}\left[\frac{1}{\omega - \varepsilon_{fj} - Z_j\Delta_{fj}(\omega)}\right] = \frac{1}{2}(1 - Z_j), \tag{6.7}$$

$$\frac{1}{\pi}\int_{-\infty}^{0} d\omega \,\mathrm{Im}\left[\frac{\Delta_{fj}(\omega)}{\omega - \varepsilon_{fj} - Z_j\Delta_{fj}(\omega)}\right] = \frac{1}{2}(\varepsilon_{fj} - E_f). \tag{6.8}$$

Eq. (6.6) in this case becomes

$$\Phi_j(\omega) = \frac{Z_j V^2}{\omega - \varepsilon_{fj}}. \tag{6.9}$$

6.2 Analytical solution in the Kondo limit

Before presenting a numerical solution of the slave boson Eqs. (6.7)-(6.8) supplemented by the self-consistency condition of Eq. (6.5), we will solve these equations analytically in the Kondo limit for a *given* conduction bath. A comparison with the numerical solution will show that the self-consistency does not qualitatively change the analytical results.

The slave boson equations simplify in the Kondo limit $Z_j \to 0$. The integral in Eq. (6.7) is dominated by the low-frequency region, and the frequency dependence in Δ_c and Δ_{fj} can be neglected. Therefore, after integration

$$\varepsilon_{fj} \approx -Z_j \mathrm{Re}\left[\Delta_{fj}(0)\right], \tag{6.10}$$

where, for simplicity, we took a semi-circle conduction bath with $\mu = 0$. In the integral of Eq. (6.8), the frequency dependence of Δ_{fj} can also be neglected. Introducing the energy cutoff D and using Eq. (6.10) we obtain (see Appendix A for the details of the derivation)

$$
\begin{aligned}
Z_j &\approx D\frac{\varepsilon_j^2+(\pi t^2\rho_o)^2}{\pi t^2\rho_o V^2}e^{-\pi^2 t^2\rho_o/J}e^{-\varepsilon_j^2/t^2\rho_o J}e^{\varepsilon_j/2t^2\rho_o} \\
&= Z_o\frac{\varepsilon_j^2+(\pi t^2\rho_o)^2}{(\pi t^2\rho_o)^2}\exp\left[-\frac{\varepsilon_j^2}{t^2\rho_o J}\left(1-\frac{J}{2\varepsilon_j}\right)\right]. \qquad (6.11)
\end{aligned}
$$

Here, ρ_o is the density of states (DOS) of the conduction electrons at the Fermi level, $J = 2V^2/|E_f|$, and $Z_o = Z(\varepsilon_j = 0)$. The Kondo temperature is proportional to the quasi-particle weight, $T_{Kj} = \pi V^2\rho_o Z_j$. In the limit $\varepsilon_j \gg J/2$ and neglecting a weak site-energy dependence in the pre-factor, we obtain

$$T_{Kj} \approx T_K^0 e^{-1/\lambda_j}, \qquad (6.12)$$

where the site dependent coupling constant is

$$\lambda_j = \frac{t^2\rho_o J}{\varepsilon_j^2}, \qquad (6.13)$$

and T_K^0 is the Kondo temperature in the clean limit (for $\varepsilon_j = 0$). From these equations, we can immediately find the desired distribution of local Kondo temperatures $P(T_K) = P(\varepsilon(T_K))|d\varepsilon/dT_K|$, which (up to a negligible logarithmic correction) is given asymptotically by

$$P(T_K) \propto (T_K/T_K^0)^{\alpha-1}, \qquad (6.14)$$

with

$$\alpha(W) = \frac{t^2\rho_o J}{2W^2}. \qquad (6.15)$$

This expression is one of the central results of this Chapter. It has exactly the form expected for a Griffiths phase, where the exponent characterizing the local energy scale distribution assumes a parameter-dependent (tunable) form.

To show how the NFL behavior appears due to the singularity in $P(T_K)$, we use the standard expression due to Wilson for the magnetic susceptibility [4]

$$\chi(T, T_K) = \frac{C}{T + aT_K}, \qquad (6.16)$$

which is an excellent approximation for a single Kondo impurity. Here C and a are constants. In the disordered case, we can split the average susceptibility $\chi(T) = \int_0^\infty P(T_K)\chi(T, T_K)dT_K$ in a regular "bulk" part

$$\chi_r(T) = \int_\Lambda^\infty P(T_K)\chi(T, T_K)dT_K, \qquad (6.17)$$

and a potentially singular part

$$\chi_s(T) = C_1 \int_0^{\Lambda} \frac{T_K^{\alpha-1}}{T + aT_K} dT_K, \tag{6.18}$$

coming from the tail with low Kondo temperatures (Λ is a crossover scale). At weak disorder, the exponent α is large and the distribution $P(T_K)$ is regular, $\chi(0) = \chi_o + C_2/(\alpha - 1)$, but NFL behavior emerges once $\alpha \leqslant 1$, which corresponds to

$$W \geq W_{nfl} = \sqrt{t^2 \rho_o J/2}. \tag{6.19}$$

For $\alpha = 1$ the magnetic susceptibility has a logarithmic divergence, $\chi(T) \propto \ln(1/T)$, characteristic of marginal Fermi liquid behavior [83], while for $\alpha < 1$ a power law divergence is obtained, $\chi(T) \propto T^{\alpha-1}$ as $T \to 0$. The same singularity also leads to an anomalous behavior in the transport properties, as shown in detail in Refs. [6] and [66].

6.3 Numerical results

In the above derivation we ignored the fact that the conduction bath Δ_c has to be self-consistently determined. This will also produce particle-hole asymmetry and an asymmetric distribution of Kondo temperatures T_{Kj}. A nonzero chemical potential will further increase this asymmetry. However, the numerical solution we obtained using the slave boson approximation at zero temperature shows that the essential physics described by Eqs. (6.12)-(6.15) remains qualitatively correct. The distribution of local Kondo temperatures in the asymptotic limit is indeed a power law, $P(T_K) \sim {T_K}^{\alpha-1}$, where the exponent α is a decreasing function of disorder.

Fig. 6.1 shows the distribution $P(T_K)$ for several values of the disorder distribution strength W. For the parameters that we here use, the system is close to the Kondo limit, and the Kondo gap of the clean system is approximately 0.04 (in energy units of the half bandwidth of bare DOS). The NFL behavior appears for $W \gtrsim 0.14$. We note that in the NFL regime the power law behavior appears already for the site energies ε_j which deviate only moderately from the mean (zero) value. In other words, the asymptotic behavior is established *well before* we attain very rare realizations of ε_j which belong to the tail of the Gaussian distribution. For example, for $W = 0.3$, sites with $\varepsilon_j \gtrsim 0.4$ (which correspond to $Z \lesssim 0.01$) are already in the power-law regime.

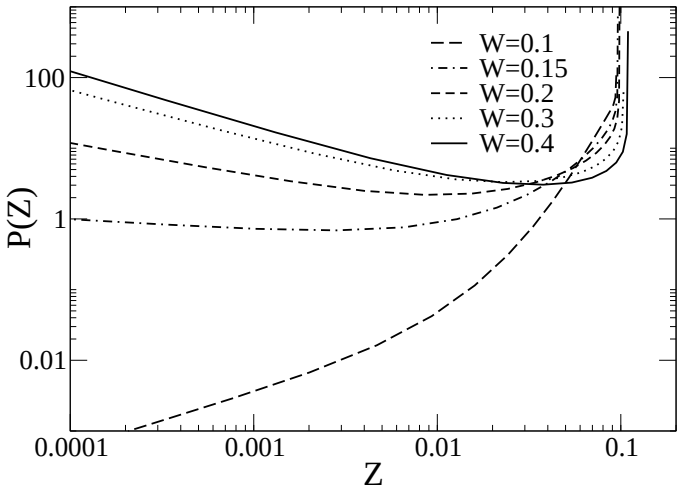

Figure 6.1. Distribution of the local Kondo temperatures. The disorder ranges from moderate $W = 0.1$ to strong $W = 0.4$. We used $V = 0.5$, $E_f = -1$, and $\mu = -0.1$.

According to the simplified derivation from Sec 6.2, the exponent α is inversely proportional to W^2. The numerical results shown in Fig. 6.2 confirm such behavior for weak and moderate disorder. For strong disorder there appear some deviations from this formula, which can be ascribed to the dependence of the DOS at the Fermi level on the disorder strength.

Before we present arguments which justify our effective DMFT model approach, let us make a direct comparison with the *stat*DMFT results from Ref. [78]. In this approach, very broad distributions of local Kondo temperatures are generated for *arbitrary* distributions of bare disorder. In particular, even if the bare distribution is bounded, sites with arbitrarily small Kondo temperatures will exist, and their distribution will have a power law tail. This is a consequence of the spatial fluctuations of the conduction electron cavity field, as we discuss in detail in the next Section. In Fig. 6.3 we compare the values of the exponent α for the effective model with Gaussian disorder of variance W^2, and the *stat*DMFT results obtained for a *bounded* uniform distribution of bare disorder with the same variance. Remarkably, not only does the electronic Griffiths phase emerge in the same fashion, but the numerical values of disorder strength determining the onset of NFL behavior are also almost the same. The comparison is made for two different values of the chemical potential. As we move further

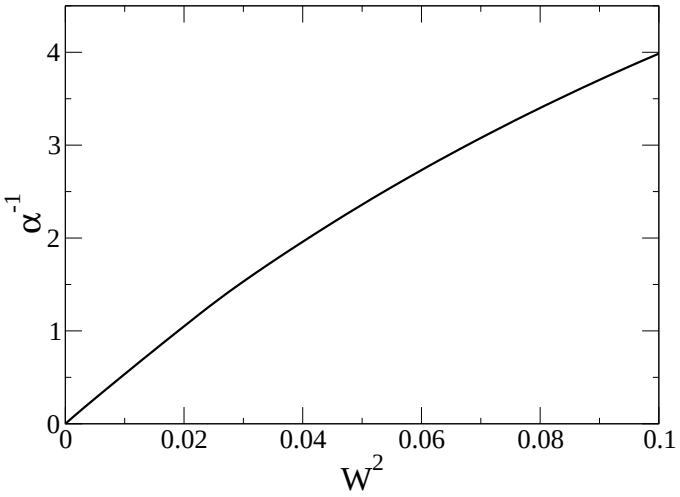

Figure 6.2. Inverse power law parameter α^{-1} as a function of W^2. For weak and moderate disorder this dependence is linear. Here $V = 0.5$, $E_f = -1$, and $\mu = -0.2$.

away from half-filling by changing the chemical potential, the critical value W_{nfl} decreases. That is expected since α should be proportional to the bare (noninteracting) DOS at the Fermi level.

6.4 The role of spatial fluctuations and the form of renormalized disorder

In this Section we explain the universal aspects of the emergence of the electronic Griffiths phase within the more generic statistical DMFT. In particular, we show how the Gaussian tails in the distribution of renormalized disorder appear for an arbitrary form of the bare disorder. Moreover, we present arguments showing that the Griffiths phase appears generically as a precursor of the Mott-Anderson metal-insulator transition.

6.4.1 Universality of the renormalized disorder distribution

In the above DMFT formulation, we had to choose a special form of disorder distribution in order to obtain the desired power-law distribution of Kondo temperatures. Had we chosen a different distribution, the results would not have held. For example, for a

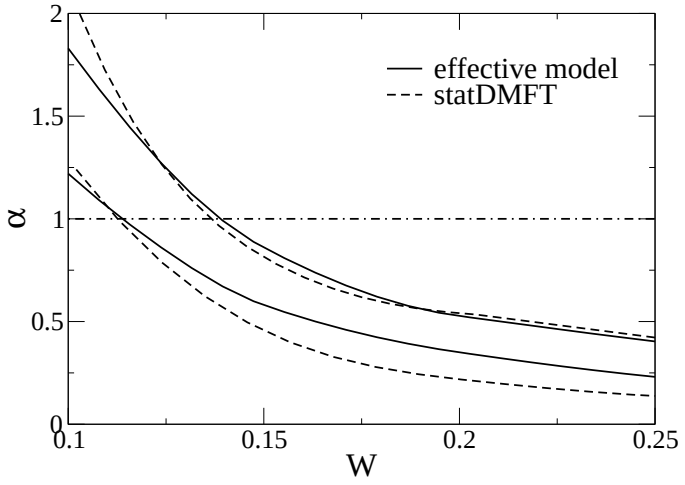

Figure 6.3. Power law exponent α as a function of disorder strength measured by the standard deviation W. Full lines are the effective model results, and dashed lines are the *stat*DMFT results. The hybridization V is taken to be 0.5 and $E_f = -1$. The chemical potential is $\mu = -0.1$ (upper lines), and -0.5 (lower lines). The onset of NFL behavior occurs at $\alpha = 1$.

bounded distribution of site energies, there would always be a minimum value of the Kondo temperature, and thus no power-law tail. On the other hand, from numerical simulations of lattices with finite coordination, it has been established that the emergence of the Griffiths phase is a universal phenomenon [78]. Why? To understand the reason for this, we note that for finite coordination (as opposed to the DMFT limit) the cavity bath Δ_c is not self-averaging, but is a site-dependent, random quantity Δ_{cj}. In this *stat*DMFT formulation, the local conduction electron Green's function is given by

$$G_{cj}(i\omega_n) = \frac{1}{i\omega_n - \varepsilon_j + \mu - \Delta_{cj}(i\omega_n) - \Phi_j(i\omega_n)}, \tag{6.20}$$

where Φ_j describes the local scattering of the conduction electrons off the f-shell at site j, and is given as before by Eq. (6.6).

For weak disorder, the corresponding fluctuations are small, and we can separate

$$\Delta_{cj} = \Delta_c^{av} + \delta\Delta_{cj}. \tag{6.21}$$

In the following, we compute the distribution function for the fluctuations of the cavity field, which will lead to the renormalized form of the disorder distribution function. The

renormalized site energies can be defined as

$$\widetilde{\varepsilon}_j = \varepsilon_j + \delta\Delta_{cj}^R, \tag{6.22}$$

where $\delta\Delta_{cj}^R = \mathrm{Re}\,[\delta\Delta_{cj}(\omega = 0)]$. We stress that the cavity fluctuations are present for a general finite coordination electronic system in the presence of disorder of any kind. In particular, the disorder in hybridization parameters V_j, or local f-energy levels E_{fj}, will induce fluctuations in the local DOS even if random site energies ε_j in the conduction band are absent. Furthermore, as we argue in the next subsection, the renormalized distribution $P(\widetilde{\varepsilon}_j)$ will have universal Gaussian tails even if the bare distribution $P(\varepsilon_j)$ is bounded. Note that $\delta\Delta_{cj}$ has a real as well as an imaginary part $\delta\Delta_{cj}^I$, due to the fact that fluctuations locally violate particle-hole symmetry. However, we show in Appendix B that $\delta\Delta_{cj}^I$ fluctuations, at least when treated to leading order, do not produce singular behavior in $P(T_K)$ and therefore can be neglected when examining the emergence of the electronic Griffiths phase.

6.4.2 The Gaussian nature of the renormalized distribution

From detailed numerical studies it has become clear that the onset of the Griffiths phase in disordered Anderson lattices generally occurs already for a relatively moderate amount of disorder. In this limit, the relevant distributions are determined essentially by the central limit theorem, therefore resulting in a Gaussian form of the tails for $P(\widetilde{\varepsilon}_j)$. This is precisely what is needed to justify the DMFT effective model, where such Gaussian tails are assumed from the outset.

Before engaging in more precise computations of these distributions, it is worth pausing to comment on the physical validity of the assumed Gaussian statistics, i.e. the relevance of the central limit theorem in the cases of interest. Quite generally, if a certain quantity can be represented as a sum of a large number of independent random variables, then the central limit theorem tells us that the resulting distribution will be Gaussian, irrespective of the specific form of the distributions of the individual terms in the sum. In our case, the fluctuations of the local cavity field result from Friedel oscillations of the electronic wave functions, induced by other impurities which may lie at a relatively long distance from the given site. This is a result of the slow ($\sim R^{-d}$) decay of the amplitude of the Friedel oscillations in d dimensions, where R is the distance from the impurity site. The situation

is very reminiscent of the Weiss molecular field of an itinerant magnet, where the RKKY spin-spin interactions have a long range character for the very same reason, being as they are a reflection of similar Friedel oscillations. Furthermore, as we will explicitly show, the leading corrections (to order $\mathcal{O}\left(W^2\right)$) at weak disorder take the form of a linear superposition of contributions from single impurity scatterers, and thus of a sum of independent random numbers, for which we expect the central limit theorem to hold.

To obtain the precise form of this distribution, it therefore suffices to compute the variance

$$\sigma_R^2 = \left\langle (\delta\Delta_{cj}^R)^2 \right\rangle, \tag{6.23}$$

to leading order in disorder strength. To compute the fluctuations $\delta\Delta_{cj}$ at weak disorder, we note that the cavity field Δ_{cj} can be computed if we consider a particular site with $\varepsilon_j = 0$ (call it site 0), and compute its Green's function in a random medium. At zero frequency for this site

$$\Delta_{co} = \mu - 1/G_{oo}. \tag{6.24}$$

The corresponding variation is

$$\delta\Delta_{co} = \delta G_{oo}/(G_{oo})^2. \tag{6.25}$$

We still need to compute the fluctuation δG_{oo}, which can be expanded in powers of the random potential ε_j. In doing this, we have ignored the interaction renormalizations of the random potential for conduction electrons. We will return to re-examine this effect in Appendix B. Note, however, that in the absence of interactions in the environment of a given site, the following expressions provide the exact leading contributions at weak disorder.

To leading order, we can write

$$\delta G_{oo} = \sum_j \varepsilon_j (G_{oj})^2 + \mathcal{O}(\varepsilon^2). \tag{6.26}$$

This gives

$$\sigma_R^2 = CW^2 + \mathcal{O}(W^4), \tag{6.27}$$

where

$$C = \sum_{\substack{j \\ (j\neq 0)}} \left[\mathrm{Re} \frac{(G_{oj})^2}{(G_{oo})^2} \right]^2. \tag{6.28}$$

The Green's function sum C will numerically depend on the lattice geometry, but will generally be a dimensionless number of order one.

The distribution of renormalized disorder $\widetilde{\varepsilon} = \varepsilon + \delta\Delta_c^R$ is given by a convolution of the distributions $P_1(\varepsilon)$ and $P_2(\delta\Delta_c^R)$

$$P(\widetilde{\varepsilon}) = \int_{-\infty}^{\infty} d\omega \, P_1(\widetilde{\varepsilon} - \omega) P_2(\omega). \tag{6.29}$$

If the bare distribution is bounded, (e.g. a standard "box" distribution), then Gaussian tails will emerge due to the fluctuations in $\delta\Delta_c^R$, and the "size" of the tails will be determined by an effective disorder corresponding to $W_{eff}^{(0)} = W\sqrt{C}$. Here, the superscript $^{(0)}$ indicates that we ignored the interaction renormalizations. In the Appendix B, we argue that the effective scattering potentials Φ_j will further renormalize the disorder distribution, but the Gaussian tails will remain as its generic feature.

Now we present numerical results which provide strong evidence for the universality of the renormalized disorder. Fig. 6.4 shows the results obtained within the *stat*DMFT [70] for uniform and binary disorder distributions with the same standard deviation $W = 0.1$. As anticipated by Eq. (6.27), the fluctuations of the cavity bath acquire an approximately Gaussian form with the same variance for both bare disorder distributions, panel (b). The renormalized disorder distribution $P(\widetilde{\varepsilon})$ exhibits long tails, panel (c), although the bare distributions are bounded, panel (a). These Gaussian-like tails are the main universal feature of the renormalized disorder, and they are crucial for the appearance of the singular behavior in $P(T_K)$ which leads to the formation of the Griffiths phase.

*Stat*DMFT results in Fig. 6.5 provide further illustration of the universality. The upper panel shows that the distributions of Kondo temperatures for uniform and binary bare disorder distributions with the same standard deviation W are qualitatively the same. The exponent α, which determines the slope of the distribution tails, is shown at the lower panel as a function of W. It depends very weakly on the particular form of disorder distribution.

6.4.3 Localization effects

In the strict DMFT formulation $\alpha \approx t^2\rho_o J/2W^2$, where $\rho_o \equiv \rho_{av}$ is simply the (algebraic) average DOS of the conduction electrons, which therefore remains finite even at the localization transition [84]. If J is chosen to be large enough, the above seems to suggest that the Griffiths phase may not emerge before the electrons localize at $W = W_c \sim 1/\rho_{av}$. However, in a theory that includes localization, the Kondo spins do not see the average,

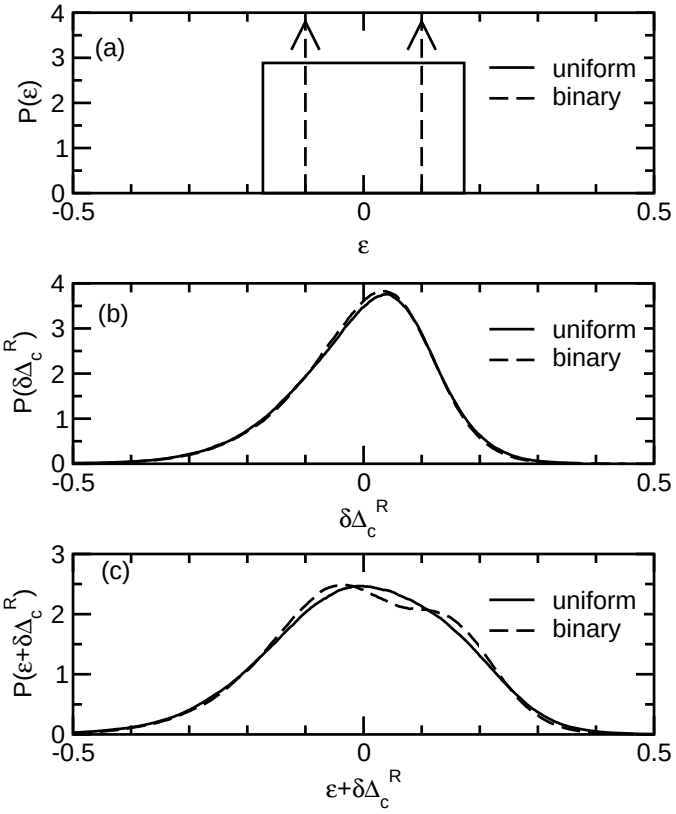

Figure 6.4. *Stat*DMFT results for uniform and binary distributions of bare disorder. Universal Gaussian-like tails appear in the cavity field fluctuations, panel (b), and the renormalized disorder distributions, panel (c), even though the bare disorder distributions are bounded (uniform and binary), panel (a). We used $V = 0.5$, $E_f = -1$, and $\mu = -0.5$.

but rather the *typical* DOS of the conduction electrons [67, 8]. Thus, in the NFL criterion, Eq. (6.19), one should actually replace $\rho_o \to \rho_{typ}$, a quantity that becomes very small (and eventually vanishes) as the Anderson transition is approached, viz.

$$\rho_{typ} = A(W_c - W)^\beta, \tag{6.30}$$

where A and β are constants. We thus get

$$W_{nfl}^2 = \frac{1}{2} A t^2 J (W_c - W_{nfl})^\beta. \tag{6.31}$$

This transcendental equation cannot be solved in closed form in general, but an approximate solution can be found for $W_c^{2-\beta}/At^2J \ll 1$. In this case, the quantity $\delta W = 1 - W_{nfl}/W_c$

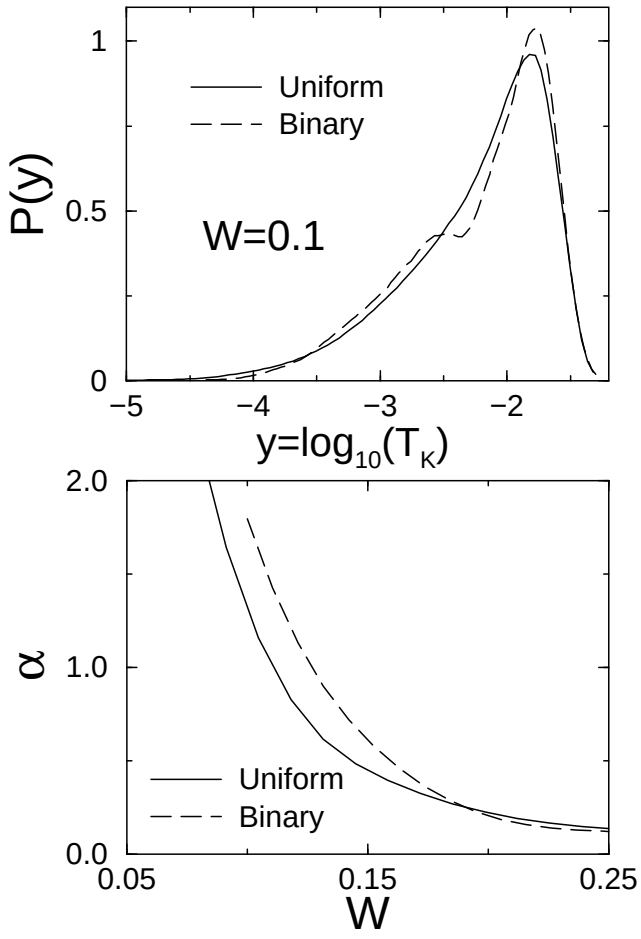

Figure 6.5. *Stat*DMFT results for the distribution of Kondo temperatures for uniform and binary bare disorder distributions (upper panel). The lower panel shows the exponent α as a function of disorder strength. The results are qualitatively the same regardless of the specific form of the disorder distribution. We used $V = 0.5$, $E_f = -1$, and $\mu = -0.5$.

will be small, and to leading order in δW

$$W_{nfl} = W_c - (At^2 J/2)^{-1/\beta} W_c^{2/\beta} < W_c. \tag{6.32}$$

Therefore, the Griffiths phase emerges strictly *before* the transition is reached.

6.5 Electronic Griffiths phase in the vicinity of the metal-insulator transition

Previous work [67] has shown that the electronic Griffiths phase appears also in a single band Hubbard model, as a precursor to the Mott-Anderson metal-insulator transition (MIT). Since the Hubbard model at half-filling is equivalent to the charge-transfer model [85] of the MIT, we examine in this Section the appearance of the Griffiths phase within this model, which can be considered a version of the Anderson lattice model that we examined in our approach.

The charge transfer model has been used to describe the Mott metal-insulator transition for various systems, including copper oxides [86]. It consists of a two band model, where one of the bands is narrow, and has large on-site interaction U (Copper d-band), while the other band is broad enough that electron-electron interactions can be neglected (Oxygen p-band). A disordered version of this model is also appropriate to describe the Mott-Anderson transition [67] in doped semiconductors such as Si:P. Here, the narrow band corresponds [87] to the impurity band of the Phosphorus donors, while the broad one is the conduction band of Silicon. This model is given exactly by the Hamiltonian of Eq. (6.1), but supplemented by the constraint

$$\overline{n_{fj}} + \overline{n_{cj}} = 1, \tag{6.33}$$

which can be enforced by adjusting the value of the chemical potential. Here n_{fj} and n_{cj} are the average number of conduction and f-electrons on site j, and the overbar denotes the average over disorder. In the mean field slave boson approach, the average occupancy of the f-site is equal to

$$n_{fj} = 1 - Z_j. \tag{6.34}$$

As the f-electron energy level is decreased ($|E_f|$ increased), the occupancy of the f-sites becomes larger: the charge is "transferred" from the conduction band. The transition to the Mott insulator is found for sufficiently large $|E_f|$. At least within DMFT, this metal-insulator transition has the same character as the more familiar Mott transition in a single band Hubbard model. As an illustration, we show on Fig. 6.6 the number of conduction electrons per site, $n_c = Z$, as a function of E_f, in the clean limit.

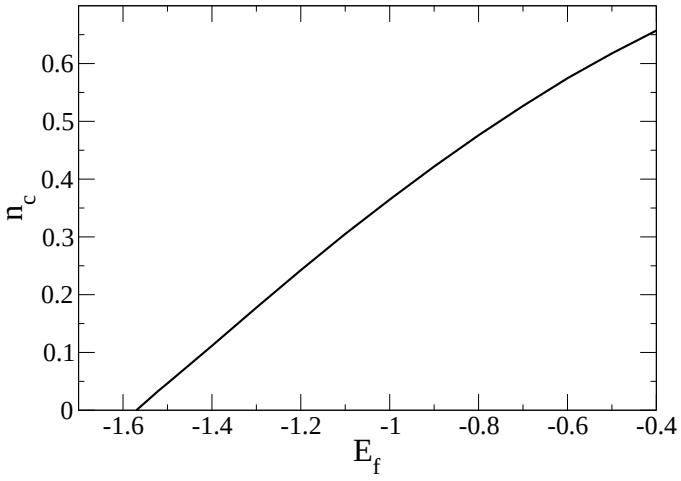

Figure 6.6. Number of conduction electrons per site as a function of the f-level energy E_f. The approach to the insulating phase is linear, $n_c \sim E_f - E_f^c$, where E_f^c is the critical value for the f-level energy. The hybridization $V = 0.5$, and E_f is measured with respect to the middle of the conduction band.

We have solved our effective model in the parameter regime relevant to the approach to the Mott-Anderson transition, and the results demonstrate the emergence of an electronic Griffiths phase in the same fashion as for the Anderson lattice model, consistent with *stat*DMFT results [67]. Here, the f-level energy in Fig. 6.7 is measured with respect to the middle of the conduction band, and not with respect to the chemical potential as in Sec. 6.3. For the parameters used in Fig. 6.7, the system is in the mixed valence regime, not in the Kondo limit, and stronger disorder is needed for the appearance of the NFL electronic Griffiths phase, again in close agreement with *stat*DMFT results [67]. These results demonstrate that our effective model proves capable to describe the emergence of the electronic Griffiths phase as a universal phenomenon in correlated electronic systems with disorder.

6.6 Summary

To summarize, we have identified an analytically solvable infinite range model, which captures the emergence of electronic Griffiths phases found within the more generic *stat*DMFT approaches [70, 78, 67]. In this effective model, a specific distribution of disorder is

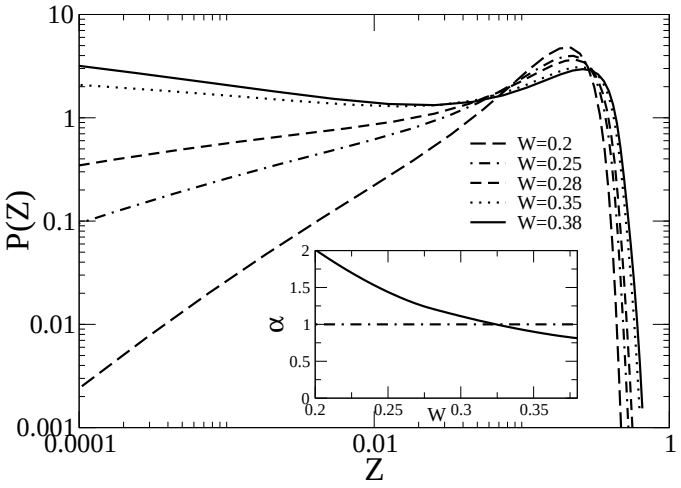

Figure 6.7. Distribution of local Kondo temperatures for several levels of disorder. The total number of electrons per unit cell is fixed to 1. The disorder ranges from $W = 0.2$ to 0.38. We used $V = 0.5$ and $E_f = -1.3$, where E_f is measured with respect to the middle of the conduction band. The inset shows the exponent α as a function of the disorder strength. The NFL phase occurs for $\alpha \leq 1$.

postulated, leading to a power-law distribution of local Kondo temperatures and NFL behavior for sufficiently strong disorder. We have also presented arguments explaining how this specific form of randomness is universally generated by renormalizations due to disorder-induced fluctuations of the conduction bath.

The main motivation for introducing this effective model lies in its simplicity, allowing an analytical solution, and thus providing further insight into the mechanism for the emergence of the electronic Griffiths phase. Nevertheless, an essential ingredient is still missing from our Griffiths phase theory, namely the inter-site RKKY interactions between Kondo spins. According to the existing picture, all the spins with $T_K < T$ will not be Kondo screened, thus providing a large contribution to thermodynamic response. These decoupled spins will, however, not act as free local moments, but will feature dynamics dominated by frustrating inter-site RKKY interactions. The simplifications introduced by our effective model open an attractive avenue to incorporate both the Kondo effect and the RKKY interaction in a single theory.

CHAPTER 7

SPIN LIQUID BEHAVIOR IN ELECTRONIC GRIFFITHS PHASES

This Chapter contains a detailed study of the interplay of the Kondo effect and RKKY interactions in the disordered Kondo lattice systems within an extended dynamical mean field theory. First we concentrate on two special cases of the model: (a) The absence of hybridization of local moments with the conduction band, when the model reduces to the infinite-ranged frustrated Heisenberg model [88]; (b) The Kondo lattice model with random infinite ranged RKKY interactions, but in the absence of disorder in the conduction band [89]. These two models have already been studied, but we review their properties as a preliminary step before we proceed to the disordered case. In addition, our results for the Kondo lattice model are in several aspects more detailed than in Ref. [89].

The presence of disorder in the conduction band leads to qualitatively different behavior than in the case of a clean Kondo lattice. The main difference is that for sufficient disorder we end up with the two fluid model, where a fraction of spins are decoupled from the conduction bath and form the spin liquid, while the other remain Kondo screened. As we will see, the existence of the the electronic Griffiths phase in absence of RKKY interactions described in Chapter 6 is crucial, since it provides the sufficient conditions for the decoupling.

7.1 Model

We consider the disordered Kondo lattice model as given by the Hamiltonian

$$\begin{aligned} H &= -t\sum_{\langle ij\rangle\sigma}(c^{\dagger}_{i\sigma}c_{j\sigma}+\text{H.c.})+\sum_{i\sigma}(\varepsilon_i-\mu)c^{\dagger}_{i\sigma}c_{i\sigma} \\ &+ J_K\sum_i \mathbf{S}_i\cdot\mathbf{s}_i+\sum_{\langle ij\rangle}J_{ij}\mathbf{S}_i\cdot\mathbf{S}_j, \end{aligned} \tag{7.1}$$

where the exchange couplings J_{ij} between localized spins, and the site energies ε_i are distributed according to the Gaussian distributions

$$P_J(J_{ij}) = \frac{1}{\sqrt{2\pi}J} e^{-J_{ij}^2/2J^2}, \tag{7.2}$$

and

$$P_W(\varepsilon_i) = \frac{1}{\sqrt{2\pi}W} e^{-\varepsilon_i^2/2W^2}. \tag{7.3}$$

In this expression, $\mathbf{S}_i$ and $\mathbf{s}_i = \frac{1}{2}\sum_{\alpha\beta} c_{i\alpha}^\dagger \sigma_{\alpha\beta} c_{i\beta}$ represent a localized spin and the conduction electron spin density at site i, respectively. The infinite-ranged nature of the RKKY interactions allows to average over the disorder in J_{ij} using the replica trick [90]. To make further progress, we take the limit of large coordination number, $z \to \infty$, in which the problem reduces to the ensemble of the single impurity problems described by the local effective action

$$\begin{aligned}
\mathcal{A}_j &= \sum_\sigma \int_0^\beta d\tau \int_0^\beta d\tau' c_{j\sigma}^\dagger(\tau)[(\partial_\tau - \mu + v_j)\delta(\tau-\tau') \\
&- t^2 G_c(\tau-\tau')]c_{j\sigma}(\tau') + J_K \int_0^\beta d\tau \mathbf{S}_j(\tau)\cdot\mathbf{s}_j(\tau) \\
&- \frac{J^2}{2}\int_0^\beta d\tau \int_0^\beta d\tau' \chi(\tau-\tau')\mathbf{S}_j(\tau)\cdot\mathbf{S}_j(\tau').
\end{aligned} \tag{7.4}$$

The spin bosonic bath $\chi(\tau) = \overline{\langle T_\tau \mathbf{S}_j(\tau)\cdot\mathbf{S}_j(0)\rangle_{\mathcal{A}_j}} = \int dv_j P_W(v_j)\langle T_\tau \mathbf{S}_j(\tau)\cdot\mathbf{S}_j(0)\rangle_{\mathcal{A}_j}$ and the conduction electron bath $G_c(\tau) = \overline{G_{cj}(\tau)} = -\overline{\langle T_\tau c_{j\sigma}(\tau) c_{j\sigma}^\dagger(0)\rangle_{\mathcal{A}_j}}$ are obtained by averaging over site disorder. For simplicity, a semicircle conduction band density of states is assumed. On the level of a single site we are dealing with the Bose-Fermi Kondo model [91, 92, 93, 94], which describes a Kondo spin embedded in a fermionic bath of conduction electrons and a bosonic bath of spin fluctuations. However, for the Kondo lattice we need to consider self-consistently an ensemble of such Bose-Fermi Kondo models, and the disorder in the Kondo couplings will lead to qualitatively different behavior than in the clean case. We will defer for a moment a discussion of the general properties of the Bose-Fermi Kondo model, and present results for two important special cases of the model given by the action (7.4).

7.2 Sachdev-Ye model of the spin liquid

We refer to the system of interacting quantum spins which does not exhibit any magnetic ordering as a spin liquid. One of the well known spin liquid models is introduced in the work of Sachdev and Ye [88]. The model describes quantum Heisenberg spins with infinite-range random interaction. Solution of such a model is made possible by extending the spin symmetry from SU(2) to SU(N). The Hamiltonian is given by

$$H = \frac{1}{\sqrt{\mathcal{N}N}} \sum_{i<j} J_{ij} \mathbf{S}_i \mathbf{S}_j, \tag{7.5}$$

where the sum extends over $\mathcal{N} \to \infty$ sites. The random exchange constants are distributed by the uncorrelated Gaussian distribution $P(J_{ij}) \sim \exp(-J_{ij}^2/2J^2)$.

This model can be reduced to a single site model with the action

$$\mathcal{A} = \frac{J^2}{2N} \int_0^\beta d\tau d\tau' \chi(\tau - \tau') \mathbf{S}(\tau) \cdot \mathbf{S}(\tau'), \tag{7.6}$$

supplemented by the self-consistency condition

$$\chi(\tau - \tau') = \frac{1}{N^2} \langle \mathbf{S}(\tau) \cdot \mathbf{S}(\tau') \rangle_{\mathcal{A}}. \tag{7.7}$$

The $N^2 - 1$ components of the SU(N) spin operator $\mathbf{S}_i = S_{i\alpha\beta}$ can be represented by the fermionic representation

$$S_{i\alpha\beta} = f_{i\alpha}^\dagger f_{i\beta} - \frac{1}{N} \delta_{\alpha\beta} \sum_\alpha f_{i\alpha}^\dagger f_{i\alpha}, \tag{7.8}$$

subject to the constraint

$$\sum_\alpha f_{i\alpha}^\dagger f_{i\alpha} = \frac{N}{2}. \tag{7.9}$$

The interaction term becomes quartic in the fermionic fields f, which can be decoupled by the Hubbad-Stratonovich transformation, and in the $N \to \infty$ limit Eqs. (7.6)-(7.7) reduce to

$$G_f(i\omega_n) \frac{1}{i\omega_n - \Sigma_f(i\omega_n)}, \tag{7.10}$$

$$\Sigma_f(\tau) = J^2 \chi(\tau) G_f(\tau). \tag{7.11}$$

The local spin-spin correlation function is given by

$$\chi(\tau) = -G_f(\tau) G_f(-\tau), \tag{7.12}$$

where G_f is the fermionic Green function given by $\delta_{\alpha\beta} G_f(\tau) = -\langle T f_\alpha(\tau) f_\beta^\dagger(0) \rangle_{\mathcal{A}}$. Since the action is invariant on the rotations in the spin space, only the diagonal terms are non-zero

and they are equal. We want to find the solution of the Eqs. (7.10)-(7.12) at zero temperature for low frequencies.

Let us first solve Eqs. (7.10)-(7.11) assuming that at large imaginary time τ the bosonic bath has the form

$$\chi(\tau) = \frac{C}{\tau^{2-\varepsilon}}, \quad \tau \gtrsim 1/\Lambda, \tag{7.13}$$

where Λ is a large frequency cut-off and $0 < \varepsilon < 2$. At particle-hole symmetry $G_f(i\omega_n)$ and $\Sigma(i\omega_n)$ are purely imaginary and odd, while $G_f(\tau)$ and $\Sigma(\tau)$ are real and odd. The Fourier transform pairs

$$F(i\omega) = \int_{\infty}^{\infty} d\tau e^{i\omega\tau} F(\tau), \quad F(\tau) = \int_{\infty}^{\infty} \frac{d\omega}{2\pi} e^{-i\omega\tau} F(i\omega) \tag{7.14}$$

then reduce to

$$F(i\omega) = 2i \int_{0}^{\infty} d\tau \sin(\omega\tau) F(\tau), \quad F(\tau) = -i \int_{0}^{\infty} \frac{d\omega}{\pi} \sin(\omega\tau) F(i\omega) \tag{7.15}$$

As we will confirm shortly, the Green function assumes the form

$$G_f(\tau) = -\frac{B}{\tau^{\varepsilon/2}}, \quad \tau \gtrsim 1/\Lambda. \tag{7.16}$$

Then the self-energy is equal to $\Sigma_f(\tau) = -J^2 BC/\tau^{2-\varepsilon/2}$, and its Fourier transform

$$\Sigma_f(i\omega) = \Sigma_f^r(i\omega) - 2iBCJ^2 \int_{1/\Lambda}^{\infty} d\tau \frac{\sin(\omega\tau)}{\tau^{2-\varepsilon/2}}, \tag{7.17}$$

where $\Sigma_f^r(i\omega)$ is the regular term which comes from short time part in $\Sigma_f(\tau)$. Similarly,

$$G_f(i\omega) = G_f^r(i\omega) - 2Bi \int_{1/\Lambda}^{\infty} d\tau \frac{\sin(\omega\tau)}{\tau^{\varepsilon/2}}. \tag{7.18}$$

After substitution $\omega\tau = x$, the self-energy and the "f-electron" Green function assume the form

$$\Sigma_f(i\omega) = \Sigma_f^r(i\omega) - 2iBCJ^2\omega^{1-\varepsilon/2} \int_{\omega/\Lambda}^{\infty} dx \frac{\sin x}{x^{2-\varepsilon/2}}, \tag{7.19}$$

$$G_f(i\omega) = G_f^r(i\omega) - \frac{2iB}{\omega^{1-\varepsilon/2}} \int_{\omega/\Lambda}^{\infty} dx \frac{\sin x}{x^{\varepsilon/2}}. \tag{7.20}$$

The integrals can be calculated explicitly,

$$\int_{\omega/\Lambda}^{\infty} dx \frac{\sin x}{x^{2-\varepsilon/2}} = \cos\left(\frac{\pi\varepsilon}{4}\right) \frac{\Gamma(\varepsilon/2)}{1-\varepsilon/2}, \quad \omega/\Lambda \to 0, \tag{7.21}$$

$$\int_{\omega/\Lambda}^{\infty} dx \frac{\sin x}{x^{\varepsilon/2}} = \cos\left(\frac{\pi\varepsilon}{4}\right)\Gamma(1-\varepsilon/2), \quad \omega/\Lambda \to 0. \tag{7.22}$$

Now it becomes clear that for $\varepsilon > 0$ the second term in Eq. (7.19) provides a leading non-analytic contribution to the self-energy at low frequencies,

$$\Sigma_f(i\omega) = -2iBCJ^2 \cos\left(\frac{\pi\varepsilon}{4}\right)\frac{\Gamma(\varepsilon/2)}{1-\varepsilon/2}\omega^{1-\varepsilon/2}, \quad \omega \to 0, \tag{7.23}$$

and the second term in Eq. (7.20) a singular contribution to the Green function

$$G_f(i\omega) = -2iB\cos\left(\frac{\pi\varepsilon}{4}\right)\Gamma(1-\varepsilon/2)\frac{1}{\omega^{1-\varepsilon/2}}, \quad \omega \to 0. \tag{7.24}$$

From Eq. (7.10) a constant $B = \left[(1-\frac{\varepsilon}{2})/(4CJ^2\cos^2(\frac{\pi\varepsilon}{4})\Gamma(1-\frac{\varepsilon}{2})\Gamma(\frac{\varepsilon}{2}))\right]^{1/2}$.

The self-energy, Eq. (7.23), and the Green function, Eq. (7.24), are obtained for a given form of the bosonic bath $\chi(\tau) = C/\tau^{2-\varepsilon}$. If we enforce the self-consistency condition for the form of the bosonic bath, Eq. (7.12), we find that the exponent ε is equal to 1. The self-energy and the Green function then assume the form

$$\Sigma_f(i\omega) = -i\left(\frac{J^2}{\pi}\right)^{1/4}\sqrt{\omega}, \tag{7.25}$$

$$G_f(i\omega) = -i\left(\frac{\pi}{J^2}\right)^{1/4}\frac{1}{\sqrt{\omega}}. \tag{7.26}$$

Analytical continuation to the upper complex half-plane gives

$$G_f(z) = \left(\frac{\pi}{4J^2}\right)^{1/4}\frac{1-i}{\sqrt{i\omega}}, \quad \mathrm{Im}z > 0, \quad |z| \to 0. \tag{7.27}$$

The most prominent feature of the Sachdev-Ye spin liquid model is the logarithmic divergence of dynamic magnetic susceptibility $\chi(\omega)$. In the imaginary time

$$\chi(i\omega) = \chi_r + \frac{1}{\sqrt{\pi}J}\int_{\omega/\Lambda}^{\infty} dx \frac{\cos x}{x}, \tag{7.28}$$

which gives

$$\chi(i\omega) = -\frac{1}{\sqrt{\pi}J}\ln\omega + \text{const.}, \quad \omega \to 0. \tag{7.29}$$

We have solved the Sachdev-Ye model numerically on imaginary frequency axis using Fast Fourier transform methods. The low frequency results shown in Fig. 7.1 and Fig. 7.2 are in excellent agreement with Eqs. (7.26) and (7.29).

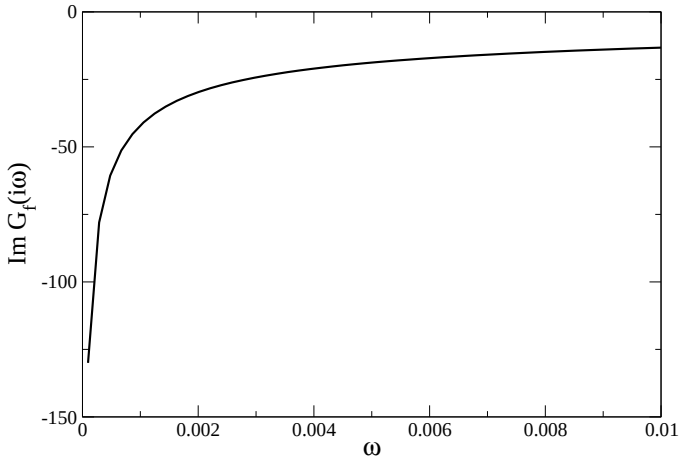

Figure 7.1. Imaginary time Green's function of the Sachdev-Ye model showing square root singularity at $\omega \to 0$. The coupling constant is set to $J = 1$.

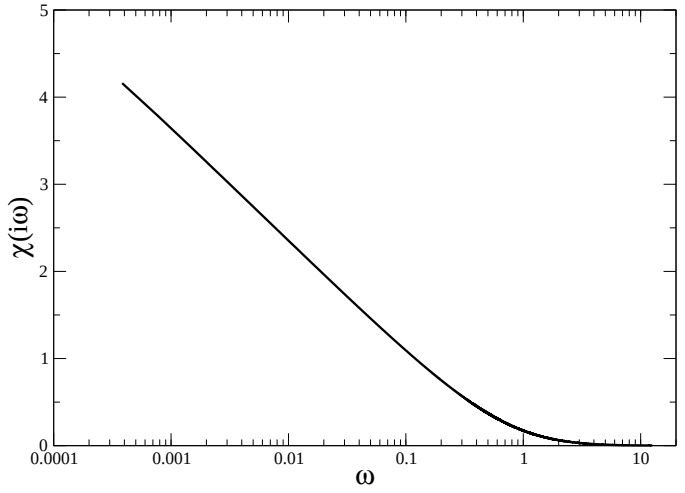

Figure 7.2. Dynamic magnetic susceptibility on imaginary frequency axis. The coupling constant is set to $J = 1$.

7.3 Clean Kondo lattice with magnetic frustration

The inter-site spin-spin interaction reduces the Kondo temperature, and may completely destroy the Kondo effect in the Kondo lattice systems. In this Section we address the following questions: (a) What is the minimum spin-spin coupling J necessary for a destruction of the Kondo effect? (b) How does the Fermi liquid coherence scale diminish as we approach to the decoupling transition, i.e. spin liquid phase? These questions can be explicitly answered within an extended DMFT model in the large N limit.

7.3.1 Critical RKKY interaction for the clean Kondo lattice

We consider the model given by action (7.4), but in absence of the disorder in the conduction bath. In the large N limit the coupling constants are rescaled as $J_K \to J_K/N$ and $J \to J/\sqrt{N}$. The localized spins in the fermionic representation are given as before by Eq. (7.8). Introducing slave boson parameters r and ε_j, and minimizing the local free energy, we come to the following saddle-point equations [89]

$$\frac{1}{\beta}\sum_{\omega_n} e^{i\omega_n 0^+} G_j(i\omega_n) = \frac{1}{2}, \tag{7.30}$$

$$\frac{1}{\beta}\sum_{\omega_n} G_j(i\omega_n)\Delta_j(i\omega_n) = -\frac{1}{J_K}. \tag{7.31}$$

The local f-pseudo-fermion Green's function $G_f(\tau) = -\langle T_\tau f_\sigma(\tau) f^\dagger_\sigma(0)\rangle$, is given by

$$G_f^{-1}(i\omega_n) = i\omega_n - \varepsilon_f - \Sigma(i\omega_n) - r^2\Delta_f(i\omega_n). \tag{7.32}$$

The self-energy is equal to

$$\Sigma(\tau) = J^2\chi(\tau)G_f(\tau), \tag{7.33}$$

and

$$\Delta_f^{-1}(i\omega_n) = i\omega_n + \mu - t^2 G_c(i\omega_n). \tag{7.34}$$

These equations for a single impurity have to be supplemented by the self-consistency conditions,

$$\chi(\tau) = -G_f(\tau)G_f(-\tau), \tag{7.35}$$

and

$$G_c^{-1}(i\omega_n) = \Delta_f^{-1}(i\omega_n) - \frac{r^2}{i\omega_n - \varepsilon_f - \Sigma_j(i\omega_n)}. \tag{7.36}$$

At the decoupling transition the Kondo temperature, proportional to the slave boson parameter r^2, vanishes. Therefore we seek for the solution of the saddle point equation (7.31) which, on the real frequency axis at zero temperature, assumes the form

$$\frac{1}{\pi}\int_{-\infty}^{0} d\omega \,\mathrm{Im}\left[G_{SY}^{J_c}(\omega)G_c^o(\omega+\mu)\right] = \frac{1}{J_K}. \tag{7.37}$$

Here $G_{SY}^{J_c}$ is the Sachdev-Ye spin liquid Green function which is approximately given by

$$G_{SY}^{J_c}(\omega) = \begin{cases} \left(\frac{\pi}{4}\right)^{1/4} \frac{1}{\sqrt{J_c}} \frac{1-i}{\sqrt{\omega}}, & |\omega| < J_c \\ \frac{1}{\omega}, & |\omega| > J_c. \end{cases} \tag{7.38}$$

For simplicity we take uniform DOS of the conduction band from $-D$ to D. Then $\mathrm{Re}G_c^o(0) = 0$, and we denote $\mathrm{Im}G_c^0 = -\pi\rho_o$. Eq. (7.37) reduces to

$$\int_{-D}^{0} d\omega \,\mathrm{Re}G_{SY}^{J_c}(\omega) = -\frac{1}{\rho_o J_K}. \tag{7.39}$$

After integration, we obtain that the critical RKKY interaction is equal to[1]

$$J_c = e^2 D e^{-1/\rho_o J_K} = e^2 T_K^o \approx 10 T_K^o. \tag{7.40}$$

This result nicely agrees with the numerical solution of the system of equations (7.30)-(7.36), Fig. 7.3.

7.3.2 Critical behavior

An important question is to determine how does the renormalized Kondo temperature T^* (defined below) decrease as we approach to the critical point $J = J_c$. As discussed in detail in the next section, the form of the bosonic bath $\chi(\tau) \sim 1/\tau^{2-\varepsilon}$, characterized by the exponent ε, is crucial for the properties of the Kondo lattice model with spin-spin (RKKY) interactions. Therefore, we will consider first the case of an impurity in a given bosonic bath. As we will see, fully self-consistent solution has the same critical behavior as a single impurity in the $\varepsilon = 1$ bosonic bath.

[1] In agreement with an improved analytical estimate of D. Grempel, private communication.

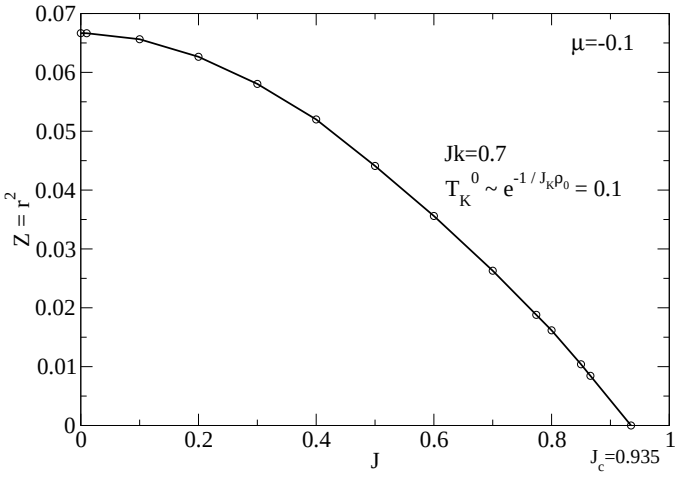

Figure 7.3. Slave boson parameter r^2 as a function of the RKKY coupling constant J. A connection between r^2 and the renormalized Kondo temperature T^* is established the text.

Bosonic $\boldsymbol{\varepsilon = 1}$ *bath.* We assume that conduction bath and the bosonic bath characterized by the exponent $\varepsilon = 1$ are given, and we use the first slave boson equation (7.30) (Friedel sum rule)

$$-\frac{1}{\pi}\int_{-\infty}^{0} d\omega \, \mathrm{Im} G_f(\omega) = \frac{1}{2}, \tag{7.41}$$

where the impurity Green function is given by

$$G_f(\omega) = \frac{1}{\omega - \varepsilon_f - \Sigma(\omega) - r^2 \Delta_f(\omega)}. \tag{7.42}$$

For the Bethe lattice $\Delta_f(\omega) = G_c(\omega)$.

The idea is to distinguish different energy (frequency) scales of the problem, and use the approximate form of $G_f(\omega)$ in each of the found regimes. First we will use the Friedel sum rule to find the value of the impurity Green function at zero frequency, $G_f(\omega = 0)$. We are interested in the limit $r^2 \to 0$ when the frequency dependence in $\Delta_f(\omega)$ in Eq. (7.42) can be neglected, and $\Delta_f(\omega)$ replaced by its value at the Fermi level $\Delta_f(0) \equiv \Delta$. The left-hand-side of Eq. (7.41) assumes the form

$$\begin{aligned}
\text{LHS} &\equiv -\frac{1}{\pi}\int_{-\infty}^{0} d\omega\, \text{Im}G_f(\omega) \\
&= -\frac{1}{\pi}\text{Im}\int_{-\infty}^{0} d\omega\, \frac{1}{\omega - \varepsilon_f - r^2\Delta' - \Sigma(\omega) + ir^2|\Delta''|} \\
&= -\frac{1}{\pi}\text{Im}\int_{-\infty}^{0} d\omega \Big\{ \frac{\partial}{\partial\omega} \ln(\omega - \varepsilon_f - r^2\Delta' - \Sigma(\omega) + ir^2|\Delta''|) \\
&+ \frac{\partial\Sigma(\omega)/\partial\omega}{\omega - \varepsilon_f - r^2\Delta' - \Sigma(\omega) + ir^2|\Delta''|}\Big\}. \qquad (7.43)
\end{aligned}$$

Performing the integration

$$\begin{aligned}
\text{LHS} &= -\frac{1}{\pi}\text{Im}\ln(\omega - \varepsilon_f - r^2\Delta' - \Sigma(\omega) + ir^2|\Delta''|)\Big|_{-\infty}^{0} \\
&- \frac{1}{\pi}\text{Im}\int_{-\infty}^{0} d\omega\, \frac{\partial\Sigma(\omega)}{\partial\omega} G_f(\omega) \\
&= -\frac{1}{\pi}\arctan\frac{r^2|\Delta''| - \Sigma''(\omega)}{\omega - \varepsilon_f - r^2\Delta' - \Sigma'(\omega)}\Big|_{-\infty}^{0} \\
&= -\frac{1}{\pi}\Big[\frac{\pi}{2} - \arctan\frac{\omega - \varepsilon_f - r^2\Delta' - \Sigma'(\omega)}{r^2|\Delta''| - \Sigma''(\omega)}\Big]\Big|_{-\infty}^{0} \\
&= \frac{1}{2} - \arctan\frac{\varepsilon_f + r^2\Delta' + \Sigma(0)}{r^2|\Delta''|} \qquad (7.44)
\end{aligned}$$

Therefore, Eq. (7.41) gives that $\varepsilon_f + r^2\Delta' + \Sigma(0) = 0$, i.e.

$$\frac{\varepsilon_f + \Sigma(0)}{r^2} = -\Delta'. \qquad (7.45)$$

In this derivation we used theorems from the Fermi liquid theory stating that $\Sigma''(0) = 0$ and $\text{Im}\int_{-\infty}^{\varepsilon_F} \partial\Sigma(\omega)/\partial\omega G(\omega)\, d\omega = 0$ [4].

Now we are ready to analyze the impurity Green function, Eq. (7.42). We distinguish three frequency intervals:

(i) $|\omega| < T^*$, where T^* denotes the Fermi liquid coherence temperature. In this interval $G_f(\omega) \approx G_f(0) = -i/r^2|\Delta''|$, where we used Eq. (7.45).

(ii) $T^* < |\omega| < J$. Here $\Sigma(\omega) \propto J\sqrt{(}\omega)$ is a dominant term in the numerator of Eq. (7.42), and $G_f(\omega)$ acquires the spin liquid form $G_f(\omega) \approx G_{SL}^J(\omega) \sim (1-i)/(J\sqrt{\omega})$.

(iii) $|\omega| > J$. Atomic limit is approached, and $G_f(\omega) \approx G_{SL}^J(\omega) \sim 1/\omega$. The coherence frequency T^* is obtained from matching $\rho_f(\omega) \equiv -\frac{1}{\pi}G_f(\omega)$ at $\omega = T^*$. It is given by

$$T^* = \frac{|\Delta''|^2}{J^2} r^4. \qquad (7.46)$$

(J and Δ are given in units of $D = 2t$.)

The easiest way to proceed is to subtract from Eq. (7.41) the corresponding equation for $J = J_c$. We obtain

$$\int_{-\infty}^{0} d\omega \, \left[\mathrm{Im}G_f(\omega) - \mathrm{Im}G_{SY}^{J_c}(\omega) \right] = 0. \tag{7.47}$$

The left-hand side is equal to

$$\begin{aligned} &\int_{-T^*}^{0} d\omega \, \left[\frac{-1}{r^2|\Delta''|} - \frac{-1}{J_c\sqrt{|\omega|}} \right] + \int_{-J_c}^{-T^*} d\omega \, \left[\frac{-1}{J\sqrt{|\omega|}} - \frac{-1}{J_c\sqrt{|\omega|}} \right] \\ &= \frac{|\Delta''|r^2}{J_c^2} - 2\left(\frac{1}{J} - \frac{1}{J_c} \right) (\sqrt{J_c} - \sqrt{T^*}) \approx \frac{|\Delta''|r^2}{J_c^2} - \frac{2}{\sqrt{J_c}}\,\delta, \end{aligned} \tag{7.48}$$

where $\delta = 1 - J/J_c$. Therefore

$$r^2 = \frac{2J_c^{3/2}}{|\Delta''|}\delta, \tag{7.49}$$

and

$$T^* \propto \delta^2. \tag{7.50}$$

Note that this derivation relies only on the first slave boson equation and it does not require small values for J and J_K.

Arbitrary ε. The critical behavior in presence of the bosonic bath with an arbitrary exponent ε, $0 < \varepsilon < 2$, can be obtained along the same lines as for $\varepsilon = 1$. Again there are three distinctive intervals:

(*i*) $|\omega| < T^*$; in this interval $G_f(\omega) \approx G_f(0) = -i/r^2|\Delta''|$.

(*ii*) $T^* < |\omega| < J$; $G_f(\omega) \approx G_{SL}^J(\omega) \sim (1-i)/(J\omega^{1-\varepsilon/2})$.

(*iii*) $|\omega| > J$; $G_f(\omega) \approx G_{SL}^J(\omega) \sim 1/\omega$. The coherence frequency T^* is obtained from matching $\rho_f(\omega) \equiv -\frac{1}{\pi}G_f(\omega)$ at $\omega = T^*$. It is given by (up to the prefactor which depends on J)

$$T^* \sim (r^2)^{2/(2-\varepsilon)}. \tag{7.51}$$

Similarly as in the as in $\varepsilon = 1$ case, we find that

$$r^2 \sim \delta^{(2-\varepsilon)/\varepsilon}, \tag{7.52}$$

which implies

$$T^* \sim \delta^{2/\varepsilon}. \tag{7.53}$$

Self-consistent solution - Kondo lattice. In the self-consistent solution for the Kondo lattice [89] the conduction bath obtains a strong frequency dependence for $|\omega| < r^2$, and the Friedel sum rule yields

$$\frac{r^2}{\varepsilon_f + \Sigma(0)} = \varepsilon_F^> - \mu. \tag{7.54}$$

$\varepsilon_F^>$ is the chemical potential corresponding to the noninteracting Fermi level with $(n_c+1)/2$ electrons per spin. Luttinger theorem is satisfied for the "large" Fermi surface containing both conduction electrons and localized spins [95]. This implies that

$$\mathrm{Im}G_f(0) = \frac{(\varepsilon_F^> - \mu)^2}{r^2}\mathrm{Im}G_c^0(\varepsilon_F^>). \tag{7.55}$$

We can then repeat the same arguments as for a single impurity Green's function. The coherence frequency, obtained by matching the density of states at zero frequency and in the spin liquid regime, is equal to

$$T^* = \left[(4\pi^3)^{-1/4}\frac{r^2}{(\varepsilon_F^> - \mu)^2\rho_0(\varepsilon_F^>)\sqrt{J}}\right]^2. \tag{7.56}$$

Following the same steps which lead to Eq. (7.49), we obtain

$$r^2 = 2\sqrt{\pi}(\varepsilon_F^> - \mu)^2\rho_0(\varepsilon_F^>)J_c\,\delta. \tag{7.57}$$

Therefore the conclusions that $r^2 \propto \delta$ and $T^* \propto \delta^2$ remain the same. This result is supported by the numerical solution, Fig. 7.3. Note that we do not find a logarithmic prefactor $\ln\delta$ from Eq. (20) in Ref. [89].

7.4 Disordered Kondo lattice: Destruction of the Kondo effect

We have seen that the solution of the Kondo lattice model with RKKY interactions reduces in the limit of large coordination number to the set of impurity problems which have to be solved self-consistently. In the previous section, we have solved such a model in a specific case of the clean Kondo lattice with random infinite-ranged RKKY interactions in the large-N approximation. However, the problem of an impurity embedded in the fermionic bath of conduction electrons and the bosonic bath of spin fluctuations ("Bose-Fermi Kondo model") is quite generic and it is of importance for various physical systems. In this

section, we will summarize the results for the Bose-Fermi Kondo model obtained within the renormalization group approach, and then use this analysis to explain how the disorder in the local Kondo couplings provides a mechanism which leads to the destruction of the Kondo effect in the Kondo lattice systems.

7.4.1 Bose-Fermi Kondo impurity model

The Bose-Fermi Kondo model (BFKM) describes a local impurity spin which couples both to the fermionic fields (describing non-correlated conduction electrons) and the bosonic fields (describing fluctuating magnetic field). As we have seen, this model naturally appears in extended DMFT theories, and its purely bosonic version emerges in the mean field theories of spin glass and spin liquid.

The local effective action of the BFKM model is given by

$$\begin{aligned} \mathcal{A}_{eff} &= \sum_{\sigma} \int_0^\beta d\tau \int_0^\beta d\tau' c_\sigma^\dagger(\tau)[(\partial_\tau - \mu)\delta(\tau - \tau') \\ &- \Delta_c(\tau - \tau')]c_\sigma(\tau') + J_K \int_0^\beta d\tau \mathbf{S}(\tau) \cdot \mathbf{s}(\tau) \\ &- \frac{J^2}{2} \int_0^\beta d\tau \int_0^\beta d\tau' \chi(\tau - \tau') \mathbf{S}(\tau) \cdot \mathbf{S}(\tau'). \end{aligned} \tag{7.58}$$

As before, $\mathbf{S}$ and $\mathbf{s} = \frac{1}{2}\sum_{\alpha\beta} c_\alpha^\dagger \sigma_{\alpha\beta} c_\beta$ represent a localized spin and the conduction electron spin density, respectively. Δ_c is (featureless) conduction bath, and $\chi(\tau)$ decays in the imaginary time as a power law, $\chi(\tau) \sim 1/\tau^{2-\varepsilon}$, $0 \leq \varepsilon < 2$.

This model is extensively studied within renormalization group approach [91, 92, 93, 94] and it provides one of the simplest examples of the zero temperature (quantum) phase transitions. For $\varepsilon = 0$, which corresponds to so-called Ohmic bosonic bath, the impurity spin is screened by the Kondo effect at zero temperature for arbitrary RKKY coupling J. However, for $\varepsilon > 0$ (sub-Ohmic bath) the Kondo effect is destroyed for strong enough J, and the spin decouples from the conduction bath. The phase diagram of the BFKM in a presence of the sub-Ohmic bosonic bath is shown in Fig. 7.4. For small J the system is in the Kondo screened phase where the only effect of the RKKY coupling is to renormalize (decrease) the Kondo temperature. The Kondo coupling J_K flows to the strong coupling

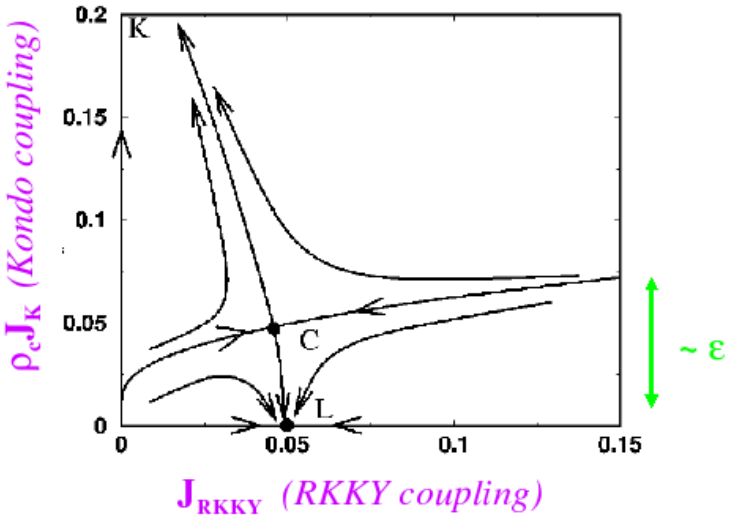

Figure 7.4. RG flow for the Bose-Fermi Kondo model.

limit which corresponds to the Fermi liquid fixed point. For stronger J, there is a decoupled phase where the Kondo coupling J_K goes to zero, and J to the spin liquid fixed point.

The form of the critical line can be determined from the RG equations. To the first order in the exponent ε, RG equations assume the form [92]

$$\beta(J_K) = \frac{1}{2}(-gJ_K + J_K^2), \tag{7.59}$$

$$\beta(g) = \varepsilon g - g^2, \tag{7.60}$$

where $\beta(J_K) \equiv dJ_K/(d\ln t)$, and $g = J^2$. Here, t is a lower cutoff on the imaginary times. Its bare value is $t_o \sim 1/D$, where D is the bandwidth. All energy scales are in units of the bandwidth, so that the conduction electron density of states $\rho_c \sim \mathcal{O}(1)$ is absorbed in the definitions of J_K and g. The phase transition is controlled by an (unstable) fixed point at $g^* = J_K^* = \varepsilon$. To eliminate the scaling variable, we can divide Eq. (7.58) by Eq. (7.59), and obtain

$$\frac{dJ_K}{dg} = \frac{1}{2}\frac{-gJ_K + J_K^2}{\varepsilon g - g^2}. \tag{7.61}$$

This nonlinear differential equation defines the family of scaling trajectories, each of which is specified by an initial condition on the boundary of the $g - J$ plane. In particular, the critical line corresponds to the solution specified by the initial condition $J_K(g = 0) = 0$.

Critical line near the origin. We first examine the form of this line close to the origin, such that both $J_K \gg \varepsilon$ and $g \ll \varepsilon$. In this case, we can drop the g^2 term in the denominator and get

$$\frac{dJ_K}{dg} = \frac{J_K}{2\varepsilon}\left[-1 + \frac{J_K}{g}\right]. \tag{7.62}$$

We can immediately see that $J_K = Ag$ is not a solution, since this would require the right-hand-side to be a constant. It is also clear that one must have $J_K > g$, otherwise J_K would not be an increasing function of g. Therefore, near the origin $J_K/g \gg 1$ so we can drop -1 term, and obtain

$$\frac{dJ_K}{dg} \approx \frac{J_K^2}{2\varepsilon g}, \tag{7.63}$$

which gives

$$g \approx e^{-2\varepsilon/J_K}. \tag{7.64}$$

The leading behavior is the same as in the large-N solution, $J \equiv \sqrt{g} \sim e^{-1\varepsilon/J_K} \sim T_K^o$, where T_K^o is the Kondo temperature in the bare ($g = 0$) model.

Critical line near the unstable fixed point. Here we need to expand the RG equations around the fixed point value $g^* = J^* = \varepsilon$. Let us define $\delta g = g - \varepsilon$, and $\delta J_K = J_K - \varepsilon$. Then Eqs. (7.59)-(7.60) take the form

$$\beta(J_K) \approx \frac{\varepsilon}{2}(\delta J_K - \delta g), \tag{7.65}$$

$$\beta(g) = -\varepsilon \delta g. \tag{7.66}$$

In vector notation,

$$\begin{bmatrix} \beta(J_K) \\ \beta(g) \end{bmatrix} = \begin{bmatrix} \frac{\varepsilon}{2} & -\frac{\varepsilon}{2} \\ 0 & -\varepsilon \end{bmatrix} \begin{bmatrix} \delta J_K \\ \delta g \end{bmatrix}. \tag{7.67}$$

The eigenvalues are

$$\lambda_{J_K} = \frac{\varepsilon}{2}, \tag{7.68}$$

$$\lambda_g = -\varepsilon. \tag{7.69}$$

The critical line corresponds to the eigenvector $\vec{x}_g$ (irrelevant direction), determined by $\delta J_K = \delta g/3$. This line has a positive slope and passes through the point $(\varepsilon, \varepsilon)$. Therefore, close to the critical point, the form of the critical line is

$$J_K(g) \approx \frac{2}{3}\varepsilon + \frac{1}{3}g. \tag{7.70}$$

Critical line for $g \gg \varepsilon$. In the asymptotic regime

$$\frac{dJ_K}{dg} = \frac{J_K}{2g}. \tag{7.71}$$

The solution is of the form $J_K = C\sqrt{g}$. To estimate the form of the critical line, we demand that this asymptotic solution "matches" in the fixed point region, i.e. we determine the constant C from the requirement $J_K(\varepsilon) = \varepsilon$. This gives $C = \sqrt{\varepsilon}$, and we can write

$$J_K(g) \approx \sqrt{\varepsilon g}. \tag{7.72}$$

7.4.2 Sub-Ohmic dissipative bath in the electronic Griffiths phase

The presence of RKKY interactions introduces a qualitative modification to the dynamics of the Kondo spins, as described by the presence of a dissipative bosonic bath of spin fluctuations. As we have seen in the previous section, this behavior depends crucially on the precise spectral form of the bosonic bath, allowing for the destruction of the Kondo effect in the presence of sub-Ohmic dissipation. For a spectrum of the low frequency (large time) form

$$\chi\left(i\omega_n\right) \sim \chi\left(0\right) - C\left|\omega_n\right|^{1-\varepsilon} \Leftrightarrow \chi(\tau) \sim \frac{1}{\tau^{2-\varepsilon}}, \tag{7.73}$$

Fermi liquid behavior is recovered for $\varepsilon = 0$, but for $\varepsilon > 0$ (sub-Ohmic dissipation), and for sufficiently small bare Kondo temperature T_K, the spin decouples from the conduction electrons. Within an electronic Griffiths phase, however, the disordered Kondo lattice has a very broad distribution of local Kondo temperatures $P\left(T_K\right) \sim \left(T_K\right)^{\alpha-1}$. Therefore, for $\varepsilon > 0$ and arbitrarily weak coupling to the bosonic bath (i.e. weak RKKY interaction), a fraction of the spins will decouple. The crucial question is under what conditions the disordered Kondo lattice model produces a sub-Ohmic dissipative bath.

To obtain a sufficient condition for decoupling, we examine the stability of the Fermi liquid solution, by considering the limit of infinitesimal RKKY interactions. To leading

order we replace $\chi(\tau) \longrightarrow \chi_o(\tau) \equiv \chi(\tau; J=0)$, and the calculation reduces to the "bare model of Chapter 6. The resulting bosonic bath, which is an average over the site-dependent local dynamic spin susceptibility,

$$\chi_o(i\omega_n) = \int dT_K P(T_K)\, \chi(T_K, i\omega_n), \tag{7.74}$$

has a Fermi liquid form in the presence of weak disorder. However, for stronger randomness, $W > W^* \approx \sqrt{t^2\rho_c J_K}/2$ corresponding to $\alpha < 2$ (here, ρ_c is the density of states for conduction electrons), the power law distribution of energy scales within a Griffiths phase produces sub-Ohmic dissipation as follows

$$\begin{aligned} \chi_o(i\omega_n) = \int_0^\Lambda dT_K^o P(T_K^o) \frac{1}{i\omega_n + T_K^o} &\sim \int_{i\omega_n}^\Lambda dT_K^o (T_K^o)^{\alpha-2} \\ &= \frac{1}{\alpha-1}\left[\Lambda^{\alpha-1} - (i\omega_n)^{\alpha-1}\right]. \end{aligned} \tag{7.75}$$

The exponent $\varepsilon = 2 - \alpha > 0$. Note that the estimate based on the bare theory sets an *upper bound* for the true critical disorder strength, i.e. $W_c < W^* = W_{nfl}/\sqrt{2}$ (here, $W_{nfl} \approx \sqrt{t^2\rho_c J_K/2}$ is the threshold for NFL behavior in the bare model, corresponding to $\alpha = 1$). We emphasize that within the electronic Griffiths phase, such decoupling emerges for $W > W_c$ even for arbitrarily small J, in contrast to the clean case where much stronger RKKY interactions ($J > J_c \approx 10\, T_K$) are required to destroy the Kondo effect.

7.5 Two fluid phase in the disordered Kondo lattice

We have seen that the properties of the Bose-Fermi Kondo impurity model depend crucially on the form of the bosonic bath. In the lattice case the solution of a set of single impurity problems determines the form of the bosonic bath, and the problem has to be solved self-consistently. In this Section we show from renormalization group analysis that the self-consistent solution has the exponent ε equal to 1. Numerical solution in the large-N limit confirms the RG results, and also provides an important quantitative estimate of the phase boundaries and crossover scales.

7.5.1 Self-consistent form of the bosonic bath

For nonzero RKKY coupling J, and for the disorder strength W larger than the critical value W_c, the spins break up into two groups: the decoupled spins and those that remain Kondo screened. Since the self-consistent bosonic bath function $\chi(i\omega_n)$ is an algebraic average over all spins, it is an additive function of the contributions from each fluid

$$\chi\left(i\omega_n\right) = n\,\chi_{dc}\left(i\omega_n\right) + (1-n)\chi_s\left(i\omega_n\right). \tag{7.76}$$

Here, n is the fraction of spins in the decoupled phase. As we shall see, the functions $\chi_{dc}\left(i\omega_n\right)$ and $\chi_s\left(i\omega_n\right)$ both have a singular, non-Fermi liquid form characterized by exponents ε_{dc} and ε_s, respectively. Deferring for a moment the study of the critical region (infinitesimally small n), we first examine the solution deep within the spin liquid phase. The first step in the self-consistent procedure is computing ε_{dc} and ε_s for a given value of the bath exponent ε. The spin autocorrelation function in the decoupled phase assumes the form $\chi_{dc}(\tau) = \langle T_\tau \mathbf{S}\left(\tau\right)\cdot\mathbf{S}\left(0\right)\rangle \sim 1/\tau^{\varepsilon}$, a result valid to all orders in ε. Since ε_{dc} is defined by $\chi_{dc}(\tau)\sim 1/\tau^{2-\varepsilon_{dc}}$, we find

$$\varepsilon_{dc}(\varepsilon) = 2-\varepsilon. \tag{7.77}$$

The non-analytic part of $\chi_s\left(i\omega_n\right)$ comes from the spins with the smallest (renormalized) Kondo temperatures T^* ("barely screened spins")

$$\chi_{bs}\left(i\omega_n\right) = \int_0^{\Lambda} dT^* P\left(T^*\right)\chi_{bs}\left(T^*, i\omega_n\right). \tag{7.78}$$

Here $P\left(T^*\right)$ is the distribution of *renormalized* Kondo temperatures (local Fermi liquid coherence scales), and $\chi_{bs}\left(T^*, i\omega_n\right)$ is the local dynamic susceptibility for a given T^*.

Properties of the Bose-Fermi Kondo model in the critical region of the decoupling transition have been extensively studied within renormalization group (RG) [91, 92, 93, 94] and large-N approaches [89], and we use these results to calculate χ_{bs}. In particular, $T^*\sim\left(\delta J_K\right)^{\nu}\sim\left(\delta T_K\right)^{\nu}$, which gives $dT^*/dT_K\sim\left(T^*\right)^{1-1/\nu}$. Therefore

$$P\left(T^*\right) = P\left[T_K\left(T^*\right)\right]\frac{dT_K}{dT^*}\sim\frac{dT_K}{dT^*}\sim\left(T^*\right)^{1/\nu-1}. \tag{7.79}$$

From scaling arguments [91, 92, 93, 94], $\chi_{bs}\left(T^*,\omega\right) = \left(T^*\right)^{\eta-1}\phi\left(\omega/T^*\right)$, where η is the anomalous dimension, which is known to be exactly ε [93, 94]. Performing the integration

in Eq. (7.78), we find at low frequencies $\chi_{bs}(i\omega_n) = \chi_{bs}(0) - C" |\omega_n|^{\eta+\frac{1}{\nu}-1}$, or, equivalently, at large times $\chi_{bs}(\tau) \sim 1/\tau^{\eta+\frac{1}{\nu}}$. By definition, $\chi_s(\tau) \sim 1/\tau^{2-\varepsilon_s}$, which gives

$$\varepsilon_s(\varepsilon) = 2 - \eta - 1/\nu. \tag{7.80}$$

Since $\eta = \varepsilon$ and $\nu > 0$ (as the relevant eigenvalue at the unstable fixed point), Eqs. (7.77) and (7.80) imply that $\varepsilon_{dc} > \varepsilon_s$. Therefore, $\varepsilon = \max\{\varepsilon_{dc}, \varepsilon_s\} = \varepsilon_{dc}$, and from Eq. (7.77) we find that the self-consistent bath is characterized by the exponent $\varepsilon = 1$, as in the spin liquid model of Sachdev and Ye [88], producing a logarithmic divergence of the average local dynamic spin susceptibility. Note that, in contrast to the bare ($J = 0$) model of the electronic Griffiths phase, the renormalized distribution $P(T^*)$ of local energy scales now assumes a *universal* form characterized by an exponent $\alpha^*(\varepsilon) = 1/\nu(\varepsilon) \approx \varepsilon/2 = 1/2$ within the spin liquid phase. The divergence of the local susceptibility does not necessarily imply that the bulk (uniform) susceptibility behaves in the same manner [95], and more work is needed to determine the behavior of the uniform susceptibility as well as specific heat.

7.5.2 Transport in the spin liquid phase

Although the renormalized Kondo coupling scales to zero for the decoupled spins, the precise form of the RG flows (scaling dimension of "irrelevant operators") near the spin-liquid fixed point still determines the finite frequency (or finite temperature) corrections. To leading order, the contribution from decoupled spins scales as $\rho(\omega) \sim [J_K^*(\omega)]^2$, while $J_K^*(\omega) \sim \omega^{1/\nu}$. To compute the appropriate exponent at the spin-liquid fixed point we have used the ε-expansion approach of Refs. [93, 94], and we find $\nu = 2/\varepsilon + O(\varepsilon^3)$. From our self-consistent solution for the spin-liquid phase ($\varepsilon = 1$), we obtain $1/\nu \approx 1/2$, producing again a marginal Fermi liquid [2] correction to the resistivity $\delta\rho_{dc}(\omega) \sim \omega$, or at $\omega = 0$ and finite temperature

$$\delta\rho_{dc}(T) \sim T.$$

7.5.3 Numerical results in the large-N limit

As an illustration of our analytical predictions, and to obtain quantitative results, we proceed to the numerical solution of our equations in the large-N limit. Introducing

[2] "Marginal" Fermi liquid model is proposed on phenomenological grounds as by Varma *et al.* [83] as a description of the electronic properties of cuprates.

site-dependent slave boson parameters r_j and ε_{fj}, and minimizing the local free energy, we come to the following saddle-point equations

$$\frac{1}{\beta}\sum_{\omega_n} e^{i\omega_n 0^+} G_{fj}(i\omega_n) = \frac{1}{2}, \tag{7.81}$$

$$\frac{1}{\beta}\sum_{\omega_n} G_{fj}(i\omega_n)\Delta_{fj}(i\omega_n) = -\frac{1}{J_K}. \tag{7.82}$$

The local f-pseudo-fermion Green's function $G_{fj}(\tau) = -\langle T_\tau f_{j\sigma}(\tau) f^\dagger_{j\sigma}(0)\rangle$, is given by $G^{-1}_{fj}(i\omega_n) = i\omega_n - \varepsilon_{fj} - \Sigma_j(i\omega_n) - r_j^2\Delta_{fj}(i\omega_n)$. The self-energy is equal to $\Sigma_j(\tau) = J^2\chi(\tau)G_{fj}(\tau)$, and $\Delta^{-1}_{fj}(i\omega_n) = i\omega_n + \mu - v_j - t^2 G_c(i\omega_n)$. This Kondo impurity problem has to be solved self-consistently, such that G_c and $\chi(\tau)$ have to be calculated by averaging over the site energies, $\chi(\tau) = -\overline{G_{fj}(\tau)G_{fj}(-\tau)}$, and $G_c(i\omega_n) = \overline{G_{cj}}(i\omega_n)$, where $G^{-1}_{cj}(i\omega_n) = \Delta^{-1}_{fj}(i\omega_n) - r_j^2/\left[i\omega_n - \varepsilon_{fj} - \Sigma_j(i\omega_n)\right]$.

These equations were solved on the imaginary axis at $T = 0$ using fast Fourier transform methods. The total average local dynamic susceptibility χ together with the contributions coming from Kondo screened χ_s and decoupled spins χ_{dc} is shown in Fig. 7.5(a). At low frequencies, the contribution from Kondo screened spins saturates to a constant, while the decoupled spins produce a logarithmic divergence. A comparison with the bare model illustrates how the strong power law divergence of χ found for $J = 0$ is suppressed by the dynamical RKKY interactions. Fig. 7.5(b) shows how χ evolves with the change of disorder. Note that marginal Fermi liquid behavior persists up to a crossover scale $\omega_{sl} \sim 0.1T_K$ $(v_j = 0)$ which has very weak dependence on the disorder strength.

7.5.4 Critical behavior

In this section we will show that the spin decoupling has a form of a continuous phase transition, where the number of decoupled spins exponentially goes to zero as the the disorder strength W approaches to the critical value W_c.

The strategy is to express the minimum site energy ε_c leading to the destruction of the Kondo effect as a function of the ratio of decoupled spins n. We will use the second slave boson equation

$$\frac{1}{\pi}\int_0^\infty d\omega\, \mathrm{Im}\left[G_{fj}(i\omega)\Delta_{fj}(i\omega)\right] = \frac{1}{J_K}, \tag{7.83}$$

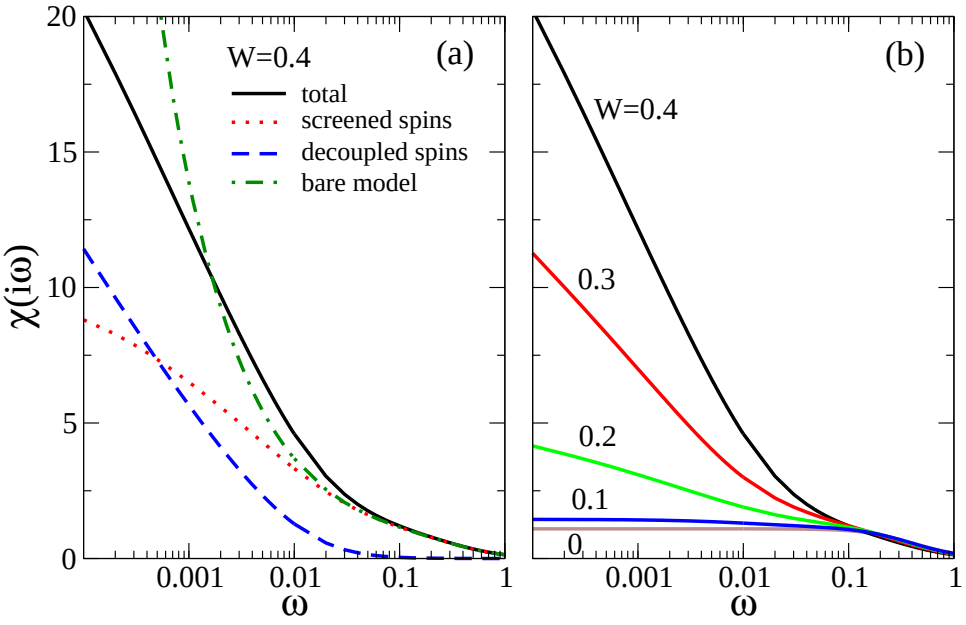

Figure 7.5. Local dynamic magnetic susceptibility. (a) At low frequencies, the decoupled spins (dashed line) provide the leading logarithmic dependence of the total averaged susceptibility (full line). For the values of the parameters used ($J_K = 0.8$, $J = 0.05$, $\mu = -0.1$ in units of the half bandwidth, corresponding to $T_K\,(v_j = 0) = 0.1$ and $W_c \approx 0.1$), there are $n = 8\%$ of decoupled spins at $W = 0.4$. The bare model ($J = 0$) leads to a stronger non-universal power law singularity (dash-dotted line). (b) $\chi(i\omega)$ for the disorder strength ranging from 0 to 0.4.

where the f-electron Green function is given by

$$G_{fj}(\omega) = \frac{1}{\omega - \varepsilon_{fj} - \Sigma_j(\omega) - r_j^2 \Delta_{fj}}. \tag{7.84}$$

Close to the decoupling point $r_j \to 0$, and G_f is determined by the form of the average dynamic susceptibility χ.

The arguments which followed Eq. (7.76) have to be modified since the relative importance of the various contributions to the average local susceptibility changes near the critical point. First, we concentrate on the contribution from the barely screened spins given by Eq. (7.78). As before, $P\,(T^*) = P\,[T_K\,(T^*)]\,dT_K/dT^*$, but close to the transition $P\,(T_K)$ is small and cannot be replaced by a constant prefactor of order 1. Since $P\,(T_K) \approx P\,(T_{Kc}) \sim (T_{Kc})^{\alpha-1}$, we find

$$n = \int_0^{T_{Kc}} dT_K P\left(T_K\right) \sim \left(T_{Kc}\right)^{\alpha}, \tag{7.85}$$

where T_{Kc} is the bare Kondo temperature at the site energy ε_c at which the spins start to decouple. Therefore

$$P\left(T_K\right) \sim n^{(\alpha-1)/\alpha}. \tag{7.86}$$

From the bare model, we know that (for small J) $\alpha \approx 2$ near the critical point. Now we are in a position to write down the general form of the total bosonic bath at low frequencies

$$\chi(i\omega_n) = \chi_o - C_1 \left|\omega_n\right| - C_2 n^{1/2} \left|\omega_n\right|^{\eta+\frac{1}{\nu}-1} - C_3\, n\, \ln\left|\omega_n\right|. \tag{7.87}$$

The first two terms come from the well screened spins and have the Fermi liquid form. The third term is due to the "barely screened" spins and the last term is the contribution from the decoupled spins. The crucial point is that the non-analytic term from the barely screened spins, being proportional to $\sqrt{n}$, is much larger than the logarithmic term due to the n decoupled spins, except at *exponentially small* frequencies. Therefore, we can neglect the last term in Eq. (7.87). Then the exponent ε of the bosonic bath can be self-consistently calculated from the equation

$$1 - \varepsilon = \eta + \frac{1}{\nu} - 1. \tag{7.88}$$

The anomalous exponent $\eta = \varepsilon$, and within large-$\mathcal{N}$ approximation $\nu = 2/\varepsilon$, which gives

$$\varepsilon = \frac{4}{5}. \tag{7.89}$$

The expression for the average susceptibility then assumes the form

$$\chi(\omega) = \chi_o - C_1\, \omega - C_2\, n^{\beta}\, \omega^{1-\varepsilon}, \tag{7.90}$$

where $\beta = (\alpha - 1)/\alpha = 1/2$ and $\varepsilon = 4/5$. The non-analytic term in Eq. (7.90) becomes dominant at frequencies smaller than the characteristic frequency

$$\omega^* = \frac{C_2}{C_1} n^{\beta/\varepsilon}. \tag{7.91}$$

Identifying the characteristic frequency ω^*, we are able to write down an approximate expression for $G_{fj}(\omega)$ close to the decoupling point, i.e. in the limit $\varepsilon_{fj} \to 0$ and $r_j^2 \to 0$

$$G_{fj}(i\omega) = \begin{cases} \dfrac{-iB\,\mathrm{sgn}\omega}{|\omega|^{1-\varepsilon/2}}, & |\omega| < \omega^* \\ -i\dfrac{1}{\omega}, & |\omega| > \omega^*. \end{cases} \tag{7.92}$$

In order to calculate the integral in Eq. (7.83), we will neglect the real part of Δ_{fj} and its frequency dependence. In other words, we assume that the cavity field Δ_{fj} has flat particle-hole symmetric DOS ρ_j with the bandwidth $2D$. Then, for large site energy ε_j, we find $-\frac{1}{\pi}\Delta_f \approx \rho_0/\varepsilon_j^2$. Eq. (7.83) reduces to

$$\int_0^D d\omega \, \mathrm{Im}\, G_{fj}(\omega) = \frac{\varepsilon_j^2}{\rho_0 J_K}, \tag{7.93}$$

and after the integration

$$\frac{2B}{\varepsilon}(\omega^*)^{\varepsilon/2} + \ln\frac{D}{\omega^*} = \frac{\varepsilon_j^2}{\rho_0 J_K}. \tag{7.94}$$

Keeping only the leading terms, we find the desired relation between the decoupling site energy ε_c and the number (ratio) of decoupled spins n

$$\varepsilon_c = \sqrt{-C \ln n}. \tag{7.95}$$

Here C is a positive constant. Since the number of decoupled spins is equal to

$$n = \int_{\varepsilon_c}^{\infty} d\varepsilon P(\varepsilon), \tag{7.96}$$

we have reached our goal: we have a single equation connecting the number of decoupled spins n and the disorder strength W

$$n = \int_{\sqrt{-C\ln n}}^{\infty} \frac{1}{\sqrt{2\pi}W} e^{-\varepsilon^2/2W^2}. \tag{7.97}$$

In the remaining part of this Section we will find $n(W)$ from Eq. (7.97).

We will use properties of the error function which is defined as

$$\mathrm{erf}(x) = \frac{2}{\sqrt{\pi}} \int_0^x dt \, e^{-t^2}. \tag{7.98}$$

The large x asymptotic behavior is given by

$$\mathrm{erf}(x) = 1 - \frac{e^{-x^2}}{\sqrt{\pi}\, x}, \;\; x \to \infty. \tag{7.99}$$

After a few steps of algebra, we find

$$n = \frac{1}{2} - \frac{1}{2}\mathrm{erf}\left(\frac{\sqrt{-C\ln n}}{\sqrt{2}W}\right), \tag{7.100}$$

and in the limit $n \to 0$

$$n = \frac{1}{2} \frac{e^{-\frac{-C \ln n}{2W^2}}}{\sqrt{\pi} \frac{\sqrt{-C \ln n}}{\sqrt{2}W}}, \tag{7.101}$$

which reduces to

$$-\frac{\ln(-\ln n)}{\ln n} = 2\left(1 - \frac{C}{2W^2}\right). \tag{7.102}$$

The critical disorder strength is equal to

$$W_c = \sqrt{\frac{C}{2}}, \tag{7.103}$$

and

$$n = \exp\left(-\frac{\sqrt{C}}{4\sqrt{2}} \frac{1}{W - W_c} \ln(-\ln n)\right). \tag{7.104}$$

If we neglect slow variations in $\ln(-\ln n)$, we find

$$n = e^{-A/(W - W_c)}, \tag{7.105}$$

where A is a positive constant. The numerical results for $n(W)$ are shown in the inset of Fig. 7.6. From numerical results we can identify that close to the transition the fraction of decoupled spins is very small, but a precise functional dependence is practically impossible to determine due to the finite numerical precision. It is limited by the size of the frequency grid on imaginary frequency axis, which is in our code of the order of 10^{-4}.

7.5.5 Spin glass instability and phase diagram.

In this paper we have concentrated on the paramagnetic solution of our model. However, the decoupled spins can be expected to form a spin glass (SG) at low temperatures in the presence of random inter-site interactions [90]. For a rigorous treatment of the spin glass phase, one needs to go beyond the $N = \infty$ limit, but a rough estimate of the temperature for SG ordering [89] may be obtained by using the large-N approach as an approximate theory

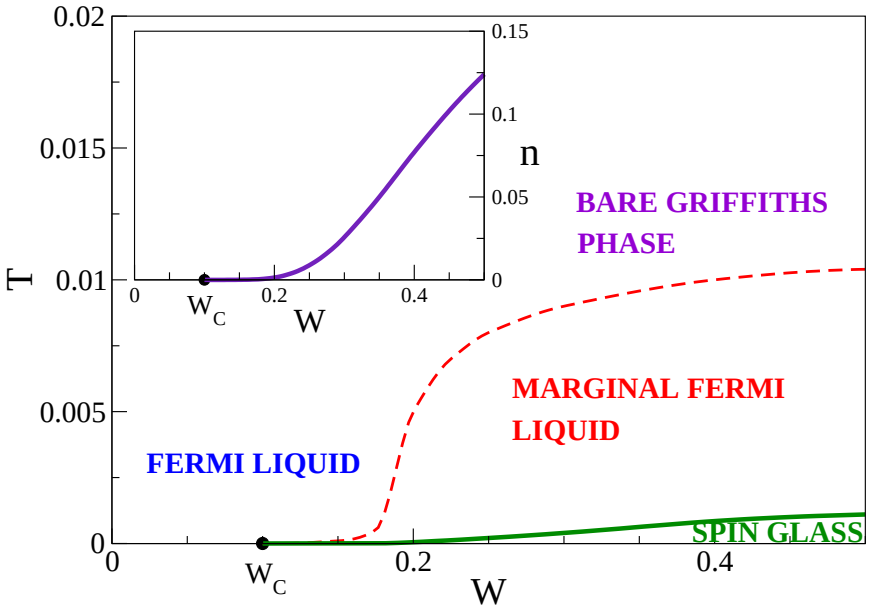

Figure 7.6. Phase diagram obtained for the same values of parameters as in Fig. 7.5. The inset shows the fraction of decoupled spins as a function of disorder. Note that the decoupling sets in already for moderate strength of disorder.

for the considered $N = 2$ case. The spin glass instability criterion [90], as appropriately generalized to the case of additional site randomness then reads

$$\sqrt{\overline{\chi_j^2}}\, J/\sqrt{2} = 1. \tag{7.106}$$

Fig. 7.6 represents a generic phase diagram of our model. For weak disorder the system is in the Fermi liquid phase, while for $W > W_c$ the marginal Fermi liquid phase emerges. The crossover temperature (dashed line) delimiting this regime can be estimated from the frequency up to which the logarithmic (marginal) behavior in $\chi(i\omega)$ is observed [3]. The spin glass phase, obtained from Eq. (7.106), appears only at the lowest temperatures, well below the marginal Fermi liquid boundary. Interestingly, recent experiments have indeed found evidence of dynamical spin freezing in the millikelvin temperature range for some Kondo alloys [96].

[3]For quantitative results, we need to solve the large-N equations at finite temperature. However, for the purpose of obtaining a rough phase diagram, we have replaced temperature with frequency in $\chi_j(T)$, using the well-known ω/T scaling of the Bose-Fermi Kondo model.

7.6 Summary

In summary, we have studied the interplay of the Kondo effect and RKKY interactions within an extended dynamical mean field theory, where we have concentrated on the model with random Kondo couplings. The disorder in the Kondo couplings is generated by the Gaussian distribution of random site energies in the conduction band, the effective disorder distribution which is earlier found to be quite generic for the disordered Kondo lattice systems. For weak disorder, for realistic values of the RKKY coupling, the local spins are screened by the conduction electrons and the system behaves as a Fermi liquid. For stronger randomness, however, spins with the smallest Kondo temperatures decouple from the conduction bath even in the presence of a weak RKKY interaction. We end up with a two fluid behavior, where a fraction of spins are decoupled from the conduction bath forming a spin liquid, while others remain hybridized with the conduction electrons in a Fermi liquid. This is to be contrasted with the clean case, where a very large spin-spin interaction is needed to destroy the Kondo effect. We have found that in the two fluid phase the decoupled spins provide the leading logarithmic divergence in the local dynamic magnetic susceptibility. Therefore, a stronger parameter dependent power law divergence in the electronic Griffiths phase is suppressed by the inter-site RKKY interactions, and replaced by universal logarithmic behavior.

CHAPTER 8

CONCLUSIONS AND OUTLOOK

In this thesis we have focused on two different problems in the physics of strongly correlated systems with disorder. First, motivated by unusual properties of the metallic phase in high mobility MOSFETs, we examined the influence of strong electron-electron interactions on the impurity dominated resistivity. We have solved the problem in the case of short ranged interactions in the limit of large coordination number. Our results favor a description of the metal-insulator transition in MOSFETs as a Mott-Anderson transition, but more work is needed to formulate and solve more realistic models. Our current results, however, clearly illustrate that the solution of the general problem should be searched for beyond the traditional perturbative theories, which are very successful in description of weakly interacting systems.

Second, we have examined, within an extended dynamical mean field theory, two competing processes in heavy fermion systems: the Kondo effect which leads to the formation of the Fermi liquid with strongly renormalized effective parameters, and the RKKY interactions which favor magnetic ordering. We have found that even a moderate amount of disorder in the Kondo couplings leads to decoupling of the spins with lower Kondo temperatures. These decoupled spins form a spin liquid with a universal logarithmic divergence of the local dynamic magnetic susceptibility. Our work provides a possible explanation of the non-Fermi liquid behavior in disordered heavy fermion systems. In this sense it is very important to carefully examine the behavior of the uniform (bulk) susceptibility and the specific heat within the present model, and also to include the RKKY interactions beyond the infinite range model, which remains as a challenge for future work.

APPENDIX A

ANDERSON IMPURITY MODEL IN THE KONDO LIMIT

A.1 Limit $|E_f| \gg 2\rho_0 V^2$ with $\varepsilon_i = 0$

In order to make comparison with the case when the Kondo limit is reached for the large site disorder, we will first recapitulate results for the well studied case of a single impurity in a clean lattice. As a criterion for the Kondo limit, we will use $|E_f| \gg 2\rho_0 V^2$. For simplicity, we will assume $\mu = 0$ and a particle-hole symmetry.

The slave boson equations on a real frequency axis are

$$-\frac{1}{\pi}\int_{-\infty}^{0} d\omega \, \mathrm{Im} G_f(\omega) = \frac{1}{2}(1 - Z), \tag{A.1}$$

and

$$\frac{1}{\pi}\int_{-\infty}^{0} d\omega \, \mathrm{Im}\left[G_f(\omega) G_c(\omega)\right] = \frac{1}{2}\frac{\varepsilon_f - E_f}{V^2}. \tag{A.2}$$

Here $G_f(\omega) = \left[\omega - \varepsilon_f - ZV^2 G_c(\omega)\right]^{-1}$ is f-electron Green's function, Z is the slave boson parameter and ε_f is the renormalized f-level energy. Let us denote $G_c(\omega) = G_c'(\omega) + iG_c''(\omega)$. Eq. (A.1) then becomes

$$-\frac{1}{\pi}\int_{-\infty}^{0} d\omega \frac{ZV^2 G_c''(\omega)}{\left(\omega - \varepsilon_f - ZV^2 G_c'(\omega)\right)^2 + \left(ZV^2 G_c''(\omega)\right)^2} = \frac{1}{2}(1 - Z). \tag{A.3}$$

In the Kondo limit, i.e. for $Z \to 0$, we neglect frequency dependence in $G_c(\omega)$, and substitute $G_c'(\omega)$ and $G_c''(\omega)$ with their values at the Fermi surface. For particle-hole symmetric case

$G_c'(0) = 0$. Now we denote $\rho_0 = -G_c''(0)/\pi$, and $-ZV^2 G_c''(0) = \pi Z V^2 \rho_0 = \Delta$. Eq. (A.1) becomes

$$\frac{1}{\pi}\int_{-D}^{0} d\omega \, \frac{\Delta}{(\omega - \varepsilon_f)^2 + \Delta^2} = \frac{1}{2}(1 - Z). \tag{A.4}$$

After integration, we obtain

$$\frac{\varepsilon_f}{\Delta} = \frac{\pi}{2} Z. \tag{A.5}$$

Within the same notation, Eq. (A.2) assumes the form

$$\frac{1}{\pi}\int_{-\infty}^{0} d\omega \frac{(\omega - \varepsilon_f - ZV^2 G_c'(\omega))\, G_c''(\omega) + ZV^2 G_c'(\omega) G_c''(\omega)}{(\omega - \varepsilon_f - ZV^2 G_c'(\omega))^2 + (ZV^2 G_c''(\omega))^2} = \frac{1}{2}\frac{\varepsilon_f - E_f}{V^2}, \tag{A.6}$$

and after we neglect frequency dependence in G_c' and G_c''

$$\frac{1}{\pi}\int_{-D}^{0} d\omega \frac{(\omega - \varepsilon_f)(-\pi\rho_0)}{(\omega - \varepsilon_f)^2 + \Delta^2} = \frac{1}{2}\frac{\varepsilon_f - E_f}{V^2}. \tag{A.7}$$

After integration

$$\left(\varepsilon_f^2 + \Delta^2\right)^{1/2} = D e^{-(\varepsilon_f - E_f)/2\rho_0 V^2}. \tag{A.8}$$

Using Eq. (2.3) we obtain the final result

$$Z = \frac{D}{\pi \rho_0 V^2} e^{-1/\rho_0 J}, \tag{A.9}$$

where $J = 2V^2/|E_f|$. The Kondo temperature is defined as

$$T_K = D e^{-1/\rho_0 J}, \tag{A.10}$$

which means that $Z = T_K/\pi V^2 \rho_0$.

Now we will make a comparison of Eq. (A.9) with a numerical solution of the slave boson equations (A.1)-(A.2). Figure A.1 shows that agreement is good, though there is some discrepancy in the prefactor of $\approx 30\%$. The explanation for the discrepancy is simple. Formula (A.7) has a divergent integral on the left-hand side. It needs to be regularized, in other words, a cutoff procedure has to be used. The formula for T_K will depend on the cutoff procedure used (the factor "D" in front). Eq. (A.7) is actually exact for a flat DOS but not for a semicircular one, which would have a different "cutoff" in front of the exponential but, and this is crucial, the same exponential dependence (that's why both curves in Figure A.1 have the same slope). Note that there is no analogous divergence in Eq. (A.1), the integral

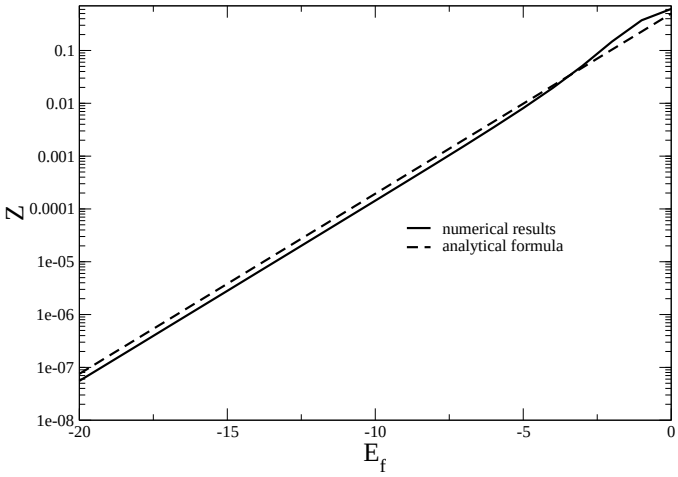

Figure A.1. Kondo temperature as a function of the bare f-energy level. Density of states is semicircular and $V = 1$.

is dominated by the region around the Fermi surface and the result is independent of cutoffs (in the Kondo limit, of course). By contrast, the integral in Eq. (A.7) has contributions from all energy scales (that's why it's sometimes said that the Kondo temperature sums up contributions from many decades in energy).

A.2 Limit $\varepsilon_i^2 \gg t^2\rho_0 J$ with fixed E_f

Now we want to solve the system of equations

$$-\frac{1}{\pi}\int_{-\infty}^{0} d\omega \,\mathrm{Im}\left[\frac{1}{\omega - \varepsilon_f - Z\Delta_{fi}(\omega)}\right] = \frac{1}{2}(1 - Z), \tag{A.11}$$

and

$$\frac{1}{\pi}\int_{-\infty}^{0} d\omega \,\mathrm{Im}\left[\frac{\Delta_{fi}(\omega)}{\omega - \varepsilon_f - Z\Delta_{fi}(\omega)}\right] = \frac{1}{2}(\varepsilon_f - E_f), \tag{A.12}$$

with

$$\Delta_{fi}(\omega) = \frac{V^2}{\omega - \varepsilon_i - \Delta_c(\omega)}. \tag{A.13}$$

Here $\Delta_c(\omega) = \Delta_c'(\omega) + i\Delta_c''(\omega)$ is the conduction electron cavity field. We will assume that it is *given* and particle-hole symmetric ($\Delta_c'(0) = 0$). Also μ is taken to be zero. For a semicircular DOS $\Delta_c''(0) = -\pi t^2\rho_0$.

We consider the limit $Z \to 0$. A crutial approximation, analogous to what we had in Section A.1, is to neglect a frequency dependence in Δ_c and in Δ_{fi}. Then, Eq. (A.11) becomes

$$-\frac{1}{\pi}\int_{-D}^{0} d\omega \frac{\frac{ZV^2\Delta_c''(0)}{\varepsilon_i^2+\Delta_c''^2(0)}}{\left[\omega-\varepsilon_f+\frac{ZV^2\varepsilon_i}{\varepsilon_i^2+\Delta_c''^2(0)}\right]^2+\left[\frac{ZV^2\Delta_c''(0)}{\varepsilon_i^2+\Delta_c''^2(0)}\right]^2} = \frac{1}{2}(1-Z). \tag{A.14}$$

After the integration

$$\varepsilon_f = \frac{ZV^2\varepsilon_i}{\varepsilon_i^2+\Delta_c''^2(0)}. \tag{A.15}$$

Within the same approximation, Eq. (A.12) gives

$$\frac{1}{\pi}\int_{-D}^{0} d\omega \frac{(\omega-\varepsilon_f)\Delta_{fi}''(0)}{\left[\omega-\varepsilon_f-Z\Delta_{fi}'(0)\right]^2+Z^2\Delta_{fi}''^2(0)} = \frac{1}{2}(\varepsilon_f-E_f). \tag{A.16}$$

We now note that Eq. (A.15) is equivalent to

$$\varepsilon_f = -Z\Delta_{fi}'(0), \tag{A.17}$$

so we get

$$\frac{1}{\pi}\int_{-D}^{0} d\omega \frac{(\omega-\varepsilon_f)\Delta_{fi}''(0)}{\omega^2+Z^2\Delta_{fi}''^2(0)} = \frac{1}{2}(\varepsilon_f-E_f). \tag{A.18}$$

Direct integration of the left-hand side leads to

$$\frac{\Delta_{fi}''(0)}{\pi}\left\{\ln\left(\frac{Z\left|\Delta_{fi}''(0)\right|}{D}\right)-\frac{\pi\varepsilon_f}{2Z\left|\Delta_{fi}''(0)\right|}\right\} \approx -\frac{E_f}{2}. \tag{A.19}$$

Using again Eq. (A.15), we obtain

$$Z = D\frac{\varepsilon_i^2+(\pi t^2\rho_0)^2}{V^2\pi t^2\rho_0} e^{-\pi^2t^2\rho_0/J} e^{-\varepsilon_i^2/t^2\rho_0 J} e^{\varepsilon_i/2t^2\rho_0}. \tag{A.20}$$

This is in a good agreement with the numerical solution of Eqs. (A.11)-(A.12), as shown in Figure A.2.

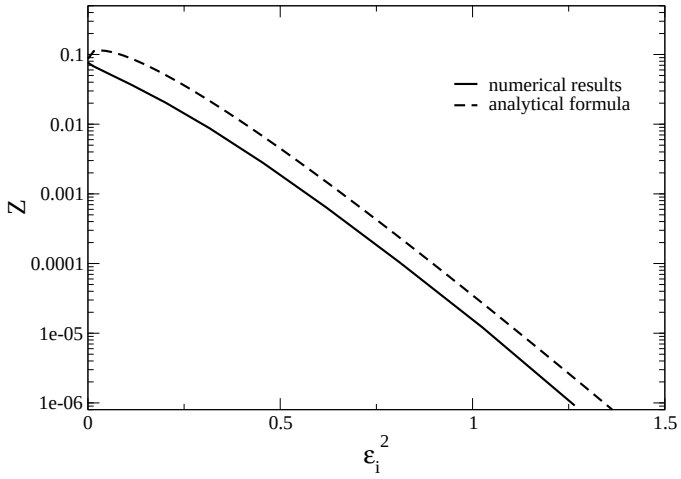

Figure A.2. Kondo temperature as a function of the site disorder. Here $V = 0.5$, $E_f = -1$, $t = 0.5$, $D = 1$ and $\rho_0 = 2/\pi$.

.

APPENDIX B

EFFECTIVE MODEL OF THE EGP: FLUCTUATIONS IN $\delta\Delta^I_{CJ}$ AND INTERACTION RENORMALIZATIONS

B.1 Fluctuations in $\delta\Delta^I_{cj}$

In Section 6.4.2 we have ignored the fluctuations in the imaginary part of the cavity function $\delta\Delta^I_{cj}$. The corresponding contribution to the low-T_K tail is sub-leading, as we now show. We need to focus on rare events that produce exceptionally small values of the local conduction electron DOS $\rho_j = -\frac{1}{\pi}G_{cj}(0)$. Using Eq. (6.20), and ignoring the fluctuations in $\delta\Delta^R_{cj}$, we see that low values for ρ_j correspond to exceptionally high values for $\delta\Delta^I_{cj}$. We therefore need to compute the form of the high-$\delta\Delta^I_{cj}$ tail of $P(\delta\Delta^I_{cj})$. Just as for the real part, we can estimate the fluctuations of $\delta\Delta^I_{cj}$ by calculating the second moment,

$$\sigma_I^2 = \left\langle (\delta\Delta^I_{cj})^2 \right\rangle , \tag{B.1}$$

and we get

$$\sigma_I^2 = C_I W^2 + O(W^4), \tag{B.2}$$

where

$$C_I = \sum_{\substack{j \\ (j\neq 0)}} \left[\mathrm{Im}\, \frac{(G_{oj})^2}{(G_{oo})^2} \right]^2 . \tag{B.3}$$

In this approximation, the quantity $\delta\Delta^I_{cj}$ has a Gaussian distribution, and we find

$$P(T_K) \sim T_K^{-1} \exp\left\{ -\frac{J^2}{2\pi^2\sigma_I^2} \ln^2(D/T_K) \right\} . \tag{B.4}$$

As we can see, because the "log" in the exponent has an extra power of two, this distribution is log-normal and not power-law. Therefore the $\delta\Delta^I_{cj}$ fluctuations, at least when treated on

the Gaussian level as we have done, do not lead to a singular $P(T_K)$ distribution. Thus, to leading order we can ignore these fluctuations when examining the emergence of the electronic Griffiths phase.

B.2 Interaction renormalizations

In the estimates of Section 6.4.2, we have omitted an important ingredient, the fact that Kondo disorder itself will produce additional scattering, i.e. disorder in the conduction channel, which needs to be self-consistently determined. As we have shown in previous work,[70] this results in a distribution of effective scattering potentials Φ_j, corresponding to the Kondo spins (note that in the uniform case, the Φ_j-s are the same on all sites, resulting in no scattering, but contributing to the formation of the Kondo gap). The resulting scattering, in the weak disorder limit again can be considered as a Gaussian distributed potential of width

$$W_\Phi = \left\langle \Phi_j^2 \right\rangle^{1/2}. \tag{B.5}$$

Note however that this additional "Kondo" scattering does not enter directly (at site 0) in the solution of the local Kondo problem, since the local f-site "sees" the corresponding c-site *with the f-site removed*. However, the presence of Φ_j-s on all other sites ($j \neq 0$) does modify the form of $\delta\Delta_{cj}^R$ which, therefore, has to be computed by including this additional scattering. At weak disorder, we expect

$$\left\langle \Phi_i^2 \right\rangle = C_1 W_{eff}^2, \tag{B.6}$$

where the constant C_1 measures the response of the Kondo spins to the hybridization disorder. Note that W_{eff} enters here, since the Φ_j-s are obtained from the solution of local Kondo problems, which are determined by the strength of the renormalized site disorder, as modified by hybridization fluctuations. We therefore need to compute W_{eff} self-consistently, and we get

$$W_{eff}^2 = W^2 + C(W^2 + C_2 W_{eff}^2), \tag{B.7}$$

or

$$W_{eff} = \sqrt{\frac{1+C}{1-CC_2}} W. \tag{B.8}$$

This reasoning, valid for weak bare disorder illustrates how the effective disorder is generated in the conduction band even if it originally was not there, or is enhanced due to additional Kondo scattering, if already present. In addition, these arguments illustrate how Gaussian tails are generated for the renormalized disorder, even if they are not introduced in the bare model. Of course, nonlinear effects at stronger disorder cannot be accounted for in this simple fashion, which is especially true for the consideration of the additional scattering introduced by disordered Kondo spins. Nevertheless, the simple arguments that we presented illustrate how universality is produced by renormalizations due to cavity field fluctuations, and seem to capture the essential features of the emergence of the electronic Griffiths phase.

REFERENCES

[1] E. Abrahams, S. V. Kravchenko, and M. P. Sarachik. Colloquium: Metallic behavior and related phenomena in two dimensions. *Rev. Mod. Phys.*, 73:251, 2001.

[2] G. R. Stewart. Non-Fermi-liquid behavior in d- and f-electron metals. *Rev. Mod. Phys.*, 73:797, 2001.

[3] T. Ando, A. B. Fowler, and F. Stern. Electronic properties of two-dimensional systems. *Rev. Mod. Phys.*, 54:437, 1982.

[4] A. C. Hewson. *The Kondo Problem to Heavy Fermions.* Cambrige University Press, Cambridge, 1993.

[5] A. Georges, G. Kotliar, W. Krauth, and M. J. Rozenberg. Dynamical mean-field theory of strongly correlated fermion systems and the limit of infinite dimensions. *Rev. Mod. Phys.*, 68:13, 1996.

[6] E. Miranda, V. Dobrosavljević, and G. Kotliar. Kondo disorder: a possible route towards non-Fermi liquid behavior. *J. Phys.: Condens. Matter*, 8:9871, 1996.

[7] V. Dobrosavljević and G. Kotliar. Dynamical mean-field studies of metal-insulator transitions. *Philos. Trans. R. Soc. London A*, 356:57, 1998.

[8] V. Dobrosavljević, A.A. Pastor, and Branislav K. Nikolić. Typical medium theory of Anderson localization: A local order parameter approach to strong disorder effects. *Europhys. Lett.*, 62:76–82, 2003.

[9] E. Abrahams, P. W. Anderson, D. C. Licciardello, and T. V. Ramakrishnan. Scaling theory of localization: Absence of quantum diffusion in two dimensions. *Phys. Rev. Lett.*, 42:673, 1979.

[10] B. L. Altshuler, A. B. Aronov, and P. A. Lee. Interaction effects in disordered fermi systems in two dimensions. *Phys. Rev. Lett.*, 44:1288, 1980.

[11] B. Tanatar and D. M. Ceperley. Ground state of the two-dimensional electron gas. *Phys. Rev. B*, 39:5005, 1989.

[12] S. V. Kravchenko, G. V. Kravchenko, J. E. Furneaux, V. M. Pudalov, and M. D'Iorio. Possible metal-insulator transition at $b = 0$ in two dimensions. *Phys. Rev. B*, 50:8039, 1994.

[13] S. V. Kravchenko, W. E. Mason, G. E. Bowker, J. E. Furneaux V. M., Pudalov, and M. D'Iorio. Scaling of an anomalous metal-insulator transition in a two-dimensional system in silicon at $b = 0$. *Phys. Rev. B*, 51:7038, 1995.

[14] S. T. Chui and B. Tanatar. Impurity effect on the two-dimensional-electron fluid-solid transition in zero field. *Phys. Rev. Lett.*, 74:458, 1995.

[15] D. Popović, A. B. Fowler, and S. Washburn. Metal-insulator transition in two dimensions: effects of disorder and magnetic field. *Phys. Rev. Lett.*, 79:1543, 1997.

[16] V. Dobrosavljević, E. Abrahams, E. Miranda, and S. Chakravarty. Scaling theory of two-dimensional metal-insulator transitions. *Phys. Rev. Lett.*, 79:455–458, 1997.

[17] D. Simonian, S. V. Kravchenko, M. P. Sarachik, and V. M. Pudalov. Magnetic field suppression of the conducting phase in two dimensions. *Phys. Rev. Lett.*, 79:2304, 1997.

[18] A. M. Finkel'stein. Weak localization and Coulomb interaction in disordered systems. *Z. Phys. B*, 56:189, 1984.

[19] S. Chakravarty, L. Yin, and E. Abrahams. Interactions and scaling in a disordered two-dimensional metal. *Phys. Rev. B*, 58:559, 1998.

[20] S. Chakravarty, S. Kivelson, C. Nayak, and K. Voelker. Wigner glass, spin-liquids, and the metal-insulator transition. *Phil. Mag. B*, 79:859, 1999.

[21] B. L. Altshuler and D. L. Maslov. Theory of metal-insulator transitions in gated semiconductors. *Phys. Rev. Lett.*, 82:145, 1999.

[22] Das Sarma and E. H. Hwang. Parallel magnetic field induced giant magnetoresistance in low density quasi-two-dimensional layers. *Phys. Rev. Lett.*, 84:5596, 2000.

[23] V. T. Dolgopolov and A. Gold. Magnetoresistance of a two-dimensional electron gas in a parallel magnetic field. *JETP Lett.*, 71:27, 2000.

[24] I. F. Herbut. The effect of parallel magnetic field on the Boltzmann conductivity and the Hall coefficient of a disordered two-dimensional Fermi liquid. *Phys. Rev. B*, 863:113102, 2001.

[25] G. Zala, B. N. Narozhny, and I. L. Aleiner. Interaction corrections at intermediate temperatures: Longitudinal conductivity and kinetic equation. *Phys. Rev. B*, 64:214204, 2001.

[26] A. A. Shashkin, S. V. Kravchenko, and T. M. Klapwijk. Metal-insulator transition in a 2D electron gas: Equivalence of two approaches for determining the critical point. *Phys. Rev. Lett.*, 87:266402, 2001.

[27] S. V. Kravchenko and M. P. Sarachik. Metal-insulator transition in two-dimensional electron systems. *Rep. Prog. Phys.*, 67:1, 2004.

[28] A. A. Shashkin. Metal-insulator transitions and the effects of electron-electron interactions in two-dimensional electron systems. *Physics-Uspekhi*, 48:129, 2005.

[29] D. Vollhardt. Normal ^{3}He: an almost localized Fermi liquid. *Rev. Mod. Phys.*, 56:99, 1984.

[30] B. Spivak. Properties of the strongly correlated two-dimensional electron gas in Si MOSFET's. *Phys. Rev. B*, 64:085317, 2001.

[31] G. D. Mahan. *Many-Particle Physics*. Plenum Press, New York, second edition, 1990.

[32] S.Doniach and E. H. Sondheimer. *Green's Functions for Solid State Physicists*. W. A. Benjamin, Inc., Massachusetts, 1974.

[33] A. V. Chubukov, V. M. Galitski, and V. M. Yakovenko. Quantum critical behavior near a density-wave instability in an isotropic fermi liquid. *Phys. Rev. Lett.*, 94:046404, 2005.

[34] A. V. Chubukov. Self-generated locality near a ferromagnetic quantum-critical point. *preprint, cond-mat/0502302*.

[35] Y. Zhang and S. Das Sarma. Quasiparticle effective-mass divergence in two-dimensional electron systems. *Phys. Rev. B*, 71:045322, 2005.

[36] V. Dobrosavljević and E. Abrahams, unpublished.

[37] M. Polini M. P. Tosi G. F. Giuliani G. Vignale R. Asgari, B. Davoudi. Many-body effective mass enhancement in a two-dimensional electron liquid. *CMT28 Conference Proceedings, cond-mat/0412665*.

[38] G. Kotliar and A. E. Ruckenstein. New functional integral approach to strongly correlated fermi systems: The gutzwiller approximation as a saddle point. *Phys. Rev. Lett.*, 57:1362, 1986.

[39] M. Gutzwiller. Correlation of electrons in a narrow s band. *Phys. Rev.*, 137, 1965.

[40] D. Tanasković, V. Dobrosavljević, E. Abrahams, and G. Kotliar. Disorder Screening in Strongly Correlated Systems. *Phys. Rev. Lett.*, 91:066603, 2003.

[41] A. A. Abrikosov, L. P. Gor'kov, and I. E. Dzyaloshinskii. *Methods of Quantum Field Theory in Statistical Physics*. Dover, New York, 1975.

[42] P. A. Lee and T. V. Ramakrishnan. Disordered eletronic systems. *Rev. Mod. Phys.*, 57:287, 1985.

[43] K. Byczuk, W. Hofstetter, and D. Vollhardt. Mott-Hubbard transition vs. Anderson localization of correlated, disordered electrons. *Phys. Rev. Lett.*, 94:056404, 2005.

[44] E. Koch. Static overscreening and nonlinear response in the Hubbard model. *Phys. Rev. B*, 64:165113, 2001.

[45] D. Goldhaber-Gordon, J. Gores, H. Shtrikman M. A. Kastner, D. Mahalu, and U. Meirav. From the Kondo regime to the mixed-valence regime in a single-electron transistor. *Phys. Rev. Lett.*, 81:5225, 1998.

[46] L. I. Glazman and M. E. Raikh. *Sov. Phys. JETP*, 47:452, 1988.

[47] T. K. Ng and P. A. Lee. On-site Coulomb repulsion and resonant tunneling. *Phys. Rev. Lett.*, 61:1768, 1988.

[48] M. C. O. Aguiar, E. Miranda, V. Dobrosavljević, E. Abrahams, and G. Kotliar. Temperature dependent transport of correlated disordered electrons: elastic vs. inelastic scattering. *Europhys. Lett.*, 67:226, 2004.

[49] S. Florens, unpublished.

[50] M. Balzer and M. Potthoff. Disorder- and correlation-driven metal-insulator transitions. *preprint, cond-mat/0406266.*

[51] S. Das Sarma and E. H. Hwang. The so-called two dimensional metal-insulator transition. *preprint, cond-mat/0411528.*

[52] Y. Meir. Percolation-type description of the metal-insulator transition in two dimensions. *Phys. Rev. Lett.*, 83:3506, 1999.

[53] C. Pethick G. Baym. *Landau Fermi Liquid Theory.* Wiley, New York, 1991.

[54] C. Castellani, B. G. Kotliar, and P. A. Lee. Fermi-liquid theory of interacting disordered systems and the scaling theory of the metal-insulator transition. *Phys. Rev. Lett.*, 56:1179, 1987.

[55] D. Belitz and T. R. Kirkpatrick. The Anderson-Mott transition. *Rev. Mod. Phys.*, 66:261–380, 1994.

[56] Peter Fulde. Introduction to the theory of heavy fermions. *J. Phys. F: Met. Phys.*, 18:601, 1988.

[57] Z. Fisk, H. R. Ott, T. M. Rice, and J. L. Smith. *Nature*, 320:124, 1986.

[58] A. Rosch, A. Schröder, O. Stockert, and H. v. Löhneysen. Mechanism for the non-Fermi-liquid behavior in $CeCu_{6-x}Au_x$. *Phys. Rev. Lett.*, 79:159, 1997.

[59] C.M. Varma, Z. Nussinov, and Wim van Saarloos. Singular or non-Fermi liquids. *Physics Reports*, 361:267, 2002.

[60] B. Andraka and G. R. Stewart. Heavy-non-Fermi-liquid behavior in U(Cu,Pd)5. *Phys. Rev. B*, 47:3208, 1993.

[61] O. O. Bernal, D. E. MacLaughlin, H. G. Lukefahr, and B. Andraka. Copper NMR and Thermodynamics of UCu5-xPdx: Evidence for Kondo Disorder. *Phys. Rev. Lett.*, 75:2023, 1995.

[62] J. A. Hertz. Quantum critical phenomena. *Phys. Rev. B*, 14:1165, 1976.

[63] A. Schröder, G. Aeppli, R. Coldea, M. Adams, O. Stockert, H.v. Löhneysen, E. Bucher, R. Ramazashvili, and P. Coleman. Onset of antiferromagnetism in heavy-fermion metals. *Nature*, 407:351, 2000.

[64] Q. Si, S. Rabello, K. Ingersent, and J. L. Smith. Locally critical quantum phase transitions in strongly correlated metals. *Nature*, 413:804, 2001.

[65] M. C. Aronson, R. Obsorn, R. A. Robinson, J. W. Lynn, R. Chau, C. L. Seaman, and M. B. Maple. Non-Fermi-Liquid Scaling of the Magnetic Response in UCu 5-xPdx (x = 1,1.5). *Phys. Rev. Lett.*, 75:725, 1995.

[66] E. Miranda, V. Dobrosavljević, and G. Kotliar. Disorder-driven non-Fermi liquid behavior in Kondo alloys. *Phys. Rev. Lett.*, 78:290, 1997.

[67] V. Dobrosavljević and G.Kotliar. Mean field theory of the Mott-Anderson transition. *Phys. Rev. Lett.*, 78:3943, 1997.

[68] V. Dobrosavljević and G. Kotliar. Dynamical mean-field studies of metal-insulator transitions. *Phil. Trans. R. Soc. Lond. A*, 356:1, 1998.

[69] R. Abou-Chacra, P. W. Anderson, and D. J. Thouless. Self-consistent theory of localization. *J. Phys. C*, 6:1734, 1973.

[70] E. Miranda and V. Dobrosavljević. Localization-induced Griffiths phase of disordered Anderson lattices. *Phys. Rev. Lett.*, 86:264, 2001.

[71] R. B. Griffiths. Nonanalytic behavior above the critical point in a random Ising ferromagnet. *Phys. Rev. Lett.*, 23:17, 1969.

[72] B. M. McCoy and T. T. Wu. Theory of a two-dimensional Ising model with random impurities. I. Thermodynamics. *Phys. Rev.*, 176:631, 1968.

[73] A. H. Castro Neto, G. Castilla, and B. A. Jones. Non-Fermi liquid behavior and Griffiths phase in f-electron compounds. *Phys. Rev. Lett.*, 81:3531, 1998.

[74] A. H. Castro Neto and B. A. Jones. Non-Fermi-liquid behavior in U and Ce alloys: Criticality, disorder, dissipation, and Griffiths-McCoy singularities. *Phys. Rev. B*, 62:14975, 1 December 2000.

[75] A. J. Millis, D. K. Morr, and J. Schmalian. Comment on "A Tale of Two Theories: Quantum Griffiths Effects in Metallic Systems". *cond-mat/0411738*, 2004.

[76] Castro Neto, A. H., and B. A. Jones. A tale of two theories: Quantum griffiths effects in metallic systems. *preprint, cond-mat/0411197*.

[77] D. Tanasković, E. Miranda, and V. Dobrosavljević. Effective model of the electronic Griffiths phase. *Phys. Rev. B*, 70:205108, 2004.

[78] M. C. O. Aguiar, E. Miranda, and V. Dobrosavljević. Localization effects and inelastic scattering in disordered heavy electrons. *Phys. Rev. B*, 68:125104, 2003.

[79] D. Tanasković, E. Miranda, and V. Dobrosavljević. Spin liquid behavior in electronic Griffiths phases. *preprint, cond-mat/0412100*, 2005.

[80] N. Read and D. M. Newns. A new functional integral formalism for the degenerte Anderson model. *J. Phys. C*, 16:L1055, 1983.

[81] P. Coleman. Mixed valence as an almost broken symmetry. *Phys. Rev. B*, 35:5072, 1987.

[82] E. Miranda and V. Dobrosavljević. Griffiths phase of the Kondo insulator fixed point. *J. Magn. Magn. Mat.*, 226-230:110, 2001.

[83] C. M. Varma, P. B. Littlewood, S. Schmitt-Rink, E. Abrahams, and A. E. Ruckenstein. Phenemenology of the normal state of Cu-O high-temperature superconductors,. *Phys. Rev. Lett.*, 63:1996, 1989.

[84] P. W. Anderson. Absence of diffusion in certain random lattices. *Phys. Rev.*, 109:1492, 1958.

[85] J. Zaanen, G. A. Sawatzky, and J. W. Allen. Band gaps and electronic structure of transition-metal compounds. *Phys. Rev. Lett.*, 55:418, 1985.

[86] F. C. Zhang and T. M. Rice. Effective hamiltonian for the superconducting Cu oxides. *Phys. Rev. B*, 37:3759, 1988.

[87] B.I. Shklovskii and A.L. Efros. *Electronic Properties of Doped Semiconductors*. Springer-Verlag, 1984.

[88] S. Sachdev and J. Ye. Gapless spin-fluid ground state in a random quantum Heisenberg magnet. *Phys. Rev. Lett.*, 70:3339, 1993.

[89] S. Burdin, D. R. Grempel, and A. Georges. Heavy-fermion and spin-liquid behavior in a Kondo lattice with magnetic frustration. *Phys. Rev. B*, 66:045111, 2002.

[90] A. J. Bray and M. A. Moore. Replica theory of quantum spin glasses. *J. Phys. C*, 13:L655, 1980.

[91] J. L. Smith and Q. Si. Non-Fermi liquids in the two-band extended Hubbard model. *Europhys. Lett.*, 45:228, 1999.

[92] A. M. Sengupta. Spin in a fluctuating field: The Bose (+Fermi) Kondo models. *Phys. Rev. B*, 61:4041, 2000.

[93] L. Zhu and Q. Si. Critical local-moment fluctuations in the Bose-Fermi Kondo model. *Phys. Rev. B*, 66:024426, 2002.

[94] G. Zaránd and E. Demler. Quantum phase transitions in the Bose-Fermi Kondo model. *Phys. Rev. B*, 66:024427, 2002.

[95] O. Parcollet and A. Georges. Non-Fermi-liquid regime of a doped Mott insulator. *Phys. Rev. B*, 59:5341, 1999.

[96] D. E. MacLaughlin, O. O. Bernal, R. H. Heffner, G. J. Nieuwenhuys, M. S. Rose, J. E. Sonier, B. Andraka, R. Chau, and M. B. Maple. Glassy Spin Dynamics in Non-Fermi-Liquid UCu5-xPdx, x = 1.0 and 1.5. *Phys. Rev. Lett.*, 87:066402, 2001.

BIOGRAPHICAL SKETCH

Darko Tanaskovic

Education

2005 Ph.D., Physics, Florida State University

2000 M.Sc., Physics, University of Belgrade, Serbia and Montenegro

1996 B.Sc., Physics, University of Belgrade, Serbia and Montenegro

Employment

From 2005, Postdoctoral Research Associate, Department of Physics, Ohio State University

2000-2005, Research Assistant, Department of Physics and NHMFL, Florida State University

1997-2000, Research Assistant, Institute of Physics, Belgrade, Serbia and Montenegro

Publications

1. J. Sobota, D. Tanasković, and V. Dobrosavljević, *RKKY interactions in the regime of Anderson localization*, in preparation.

2. M. Kollar, M. Eckstein, K. Byczuk, N. Blümer, P. van Dongen, M. H. Radke de Cuba, W. Metzner, D. Tanaskovic, V. Dobrosavljevic, G. Kotliar, D. Vollhardt, *Green functions for nearest- and next-nearest-neighbor hopping on the Bethe lattice*, submitted for publication to Annalen der Physik, preprint cond-mat/0504637.

3. D. Tanasković, V. Dobrosavljević, and E. Miranda, *Spin Liquid Behavior in Electronic Griffiths Phases*, submitted for publication to Phys. Rev. Lett., preprint cond-mat/0412100.

4. D. Tanasković, E. Miranda, and V. Dobrosavljević, *Effective Model of the Electronic Griffiths Phase*, Phys. Rev. B. **70**, 205108 (2004).

5. S. Nakatsuji, V. Dobrosavljević, D. Tanasković, M. Minakata, H. Fukazawa, and Y. Maeno, *Mechanism of Hopping Transport in Disordered Mott Insulators*, Phys. Rev. Lett. **93**, 146401 (2004) .

6. D. Tanasković, V. Dobrosavljević, E. Abrahams, and G. Kotliar, *Disorder Screening in Strongly Correlated Systems*, Phys. Rev. Lett. **91**, 066603 (2003).

7. V. Dobrosavljević, D. Tanasković, and A. A. Pastor , *Glassy Behavior of Electrons Near Metal-Insulator Transitions*, Phys. Rev. Lett. **90**, 016402 (2003).

8. D. Tanasković, Z. Radović, and L. Dobrosavljević-Grujić, *Spin paramagnetism in d-wave superconductors*, Phys. Rev. B **62**, 138 (2000).